

One-Dimensional Nanostructures of π -Conjugated Molecular Systems: Assembly, Properties, and Applications from Photovoltaics, Sensors, and Nanophotonics to Nanoelectronics[†]

Felix Sunjoo Kim, Guoqiang Ren, and Samson A. Jenekhe*

Department of Chemical Engineering and Department of Chemistry, University of Washington, Seattle, Washington 98195-1750, United States

Received September 27, 2010. Revised Manuscript Received November 2, 2010

This paper presents a comprehensive review of the literature on one-dimensional (1D) nanostructures (nanowires, nanoribbons, nanotubes, nanobelts, and nanofibers) of π -conjugated small molecules, oligomers, and polymers. The diverse methods used in assembling the molecular building blocks into 1D functional nanostructures and nanodevices are discussed, including hard and soft template-assisted synthesis, electrospinning, nanolithography, self-assembly in solution and at interfaces, physical vapor transport, and other strategies. Optical, charge transport, electronic, and photoconductive properties of nanowires and nanotubes of selected classes of π -conjugated molecular systems are discussed next, highlighting unique features of the 1D nanostructures compared to 2D thin films. Overview of applications of these 1D organic nanostructures ranging from nanoscale light-emitting diodes, field-emission devices, organic photovoltaics, sensors/biosensors, spin-electronics, and nanophotonics to nanoelectronics is then given. The final section provides our brief concluding comments on the status of the field and on areas of outstanding challenges and opportunities for future work. We believe that the emerging confluence of nanoscience and organic semiconductors will greatly enrich both fields while leading to enhanced performance in organic electronics and affordable nanotechnologies.

1. Introduction

The spectacular rise of nanoscience in the last two decades has been stimulated by advances in the synthesis and interdisciplinary investigation of the properties of low-dimensional nanostructures and nanomaterials in which at least one of the dimensions falls in the 1–100 nm.^{1–14} The expected size effects on electronic, optical, magnetic, and mechanical properties due to quantum confinement of electrons or Wannier excitons in two-dimensional (2D), one-dimensional (1D), and zero-dimensional (0D) nanostructures coupled with their possible technological applications have fueled the exponential growth of the field.^{1–14} The synthesis of 0D and 1D nanostructures of inorganic semiconductors and metals has advanced to the point where there is excellent control over the size, composition, crystal structure, surface chemistry, and solid-state properties of the nanomaterials.^{1–10} A rich array of nanoscale devices with enhanced performance compared to conventional microelectronics and optoelectronics has been demonstrated.^{1–10} A substantial majority of the focus of nanoscience has been on inorganic semiconductors and metals as well as carbon nanotubes.^{1–10,15–19} In part because the supposed revolutionary new nanotechnologies promised by nanoscience have not materialized after two decades, there is an ongoing discussion of possible new directions for the field.^{12–14}

A similar rise in the interdisciplinary study of π -conjugated organic semiconductors in the past two decades, essentially in parallel with nanoscience, has led to major advances in the fundamental understanding of their diverse electronic, optoelectronic, and photonic properties while enabling their applications in information, energy and other technologies.^{20–23} For example, the efficient exciton luminescence of organic semiconductor thin films has enabled the development of organic light-emitting diodes (OLEDs) for large-area full-color displays and solid-state lighting.^{24–30} High-mobility charge transport in organic semiconductor thin films is enabling the development of thin-film transistors for printable and flexible electronics.^{31–38} The combination of efficient solar light absorption and good charge transport in organic semiconductor thin films is facilitating the development of large-area, low-cost, photovoltaic devices.^{39–46} The considerable progress in the science and applications of organic semiconductors during this period has been made possible by the spectacular advances in the molecular design and synthesis of this class of electronic and optoelectronic materials, including π -conjugated small molecules, oligomers and polymers^{47–52} as exemplified by typical molecular structures in Figure 1. There is now very good synthetic control and tunability of the electronic band structure (e.g., highest occupied/lowest unoccupied molecular orbital, HOMO/LUMO, energy levels, band gap), optical, electrochemical redox, and other properties of organic semiconductors at the molecular level.^{48–57}

[†] Accepted as part of the “Special Issue on π -Functional Materials”.

*Corresponding author. E-mail: jenekhe@u.washington.edu.

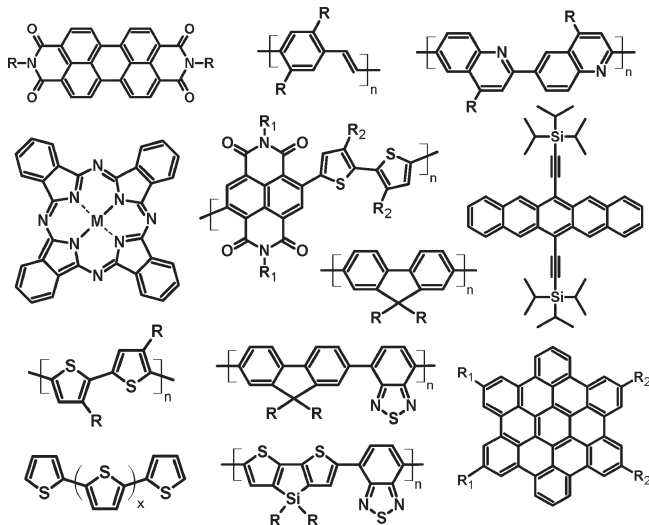


Figure 1. Molecular structures of representative organic semiconductors including π -conjugated small molecules, oligomers, and polymers.

What synergies or new opportunities can the confluence of nanoscience and organic semiconductors promise? This question can be addressed in two ways. First, we exemplify some of the potential benefits of broadening the focus of 1D nanostructures and nanomaterials to include π -conjugated molecular building blocks. The huge diversity of π -conjugated organic semiconductors (small molecules, oligomers, and polymers) and the facile tunability of their electronic, optical, optoelectronic, and mechanical properties could dramatically enlarge the scope of 1D nanomaterials and their possible technological applications. The “soft nature” of organic semiconductor nanostructures could facilitate their ready hybridization with inorganic or metallic nanostructures, biomaterials, or other organic materials to create more complex advanced functional nanocomposite systems. Although supramolecular self-assembly was recognized early as a powerful “bottom-up” method in nanochemistry,^{58–62} it remains to be fully exploited in producing solid-state 1D nanostructures for applications in electronics and optoelectronics. Solution-based large scale synthesis of π -conjugated molecular building blocks and their self-assembly into functional 1D nanostructures, nanodevices, and nanosystems represent a viable approach to high-volume, low-cost, and affordable nanotechnologies. Second, regarding the possible benefits of nanoscience to organic semiconductors, we note that many of the limitations in the performance of current organic electronics, including thin-film transistors and photovoltaic devices, are largely due to the inability to control the morphology and properties of 2D thin films at the nanoscale.⁶³ Because one of the towering achievements of nanoscience to date is the high degree of control of the size, composition, morphology, and properties of 2D, 1D, and 0D inorganic solid-state materials, one can imagine the impact of a similar level of control in organic solid-state materials.

In this review paper, we focus the discussion on 1D nanostructures assembled from π -conjugated molecular building blocks, including small molecules, oligomers,

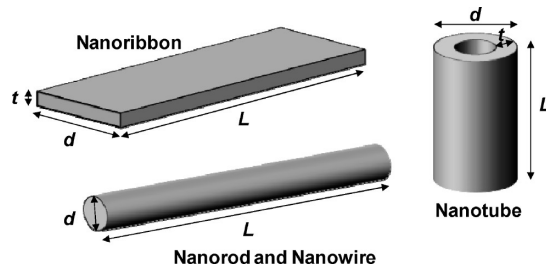


Figure 2. One-dimensional (1D) nanostructures: nanorod, nanowire, nanoribbon, and nanotube.

and polymers. Thus, although single-walled and multiwalled carbon nanotubes^{15–17,64} are strictly also π -conjugated molecular systems and have occupied a central place in the field of nanoscience and nanotechnology, they are not covered here. There are many reviews on carbon nanotubes.^{15–19} Single-molecule nanostructures such as dendron-functionalized π -conjugated polymers,⁶⁵ cylindrical π -stacked bottlebrush conjugated polymers,⁶⁶ and related “molecular wires”^{67,68} are similarly excluded. We note that 0D nanostructures or nanoparticles of conjugated polymers and π -conjugated small-molecule dyes, which are also of growing interest, have been discussed in other recent reviews^{69,70} and thus are not discussed.

This review is organized as follows. We first present in section 2 the main approaches to creating 1D organic semiconductor nanostructures from diverse π -conjugated molecular building blocks, including small molecules, oligomers, and polymers. We discuss the common synthetic strategies for producing functional 1D nanostructures, including the use of hard and soft templates, electrospinning, nanolithographic fabrication methods, supramolecular self-assembly in solution and at interfaces, and physical vapor transport. The morphology of the 1D nanostructures, including type (nanowires, nanorods, nanoribbons/nanobelts, or nanotubes) and dimensions (width/diameter d , thickness t , and length L), illustrated in Figure 2, and crystallinity (as characterized by X-ray diffraction, transmission electron microscopy (TEM) and/or electron diffraction) are included in the discussion.

We next summarize the optical, charge transport, and optoelectronic properties of 1D organic semiconductor nanostructures in sections 3.1–3.3. The 2D confinement of Frenkel or charge transfer excitons in these 1D nanostructures of π -conjugated molecular systems can lead to a range of novel and tunable optical, nonlinear optical, and optoelectronic properties. The characteristic length scales relevant to various supramolecular and mesoscopic phenomena in organic semiconductor nanostructures are illustrated in Figure 3. By virtue of the high crystallinity, and often single-crystallinity, of 1D nanostructures of π -conjugated small molecules, oligomers, and polymers, they have enhanced charge transport properties compared to polycrystalline or amorphous 2D thin films. Most of the studies on the charge-transport properties of organic semiconductor nanowires were focused on field-effect charge carrier mobilities in either a single

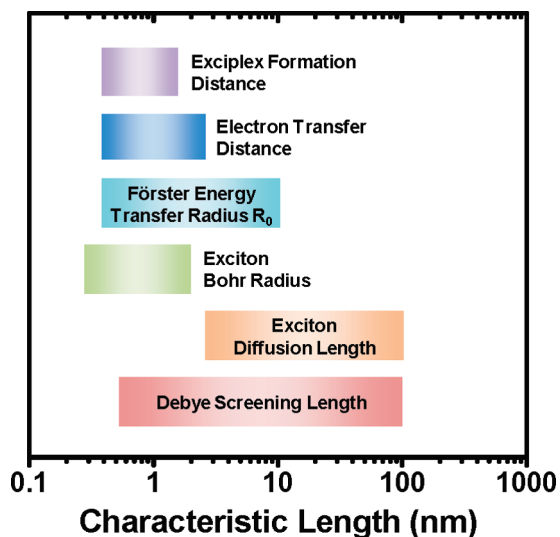


Figure 3. Some characteristic length scales relevant to various supramolecular and mesoscopic phenomena in organic semiconductor nanostructures. Partially adapted with permission from ref 9. Copyright 2004 Annual Reviews.

nanowire or an ensemble of nanowires. We also discuss studies of electrical properties of conducting polymer nanowires and nanotubes, including size-dependent charge transport in this class of organic nanostructures. The photoconductive properties of a single nanowire or bundles of nanowires as well as similar studies on nanotubes of selected π -conjugated molecular systems are presented in section 3.3.

The many different applications of 1D nanostructures of π -conjugated molecular systems are discussed in sections 3.4–3.9. These include organic light-emitting diodes (OLEDs), field emission devices, nanoscale field-effect transistors and nanoelectronics, organic photovoltaics, sensors and biosensors, lasers and nanophotonics, and others. We highlight the unique features and advantages of 1D organic semiconductor nanostructures in these applications compared to 2D thin films and bulk solids. In the case of OLEDs, the main goal of exploiting 1D nanostructures is to develop efficient nanoscale subwavelength light sources, that could be used in areas such as near-field optical microscopy, nanolithography, and data storage. Nanoscale field-effect transistors based on single-crystalline organic semiconductor nanowires represent one of the key building blocks toward high performance nanoelectronic circuits and systems as demonstrated in recent work discussed. Crystalline nanowires and nanotubes of p-type and n-type organic semiconductors offer many potential advantages in developing more efficient organic photovoltaic (OPV) devices, including the larger exciton diffusion length, the ultra-large p-type/n-type interface for exciton dissociation, and the unique nanoscale morphology. The well-defined morphology of polymer semiconductor nanowire-based bulk heterojunction solar cells also provide unique opportunities for systematic basic studies of the photoconversion processes in the bulk and at the nanoscale. We also highlight the great potential of 1D nanostructures of

π -conjugated molecules and polymers for developing ultrasensitive and fast-responding chemical-/biosensors by virtue of their large surface area-to-volume ratios, huge dynamic range for tunability of their optical, electronic, and optoelectronic properties, and the potential low cost for developing and deploying such sensors. The narrow width, large aspect ratio (L/d), high crystallinity, and smooth surfaces of organic semiconductor nanowires make them useful for developing low-loss subwavelength waveguides and nanoscale light sources in nanophotonic devices and circuits.

Finally, in section 4, we offer brief concluding personal comments on the advances discussed in this review as well as areas of outstanding challenges and opportunities for research in the field of 1D organic nanoscience and nanotechnology.

2. Assembly and Morphology

2.1. Templated Methods. The basic concept of using an existing material (or template) as a scaffold for the growth of a complementary one ultimately originates in biology, with spectacular examples in Mother Nature such as the synthesis of proteins with information encoded in DNA. Such a template-directed strategy provides a natural way to produce 1D nanostructures with controlled dimensions and morphology.^{71–82} This method has been extensively studied as a route to nanowires and nanotubes of semiconducting and conducting organic materials. Notable among the early efforts in the template-directed synthesis of organic semiconductor nanowires were studies by the Martin^{71,72,80,83–91} and Bein^{81,92–94} groups. Templates commonly employed in the synthesis of nanomaterials are broadly of two classes: hard templates and soft templates. Particle track-etched membranes (PTMs),^{71,86,90,91,95–105} anodic aluminum oxide (AAO) membranes,^{71–73,77,80,95,105–134} mesoporous silica and other mesoporous rigid solids^{81,82,92–94,135} exemplify hard templates. Assemblies of block copolymers,^{136–146} surfactants and aggregates,^{147–152} liquid crystals,^{153–163} biomolecules,^{164–179} and polymer nanofibers^{180–186} are common examples of soft templates that have been used in the templated synthesis of 1D nanostructures of semiconducting and conducting oligomers/polymers. We briefly discuss a few each of the hard and soft templates as applied in the preparation of 1D organic nanomaterials, highlighting their potentials and limitations.

2.1.1. Hard Templates. The use of hard templates represents a versatile approach in the synthesis of various 1D nanomaterials, including nanorods, nanowires and nanotubes. Although other hard templates, such as mesoporous silica or zinc oxide, have been used to fabricate various 1D organic nanomaterials, e.g., polyaniline (PANI),^{81,94} polypyrrole (PPy),¹³⁵ poly(3,4-ethylenedioxythiophene) (PEDOT),¹⁸⁷ and poly(*p*-phenylenevinylene) (PPV) derivatives,⁸² we will focus on particle track-etched membranes (PTMs) and anodic aluminum oxide (AAO) membranes which are the most commonly discussed (Figure 4). In general, good control of diameter and length is possible with hard templates since the

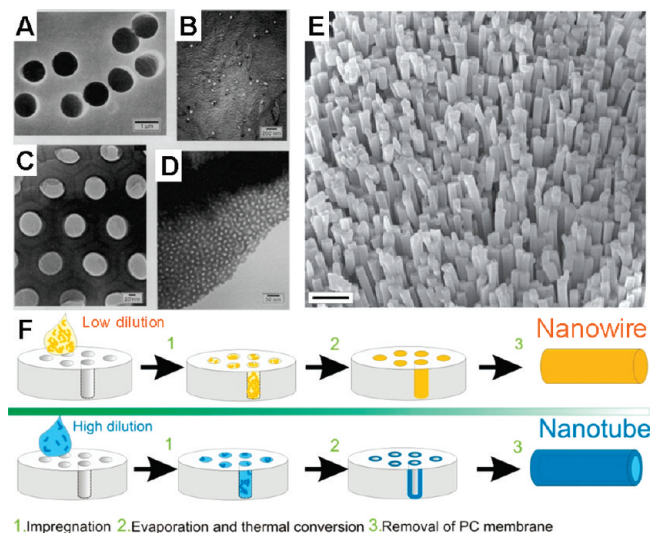


Figure 4. (A–D) Electron microscope images of hard templates: (A) SEM image of particle track-etched membranes (PTMs) with pore diameter of 1 μm ; (B) TEM image of graphite replica of PTM with pore diameter of 30 nm; (C) SEM image of anodic aluminum oxide (AAO) membranes with pore diameter of 70 nm; and (D) TEM image of sectioned AAO membrane with pore diameter of 10 nm. Scale bars: (A) 1 μm , (B) 200 nm, (C) 20 nm, and (D) 50 nm. Reprinted with permission from ref 71. Copyright 1994 American Association for the Advancement of Science. (E) Arrays of PFO (**6a**) nanowires after removal of the AAO template. Reprinted with permission from ref 126 Copyright 2007 Nature Publishing Group. (F) Schematic of the synthesis of nanowires and nanotubes with assistance of track-etched polycarbonate (PC) hard templates. Scale bars: 1 μm . Reprinted with permission from ref 96. Copyright 2009 Institute of Physics.

geometry and morphology of the resulting nanomaterials are endowed by the template itself. In addition, the control of pore density on the template allows production of aligned nanowire (nanorod, nanotube) arrays with desired density and yield. In a typical hard-template synthesis, the pores are filled with a solution of a monomer or precursor and a subsequent electropolymerization (or electrodeposition) in the nanochannels of the template produces polymer nanostructures that mimic the pore dimension. The template is then removed by acidic or basic etching to release the free-standing nanostructures. Several reviews have previously been dedicated to the hard template-based synthesis of nanostructures from organic and inorganic materials.^{71,73,78}

2.1.1a. Particle Track-Etched Membranes (PTMs). Microporous polymeric membranes, especially polycarbonate membranes, are commonly used as a hard template for the synthesis of nanowires. These porous membranes, called particle track-etched membranes (PTMs), are commercially available in various pore sizes. Figure 4A,B shows electron microscope images of PTMs.⁷¹ Pore diameters of membrane A and membrane B are 1 μm and 30 nm, respectively. PTMs have been widely used as templates in the synthesis of nanofibers and nanotubes of polyaniline (PANI) (**1**),^{90,91,95} polypyrrole (PPy) (**2**),^{86,97,98,102–104,188,189} poly(*p*-phenylene vinylene) (PPV) (**3**),^{96,105} poly(3-methylthiophene) (P3MT) (**4b**),⁸⁶ poly(3,4-ethylenedioxythiophene) (PEDOT)^{99–101} (**5**) (see Charts 1 and 2). Figure 4F shows the schematic procedures of the synthesis of nanofibers and nanotubes by means of track-etched polycarbonate templates.⁹⁶ The

Chart 1. Chemical Structures of 1–3

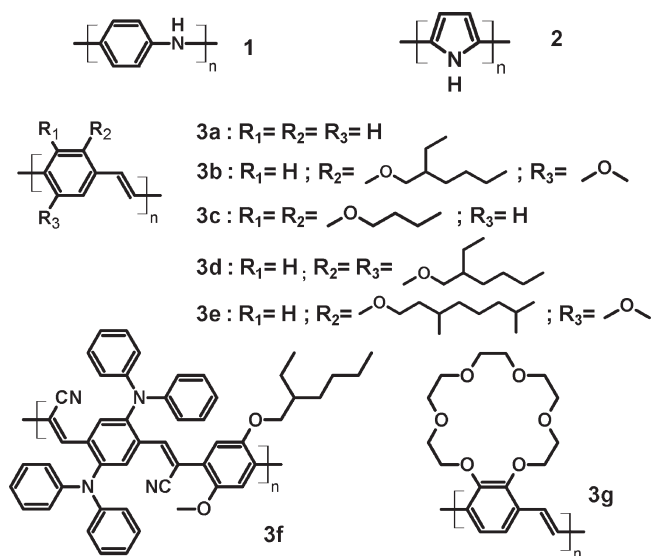
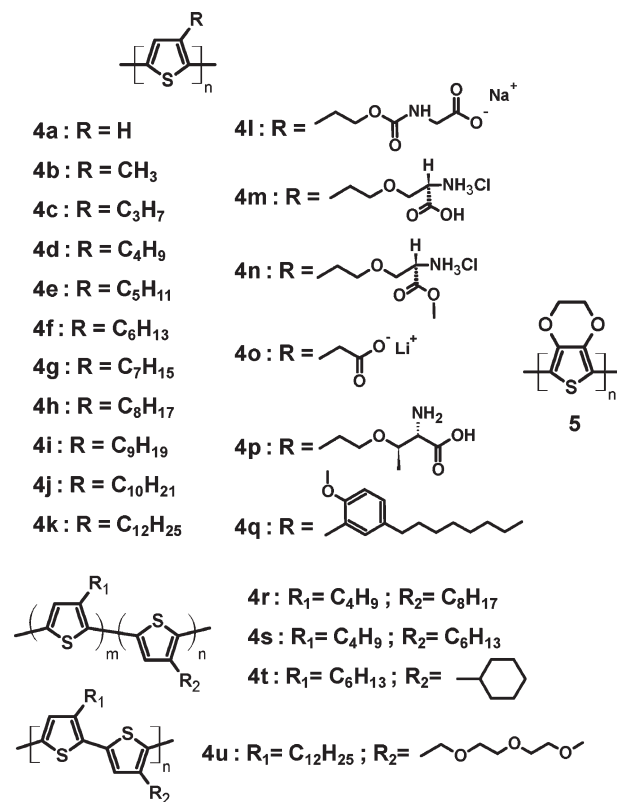


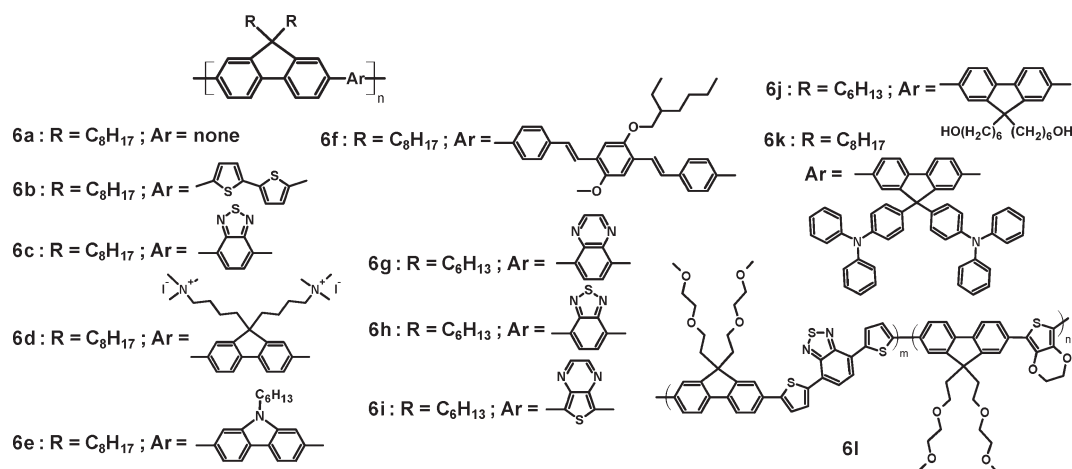
Chart 2. Chemical Structures of 4–5



polymerization of a monomer takes place in the membrane pores and thus, the diameter of 1D nanostructure produced is dependent on the dimension of the template pores. However, these PTM templates are usually produced by random bombardment of ions, and thus the porous structure is not well-controlled and organized.

2.1.1b. Anodic Aluminum Oxide (AAO) Membranes. AAO templates with arrays of cylindrical pores of diameters ranging from 5 to 270 nm are produced following a two-step anodization process.^{73,106,107} A thin sheet of

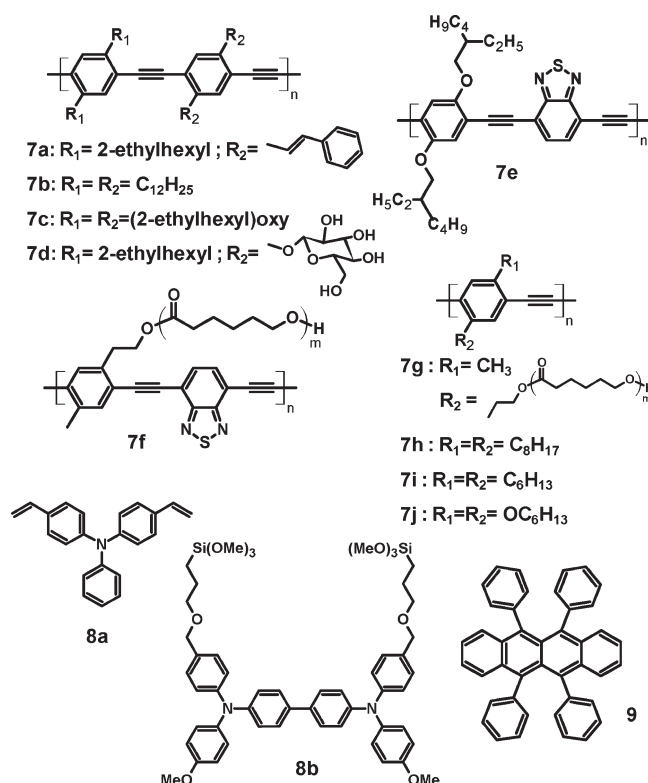
Chart 3. Chemical Structures of 6



aluminum is electropolished to remove the oxide and then is subject to an anodization process in an acidic electrolyte solution. Any generated oxide is removed in a chromate solution, and a second anodization is performed to produce honeycomb structures in the alumina.¹⁰⁶ The pore size can be controlled by adjusting the composition, concentration, and temperature of the acidic electrolyte solution and the applied voltage, whereas the length of the cylindrical pores can be tailored by the anodization time. Figure 4C,D shows SEM and TEM images of the AAO templates with 70 and 10 nm pores.⁷¹ Well-aligned, hexagonally patterned cylindrical pores with uniform diameter can be obtained in high pore density (up to $1 \times 10^{11}/\text{cm}^2$). AAO membranes of various pore sizes are commercially available.

Organic materials can infiltrate into the pores of AAO templates and be solidified from vapor-phase, solution, or precursor fluid state to produce nanowires or nanotubes. After synthesis, the AAO template is removed by immersing and dissolving the template in NaOH solution. Nanowires and nanotubes of PANI (1),¹¹¹ PPy (2),^{108–111} PEDOT (5),^{110–114} P3MT (4b),¹¹⁷ P3HT (4f),^{118–122,133} PPV (3a),^{105,110} polyfluorene (PFO) (6a),^{123–126} poly[(9,9-dioctylfluorenyl-2,7-diyl)-co-(bithiophene)] (F8T2) (6b),¹²⁷ poly(arylene ethynylene)s (7a–e),¹³⁴ cross-linkable triphenylamines (8),^{115,116} and rubrene (9)¹²⁸ (see Charts 3 and 4) have been synthesized by chemical/electrochemical polymerization, infiltration, or vapor-deposition in AAO templates. Figure 4E shows a representative SEM image of PFO (6a) nanowires after removal of the AAO template.¹²⁶ In addition to these single-component nanowires, AAO-template-directed synthesis of multi-component nanowires, creating 1D semiconductor heterojunctions and diodes, has been demonstrated. For example, by sequential polymerization of P3MT (4b), P3BT (4d), and PEDOT (5) in AAO templates, nanoscale barcodes with optically distinct compartments have been demonstrated (Figure 5).¹²⁹ This method is even demonstrated to be suitable for organic/inorganic hybrid heterojunction nanowires composed of p- and n-type semiconductors or semiconductor and metal components. Along this vein, Au-PPy (2), Au-Cd-PPy (2)-Au, and CdSe-PPy

Chart 4. Chemical Structures of 7–9



(2)-Au hybrid nanowires with diameters of 360–400 nm have been produced and studied as mesoscopic amphiphiles and nanoresistor/diodes.^{190,191} CdS-PPy (2) hybrid semiconductor nanowires with diameters of 200–400 nm have also been produced and shown to exhibit a strong photoinduced rectification and photovoltaic properties.^{130,131} Similarly, organic/inorganic hybrid semiconductor nanowires consisting of segments of CdS and polythiophene (4a) and nanowires with a polythiophene (4a) core and a CdS shell have been produced by electrodeposition of materials in AAO templates.¹³²

2.1.2. Soft Templates. **2.1.2a. Block Copolymers as Templates.** Block copolymers are suitable as templates for the synthesis of various nanomaterials due to their intrinsic ability to assemble into ordered structures with

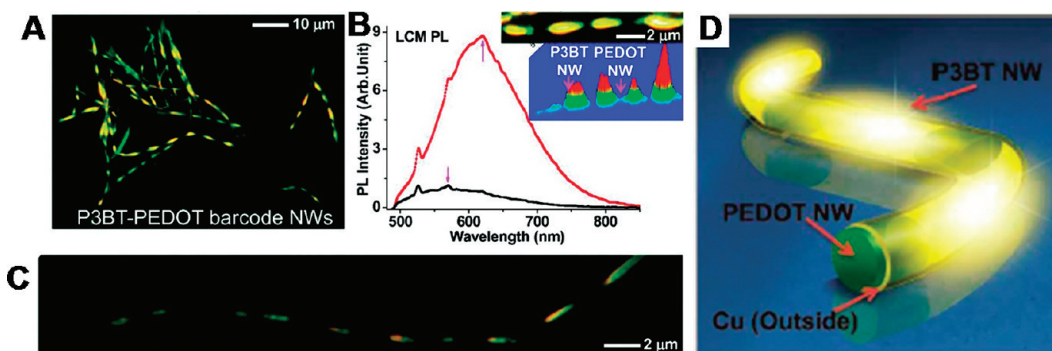


Figure 5. Light-emitting barcode nanowires based on P3BT (**4d**) and PEDOT (**5**) synthesized by AAO template. (A) Color CCD images of P3BT (**4d**)-PEDOT (**5**) barcode nanowires under excitation of 435 nm light. (B) Photoluminescence spectra of P3BT (**4d**) and PEDOT (**5**) compartments of a single barcode nanowire. Inset shows color CCD and laser confocal microscope photoluminescence images of a single nanowire. (C) Color CCD image of a single barcode nanowire with 22 compartments. (D) Schematic illustration of a single barcode nanowire coated with copper to enhance the intensity of photoluminescence. Reprinted with permission from ref 129. Copyright 2010 American Chemical Society.

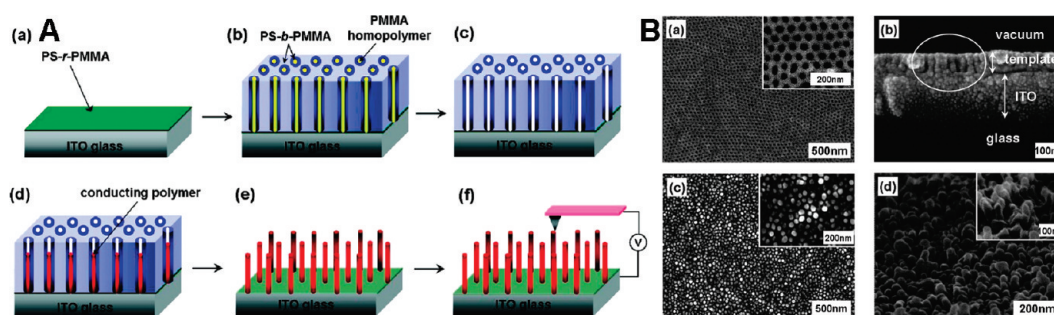


Figure 6. (A) Illustration of block-copolymer-templated fabrication of ultrahigh density array of conducting polymer nanorods. (B) SEM images of nanoporous templates and PPy (**2**) nanorods: (a) top and (b) cross-sectional images of PS-*b*-PMMA/PMMA mixture film on the ITO glass; and (c) top and (d) cross-sectional images of PPy (**2**) nanorods after removal of the template. Reprinted with permission from ref 143 Copyright 2008 American Chemical Society.

nanoscale phase-separated domains.^{136–142} By tuning the block composition, nanoscale morphology of the block copolymer assemblies can be tuned from spherical, cylindrical, lamellae, to ordered bicontinuous double diamond (OBDD).^{136–138} For the synthesis of 1D nanomaterials, the block copolymer assemblies should form a cylindrical morphology (Figure 6). Reactive ion etching, UV irradiation, and mild base treatment can selectively remove a specific block of the copolymer.¹³⁸ By preferential removal of the cylindrical domains, hollow nanopatterns or nanochannels result and thus the block copolymer film can serve as a template. Infiltration with a precursor solution and upon polymerization or electrodeposition, polymer nanostructures mimicking the nanochannels form. Complete removal of the block copolymer template, by either dissolving,¹⁴³ thermally decomposing,¹⁴⁴ or etching with plasma,¹⁴⁵ releases the nanostructures.^{143–145} Figure 6B shows SEM images of block copolymer template (PS-*b*-PMMA) and generated arrays of vertical nanorods of PPy (**2**).¹⁴³ Block copolymers, such as polystyrene-*b*-poly(2-vinylpyridine) (PS-*b*-P2VP),¹⁴⁶ and polystyrene-*b*-poly(methyl methacrylate) (PS-*b*-PMMA),¹⁴³ have been successfully demonstrated in the synthesis of PPy (**2**)¹⁴³ and PANI (**1**)¹⁴⁶ nanorod arrays on various substrates. In principle, very high densities of 1D nanostructures ($\sim 1 \times 10^{11} / \text{cm}^2$) could be attained by using block copolymer assemblies as templates.^{192,193}

2.1.2b. Surfactants and Aggregates as Templates. Surfactants are amphiphilic molecules that can self-assemble in solution into various nanostructures such as micelles (or inverse micelles) of various shapes, when the concentration of the surfactant is above the critical micelle concentration (CMC).¹⁹⁴ These micelles can provide a microenvironment for polymerization, and the morphology and dimension of the resulting polymer nanostructures will be complementary to those of the surfactant assembly. For example, chemical polymerization of PPy (**2**) (Figure 7)¹⁴⁷ or PEDOT (**5**)¹⁴⁸ in solutions with sodium bis(2-ethylhexyl) sulfosuccinate (AOT) yielded nanowires and nanotubes with diameters of 40–300 nm. PPy (**2**) nanowires have also been synthesized by chemical polymerization with cationic surfactants in combination with anions of the oxidizing agent ammonium persulfate.^{149,150} Choice of surfactant turned out to be important to produce desirable morphology. The use of cationic surfactants with long alkyl chains, such as cetyltrimethylammonium bromide (CTAB) and dodecyltrimethylammonium bromide (DTAB), yielded nanowirelike morphology of PPy (**2**), with widths of 25–85 nm and lengths of several micrometers.¹⁵⁰ Spheres with diameters of 45–70 nm were observed when nonionic surfactant, poly(ethylene glycol) mono-*p*-nonylphenyl ether (O π -10), or short-chain cationic surfactant octyltrimethylammonium bromide (OTAB) was used, whereas no characteristic feature was observed from

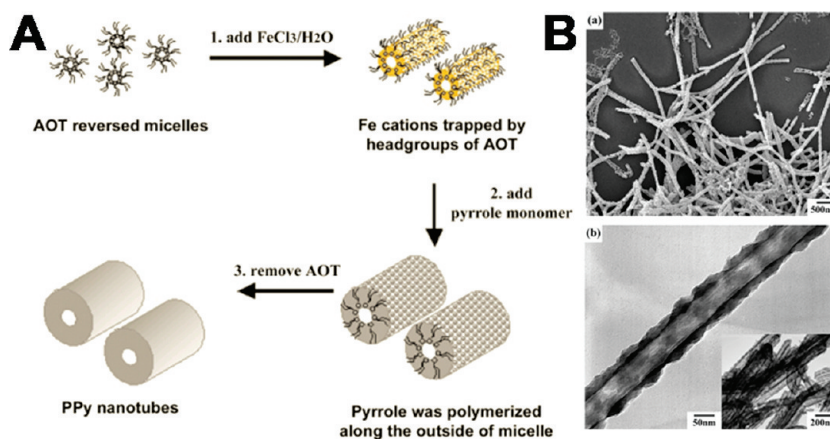


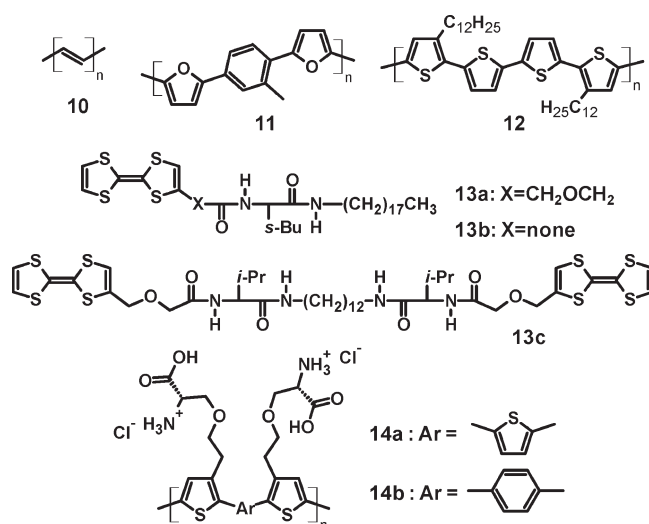
Figure 7. (A) Illustration of surfactant-assisted synthesis of PPy (2) nanotubes. (B) (a) SEM and (b) TEM images of PPy (2) nanotubes. Reprinted with permission from ref 147. Copyright 2003 Royal Society of Chemistry.

anionic surfactant sodium dodecyl sulfate (SDS).¹⁵⁰ In another study, PANI (1) nanowire networks were synthesized using a cationic surfactant, hexadecyltrimethylammonium bromide (HTAB), as an emulsifier and an organic diacid, oxalic acid, as a dopant during an oxidative polymerization of aniline monomer.¹⁵¹ The diameters of PANI (1) nanowires were controlled from 35–45 to 100 nm, by adjusting reaction conditions.¹⁵¹ Besides such amphiphilic surfactants, an anionic 5,10,15,20-tetrakis(4-sulfonatophenyl)porphyrin (TPPS) has been employed as a template due to its ability to aggregate into 1D rod-like nanostructure.¹⁵² Electrochemical polymerization of 3,4-ethylenedioxythiophene (EDOT) or pyrrole resulted in PEDOT (5) or PPy (2) nanostructures with lengths of 300–500 nm and diameters of 30–80 nm.¹⁵²

2.1.2c. Liquid Crystals as Templates. The use of liquid crystals (LCs) as soft templates to produce 1D organic nanomaterials has been fully demonstrated in the last two decades.^{153–163} The ordering of the nematic LCs, which have a directional ordering, can direct the self-assembly of small-molecules and polymers during synthesis of the nanostructures.^{153–160} Nanowires based on polyacetylene (PA) (10),^{153–155} PPy (2),¹⁵⁶ a furan-based copolymer (11),¹⁵⁷ polythiophene derivatives (4a,12),^{159,160} and tetrathiafulvalene (TTF) derivatives (13)¹⁵⁸ (see Chart 5) have been synthesized by using LCs as a template. For example, PA (10) is known to form a network of nanowires with a diameter of 20 nm when chemically polymerized without any template.^{153,195} When the polymerization was carried out in an LC solvent, highly aligned PA (10) nanowires were produced.^{153–155}

A high-mobility semiconducting polymer, poly(3,3'-didodecylquaterthiophene) (PQT12) (12) (Figure 8A), is an example of the materials that have been studied in the form of nanowires synthesized by using an LC template.¹⁶⁰ PQT12 (12) was selected because it is miscible with a nematic LC (E44). Large-scale aligned nanowires of PQT12 (12) were obtained by utilizing this anisotropic crystallization of the nematic LC assembly. The alignment of the nanowires was confirmed by polarized absorption and AFM imaging (Figure 8B). An individual PQT12 (12) nanowire and bundles of the nanowires

Chart 5. Chemical Structures of 10–14



produced with this method have heights of ~10 and ~100 nm, respectively.¹⁶⁰ The proposed mechanism of the synthesis follows (Figure 8C):¹⁶⁰ (1) the polymer chains are randomly oriented at very high temperature ($T > 120^\circ\text{C}$; isotropic phase); (2) in the nematic phase at relatively high temperature ($102^\circ\text{C} > T > 60^\circ\text{C}$), the PQT12 (12) chains are still isolated, but are unidirectionally aligned by the nematic ordering of the LC along the director (i.e., rubbing direction of a polyimide layer); and (3) upon further cooling ($T < 60^\circ\text{C}$), the polymer chains are crystallized and self-assembled into nanowires consisting of stacked polymers that preserve their alignment. This mechanism was supported by the fact that PQT12 (12) nanowires were randomly oriented when another LC, 5CB, which has a lower transition temperature, was used.¹⁶⁰

2.1.2d. Polymer Nanofibers as Templates. Electrospun nanofibers of insulating polymers have been shown to act as soft templates to synthesize nanofibers and nanotubes of various materials.^{180–186} This templation process is often termed as “tubes by fiber templates,” also known as TUFT.¹⁸⁰ A typical TUFT-directed synthesis of nanotubes includes three processes – fabrication of the core

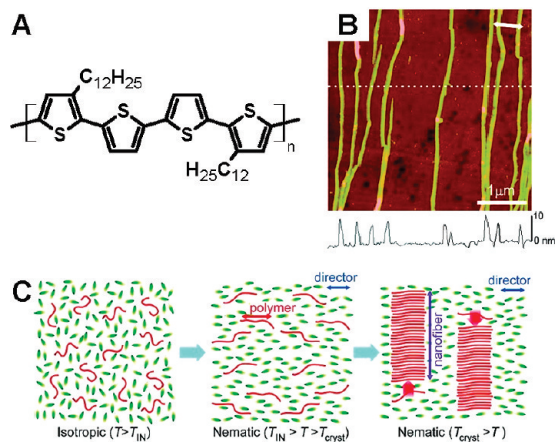


Figure 8. (A) Chemical structure of PQT12 (**12**). (B) AFM topographic image of PQT12 (**12**) nanowires assembled via LC template. (C) Illustration of the nanowire assembly mechanism. Reprinted with permission from ref 160. Copyright 2009 American Chemical Society.

fibers by electrospinning, coating of the fibers with the desired material, and removal of the core fiber material. Several key requirements need to be met in order to use the process. The morphology and dimension of core fiber are critical in determining the nanotube morphology and dimension. To fabricate nanotubes, the core fiber material has to be electrospinnable into ultrafine nanofibers. Poly(L-lactide) (PLA),^{180–182} poly(lactide-co-glycolide) (PLGA),¹⁸² polystyrene (PS),¹⁸⁴ poly(methyl methacrylate) (PMMA),¹⁸⁴ poly(vinyl pyrrolidone) (PVP),¹⁸⁵ and cellulose acetate¹⁸⁶ have been shown to be effective in producing nanofibers used as soft templates in the synthesis of organic nanotubes. The removal of the core materials can be done by selective dissolution or by thermal decomposition of the fiber templates. To remove the core fibers by dissolution, the constituent core fiber and shell materials must have mutually exclusive solubility in some solvents.^{182,185} Figure 9 shows SEM images of electrospun PVP nanofibers, vapor-polymerized PEDOT (**5**) on PVP, and PEDOT (**5**) nanofibers after removal of PVP.¹⁸⁵ To remove the core fibers by thermal decomposition, the decomposition temperature of the core fiber material must be lower than the shell material to prevent any potential destruction of the nanotube.¹⁸⁴ Taking PLA as an example, nanofibers with an average diameter of 200 nm were produced by electrospinning.¹⁸⁰ The PLA nanofibers decomposed at 235–255 °C, which is much lower than the decomposition temperature of conjugated polymers such as PANI (**1**) (~280 °C).¹⁸⁴ Coating of the shell material onto the core fiber can be done using solution-phase polymerization,^{182,184} vapor-phase polymerization,¹⁸⁵ or layer-by-layer deposition.¹⁸⁶ Nanotubes of PANI (**1**),¹⁸⁴ PEDOT (**5**),^{182,185} and hydrolyzed poly[2-(3-thienyl) ethanol butoxy carbonyl-methyl urethane] (H-PURET) (**4l**)¹⁸⁶ have thus been produced by this process.

2.1.2e. Biomolecules as Templates. Biomolecules, such as DNA,^{164–172} proteins,^{173–176,196} and lipid vesicles,^{177,178} and microorganisms, such as fungi,^{179,197} have been explored as a soft template for the synthesis of various organic and inorganic nanostructures. Among such

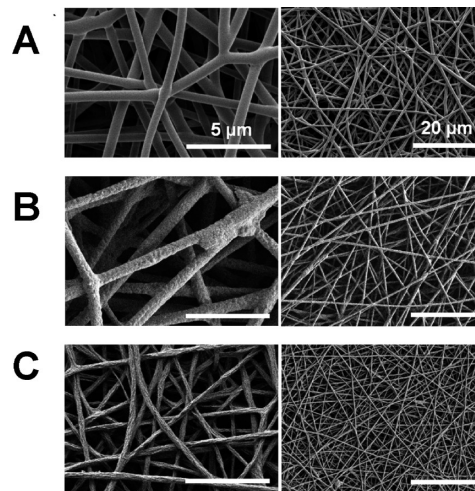


Figure 9. SEM images of the nanofibers at each fabrication step of nanofiber-template synthesis: (A) after electrospinning of PVP; (b) after vapor-phase polymerization of EDOT; and (c) PEDOT (**5**) nanofibers after rinsing of the template with methanol. Reprinted with permission from ref 185. Copyright 2010 American Chemical Society.

templates, DNA is one of the first and often studied examples of biomolecular templates used to produce conducting and semiconducting organic nanowires.¹⁶⁴ DNA is relatively stable, programmable in length, and easy to chemically functionalize.¹⁶⁵ The synthetic approach utilizes the noncovalent interactions between DNA and other molecules (monomers and oligomers), which results in the formation of hybrid materials.¹⁶⁵ Figure 10 shows illustration of a PANI (**1**) nanowires synthesized by using DNA as a template.¹⁶⁶ Several conducting and semiconducting polymers, including PPV (**3a**),¹⁶⁴ PANI (**1**),^{166–169} PPy (**2**),^{170,171} and polythiophene derivatives (POWT (**4m**) and POMT (**4n**))¹⁷² have been made into nanowires with this approach.

Some proteins are destabilized from their native state and reorganized into amyloid fiber under certain environmental conditions. These amyloid fibers of bovine insulin have been used to assemble nanofibers of various organic semiconductors, such as derivatives of oligothiophene (**14**), polythiophene (**4o**), and polyfluorene (APFO12) (**6l**).^{173–175} Individual nanofiber had a width less than 10 nm, whereas bundles of the nanofibers had a width on the order of micrometers.^{173–175} Nanoribbon-like structures of a polythiophene derivative (**4p**) have been produced via synthetic polypeptides as well.¹⁷⁶ Lipid bilayers are another example of a biomolecular templated used in the chemical polymerization of PPy (**2**), yielding the PPy (**2**) nanowires with widths of 10–200 nm.^{177,178} Fungi have been shown to be a good template for micrometer-wide tubular assembly of a polythiophene derivative.¹⁷⁹ In principle, other microorganisms such as viruses^{198–201} can similarly serve as templates to direct the synthesis of 1D nanostructures of diverse organic/polymer semiconductors.

2.2. Electrospinning. Electrospinning is a simple, inexpensive, and scalable method for producing long and continuous nanofibers of diverse materials under a high electric field.^{202–205} Use of this method of fiber drawing

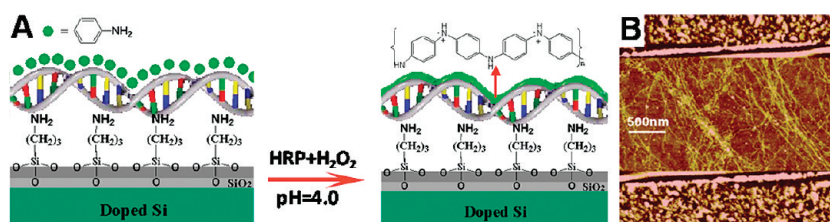


Figure 10. (A) Illustration of a PANI (**1**) nanowire synthesis on a Si surface with stretched double-stranded DNA as a template. (B) AFM image of PANI (**1**) nanowires bridging gold electrodes. Reprinted with permission from ref 166. Copyright 2004 American Chemical Society.

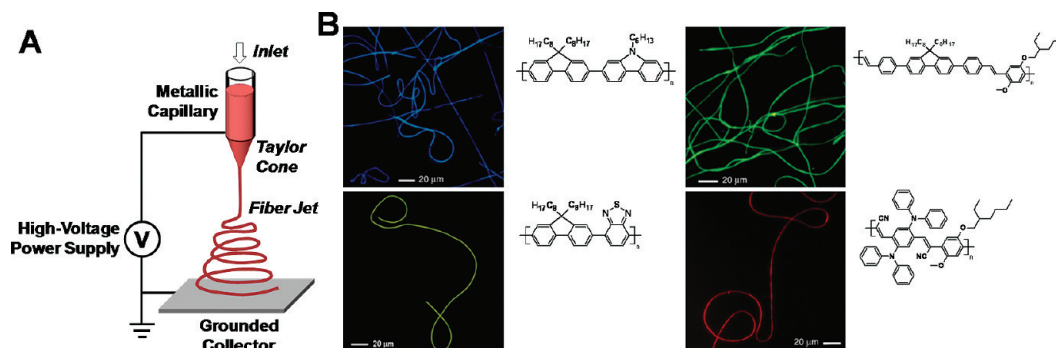


Figure 11. (A) Illustration of the experimental setup of electrospinning. (B) Fluorescent optical microscope images of electrospun nanofibers based on polymer semiconductors and their corresponding chemical structures. Reprinted with permission from ref 230. Copyright 2008 Nature Publishing Group.

from solutions and melts has seen a tremendous growth in the last 15 years,^{202–205} including the preparation of nanofibers, nanowires, and nanotubes of π -conjugated organic semiconductors and conducting polymers. Electrospinning of nanofibers of various materials is the subject of several reviews.^{202–205}

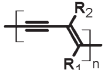
The electrospinning equipment consists of a high-voltage power supply, a metallic capillary, and a grounded collector as a counter electrode (Figure 11A).^{202–205} Electric potential across the setup can be from a few to tens of kilovolts in a distance of ~ 5 –50 cm between a capillary nozzle and a grounded collector, resulting in an electric field on the order of 1×10^5 V/m. As droplet at the tip of the capillary is electrically charged, a fluid jet ejects from the tip of the capillary when the electrostatic force surpasses a threshold point and the charged jet of the fluid accelerates to a velocity of ~ 10 m/s. The feed rate can be adjusted with a syringe pump if necessary. The polymeric fluid stretches out, narrows its diameter, forms a continuous fiber of the polymer if the fluid is viscous enough and has low surface tension, and travels all the way down to a grounded collector where discharge occurs. This jet experiences instability due to the competition of electrostatic repulsion, viscoelastic forces, and surface tension, having fiber elongation, bending, looping, and splaying.²⁰⁶ Under the right conditions, the diameter of the fiber continues to narrow from ~ 100 μm at the capillary tip to ~ 10 nm– 10 μm until the fiber is solidified as the solvent evaporates or the fluid cools down. The length of the electrospun fiber can range from a few centimeters to kilometers, resulting in very high aspect ratios ($> 1 \times 10^6$).^{202,206}

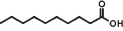
The dimensions and morphology of electrospun nanofibers are determined by many variables: (1) intrinsic properties of the materials, such as chemical structure,

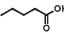
molecular weight, and solubility; (2) properties of the solvent, such as surface tension, viscosity, conductivity, vapor pressure, and dielectric constant; (3) external processing parameters, such as electric potential and field distribution, concentration of constituent materials and any additional ions, number and structure of inlet capillaries, feed rate, shape and motion of the collector, ambient temperature, relative humidity, flow of air, and time of fiber collection.^{202–205,207,208} Therefore, many


intrinsic and external processing parameters have to be adjusted to enable electrospinning of each specific system and to control the size and morphology.^{207,208} For example, diameters of the nanofibers of PANI (**1**)/poly(ethylene oxide) blends varies from 5–50 nm²⁰⁹ to 100–500 nm,^{210,211} and to 1–2 μm ,²¹² from small changes in processing conditions. Once these parameters are optimized, electrospinning can produce uniform nanofibers with targeted dimension and secondary structures (e.g., alignment). Deposition of nanofibers can be guided to align nanofibers or to isolate a single fiber by design of collector motion and electric field distribution.^{213–217} Electrospinning may occur during electrospinning of fibers, resulting in beadlike morphology. This is a consequence of imbalance in the competing forces of electrostatic repulsion, viscoelastic forces, and surface tension. Increase in viscosity and reduction of surface tension of the fluid by selection of an appropriate polymer/solvent pair reduce or eliminate the formation of beads. High-molecular-weight flexible-chain polymers such as poly(ethylene oxide), polystyrene, and poly(vinyl pyrrolidone) are well-known to form bead-free nanofibers by electrospinning.^{208,210,218–220} The high degree of entanglement in such high molecular weight polymers confers viscoelastic properties to the polymeric fluid, precluding

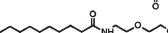
Polyaniline (PANI) (**1**) was one of the first semiconducting or conducting polymers investigated in the form of electrospun nanofibers.^{202,209–212,225,236} Electrospinning was performed from a PANI (**1**) solution in sulfuric acid,^{202,210} a blend of PANI (**1**) and poly(ethylene oxide) (PEO) in chloroform,^{209–212,225} or core/sheath structures of PANI (**1**) and poly(vinyl alcohol) (PVA) in water.²³⁶ Polystyrene and polyacrylonitrile have also been used as

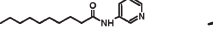


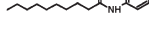
15a: $R_1 = C_{12}H_{25}$; $R_2 =$ 


15b: $R_1 = C_{12}H_{25}$; $R_2 =$ 


15c: $R_1 = C_{12}H_{25}$; $R_2 =$ 


15d: $R_1 = C_{12}H_{25}$; $R_2 =$ 

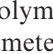
15e: $R_1 = C_{12}H_{25}$; $R_2 =$ 

15f: $R_1 = C_{12}H_{25}$; $R_2 =$ 

15g: $R_1 = C_{12}H_{25}$; $R_2 =$ 

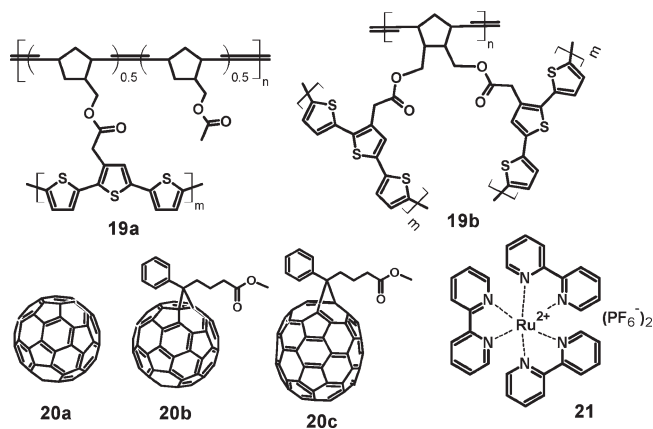
15h: $R_1 = C_{10}H_{25}$; $R_2 =$ 

15i: $R_1 = C_{16}H_{33}$; $R_2 =$ 

15j: $R_1 = R_2 =$ 

Electrospun nanofibers of PPV derivatives (**3a–d**, **f**)^{208,215,217–220,230,234,237–244} and PFO derivatives (**6a**, **c–k**)^{215,216,219,230,235,238,244–246} and their properties have been widely studied. Diameters of the nanofibers varied from 100 to 2500 nm depending on the electrospinning conditions (Figure 11B). The polymer semiconductors were often incorporated with electrospinnable insulating polymers to achieve their nanofibers and investigate their morphology and photophysical properties compared to the corresponding thin films. PL spectra of electrospun nanofibers of the polymer semiconductor/insulating polymer blends show higher intensity of high-energy bands than the spectra in the thin films of the blends.^{216,220,235} This implies that the conjugated polymers are less aggregated in the nanofibers as a result of dilution effect of the insulating polymer. As the amount of the insulating component in the nanofiber increased,

Chart 7. Chemical structures of 19–21



the PL emission peak is blue-shifted, supporting the fact that interchain interaction and charge delocalization is weaker in the nanofibers.^{220,235} The PL quantum efficiency was also higher in the nanofibers than in thin films.²³⁵

Nanofibers of binary blends of conjugated polymer semiconductors have also been produced by electrospinning. Förster-type energy transfer between the constituent conjugated polymers resulted in the change of emission colors depending on the blend composition.^{215,218,219,238,244} Nanofibers of MEHPPV (**3b**)/P3HT (**4f**) blends were found to be phase-separated with smaller domain sizes than in the spin-coated thin films, resulting in significant energy transfer.^{218,219} In contrast, electrospun nanofibers of MEHPPV (**3b**)/PFO (**6a**) blends were free of such energy transfer as in the thin films, likely because of the larger scale of the phase separation in the nanofibers.²¹⁹ The effect of phase separation on energy transfer is also confirmed by an independent study. The electrospun nanofibers of PFO (**6a**)/DB-PPV (**3c**)/PMMA blends from chloroform as a solvent have small-scale phase separation and significant energy transfer, whereas the nanofibers from chlorobenzene as a solvent have larger phase separation and limited energy transfer.²¹⁵ By controlling the solvent and the composition of PFO (**6a**)/DB-PPV (**3c**), the emission color was tuned from blue to green.²¹⁵ Tuning of the PL emission color from blue to white to red by changing the composition of the constituent conjugated polymers in blends and controlling the degree of the energy transfer was also demonstrated by others.^{238,244,246} Electrospun nanofibers of blends of a conjugated polymer (BEHPPV) (**3d**) with a strong electron acceptor, phenyl-C₆₁-butyric acid methyl ester (PCBM) (**20b**), resulted in complete quenching of PL emission because of the ultrafast charge transfer from the polymer to the PCBM (**20b**).²³⁴

Highly polarized PL emission has been observed in nanofibers of PPV and PFO derivatives (**3b,c,6a,d**), proving that the conjugated polymer chains are highly aligned within the fibers.^{215–217} Nanofibers of PFO derivatives (**6c,e,f**) and PPV derivatives (**3b,f**) with diameters ranging from 75 nm to 5 μ m were also obtained without any assistance of inert polymers.^{230,245} These electrospun

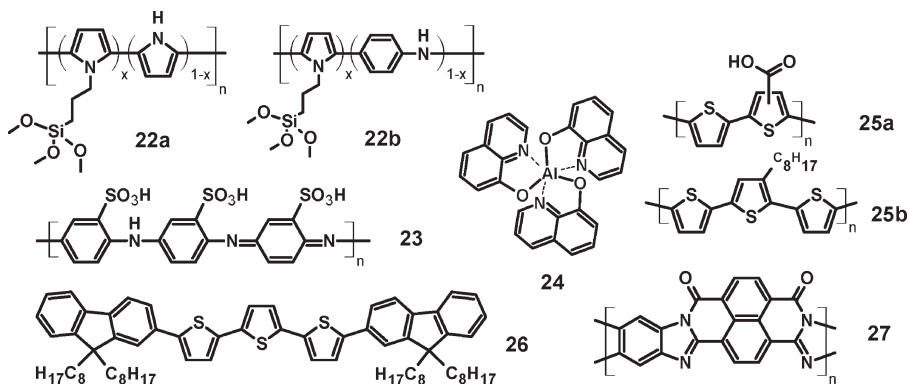
nanofibers were a subject of further nanopatterning in combination with room-temperature nanoimprinting lithography to make photonic nanostructures on a single nanofiber (see section 2.3.3).^{230,245}

Nanofibers of organic/inorganic semiconductor hybrid materials have been prepared by electrospinning. Simultaneous electrospinning of MEHPPV (**3b**) and mesoporous molecular sieve (SBA-15) nanofibers from two syringes in parallel have been shown to tune the photoluminescence (PL) spectra.²⁴³ Blends of polyfluorene derivative PFTPA (**6k**) and organic-dye-modified zeolite L have been electrospun to tune the emission wavelength by using Förster-type energy transfer.²⁴⁶ Sequential electrospinning of an inorganic oxide semiconductor SnO₂ nanofiber and a P3HT (**4f**) nanofiber was applied to form a rectifying p-n hybrid junction.²²⁸ PPV (**3a**)/TiO₂ or PPV (**3a**)/ZnO nanocomposite fibers have also been produced from blends of a PPV (**3a**) precursor and a sol-gel solution or the dispersion of the oxide semiconductor nanoparticles, and their photophysical properties were investigated.^{241,242}

Electrospun nanofibers of organic semiconductors have been explored in functional electronic devices, such as field-effect transistors (FETs),^{219,228,229,248} rectifying diodes,²²⁸ electroluminescent (EL) devices²²⁷ and electrochromic devices.²⁵⁵ FETs of P3HT (**4f**) nanofibers, with a flexible-chain insulating polymer^{219,228,248} and P3HT (**4f**) alone,^{229,248} were studied. Hybrid diodes based on a p-type nanofiber of P3HT (**4f**) and an n-type nanofiber of oxide semiconductor SnO₂ were also demonstrated.²²⁸ In EL nanofibers, ruthenium complex ions, [Ru(bpy)₃]²⁺-(PF₆)₂ (**21**), were embedded in PEO fibers of diameter ~150 nm to 5 μ m.²²⁷ The nanofiber EL device with maximum emission wavelength of 600 nm clearly suggests that the nanofiber can be used as a point light source. For electrochromic devices, a nonconjugated polynorbornylenes with oligothiophene pendants (PNP3T-PN) (**19a**) was electrospun to prepare nanofibers with diameters as small as 119 nm.²⁵⁵ The oligothiophene pendants were then chemically or electrochemically cross-linked, as indicated from the visual change of color from colorless to deep blue. The resulting nanofibers switched the color from blue to orange depending on the oxidation state.²⁵⁵

2.3. Nanolithography. Nanolithography is a printing process for generating numerous copies of a master pattern with features in the nanometer scale. Various methods have been developed for implementing nanoscale lithography.^{256–260} Examples of nanolithographic techniques that have been applied to synthesize organic semiconductor nanowires include electron-beam lithography (EBL), scanning probe lithography (SPL), soft lithography, and others. Unlike other strategies for the synthesis of nanowires, nanolithographic approaches can generate 1D and 2D patterns on an organic semiconductor thin film with precisely controlled direction, size, aspect ratios, and periodicity. The patterns may or may not become separate nanowires at the end of the process. In general, organic nanostructures fabricated by

Chart 8. Chemical Structures of 22–27



nanolithography tend to be amorphous except in a few cases where self-assembly of crystalline molecules is carefully introduced into the process.^{261–264} Minimum widths of the patterns generated vary as the size of the master or resolution of the translational scanner equipment, typically ranging from ~ 10 nm to ~ 1 μ m. Lengths of patterns constructed by nanolithography vary depending on the size of the master or the scanning capability of the equipment, ranging from the order of ~ 100 nm to ~ 10 cm. EBL,^{265–273} SPL,^{274–283} nanoimprinting and soft lithography,^{230,245,262–264,284–299} and others^{300–302} have all been used to synthesize various organic semiconductor nanowires.

2.3.1. Electron Beam Lithography. Electron beam lithography (EBL) is a maskless method of patterning nanostructures that conventional photolithography is unable to reach because of the diffraction limit of light.²⁵⁶ EBL scans electron beam to generate a designed pattern onto a thin film. A thin polymer film, such as poly(methyl methacrylate) (PMMA), is typically used as a resist layer that can be developed afterward, although direct writing of electron beam on patternable materials is also possible. After deposition of additional layer and lift-off, the designed pattern remains on the substrate. EBL can generate high-resolution patterns with a feature size less than 100 nm. However, scanning of electron beam is a serial process and substrate size is limited to the scan range, limiting EBL to a low-throughput process.

Nanopatterning of organic semiconductors by EBL has developed in two directions: positive method (with resist) and negative method (without resist). Positive method involves deposition of a resist such as PMMA, followed by additional deposition or etching. Nanowires of conducting polymers with widths of ~ 80 – 150 nm have been produced.^{265–269} Chemical polymerization of PPy (2) and PANI (1) has been used to synthesize polymer nanowires defined by EBL.²⁶⁵ After PMMA resist is exposed and developed, the substrate was immersed in a solution of the monomer and initiator. To promote adhesion of nanowires on a silicon substrate, silane-functionalized comonomers of pyrrole and aniline were used in the polymerization to synthesize PPy-silane (22a) and PANI-Py-silane (22b) (see Chart 8). Lift-off of PMMA results in the nanowires of the conducting polymers.²⁶⁵ In

other studies, electrochemical polymerization for synthesis of PPy (2),^{266–269} PANI (1),^{266–268} polythiophene (4a),²⁶⁹ and PEDOT (5)²⁶⁹ nanowires has been performed on patterns defined by EBL. Developed PMMA layer acted as mask for reactive ion etching to define a channel for polymerization. The resulting conducting polymer nanowires were used as electrolyte-gated FETs and pH sensors,^{266–268} as well as chemical sensors for volatile organic compounds.²⁶⁹

Direct writing of electron beam patterns onto polymer semiconductors without PMMA resist has been utilized to synthesize various nanowires. In this case, the polymer semiconductor irradiated by electron beam undergoes cross-linking, resulting in insoluble polymer 1D nanostructures. Additional agents for cross-linking were introduced in some cases to increase the sensitivity.²⁷⁰ Unreacted polymers were washed out by solvent. Nanowires of P3OT (4h),²⁷¹ MEHPPV (3b),²⁷² and PFO derivatives (PFC) (6j),²⁷⁰ with line widths as narrow as $d \approx 50$ – 70 nm, have been synthesized. The studies showed that only a small fraction in the polymer semiconductor was affected by the irradiation of electron beam as was confirmed by the measured electrical and optical properties.^{270–272} Very smooth films of MEHPPV (3b) have been patterned as optical grating with periodicity of 580–610 nm by EBL.²⁷³ The irradiation of electron beam reduced the conjugation length of MEHPPV (3b) and led to cross-linking. Irradiated region shrank only about 0.5–1 nm, resulting in very small topographical modulation.²⁷³

2.3.2. Scanning Probe Lithography. Scanning probe lithography (SPL) is a very powerful technique that can address positions with a spatial resolution less than 10 nm.²⁵⁸ As scanning probe microscopy (SPM) has many variations depending on the mechanisms of interaction, SPL-based nanopatterning has thus evolved in several directions. Scanning near-field optical lithography, scanning thermochemical nanopatterning, scanning electrochemical lithography, and dip-pen nanolithography are examples of SPL techniques that have been utilized to synthesize organic semiconductor nanowires (Figure 12). Most of SPL techniques involve the conversion of a precursor of an organic semiconductor, except dip-pen nanolithography which generates nanowires by

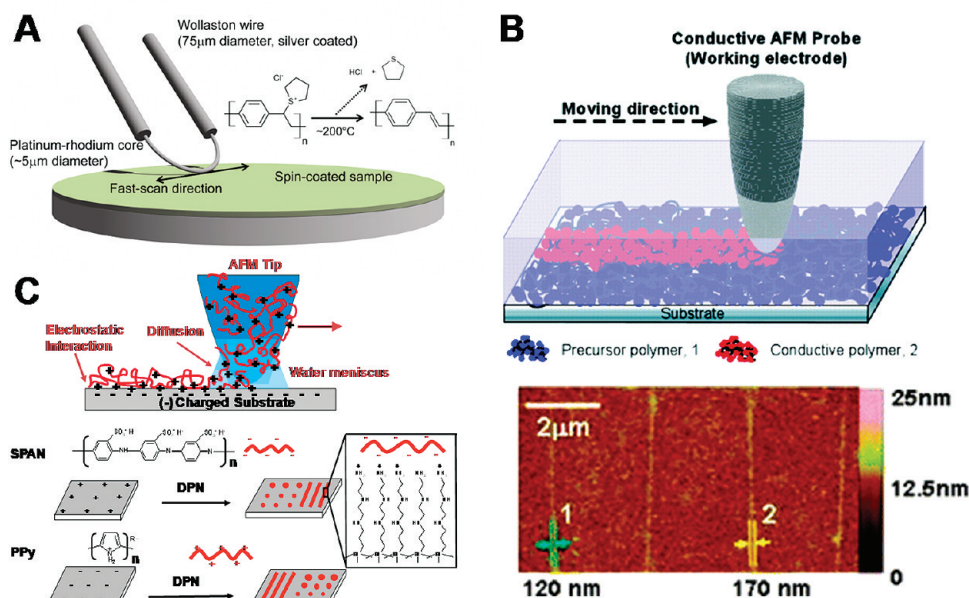


Figure 12. Schematic illustrations of scanning probe lithographic techniques: (A) Scanning thermochemical lithography. Reprinted with permission from ref 278. Copyright 2009 Nature Publishing Group. (B) Scanning electrochemical lithography and height image of produced polymer nanolines. Reprinted with permission from ref 277. Copyright 2004 American Chemical Society. (C) Dip-pen nanolithography. Reprinted with permission from ref 279. Copyright 2002 Wiley-VCH.

an additive process. Nanopatterns fabricated by SPL have feature sizes as narrow as $d \approx 6\text{--}45\text{ nm}$,^{274–278} although larger dimensions were also reported in some cases.^{279–281} The width is largely affected by the size of tip, strength of the patterning force, and the scanning speed.^{275–279,282} Lengths of the nanowires are mainly limited by the available scanning range of the stage. In the case of dip-pen nanolithography, dimensions of the nanowires are also governed by the amount of material on the tip and ambient conditions.^{279,282} SPL is a serial and low throughput process; the scan rate of the tip for the lithography is usually less than $\sim 20\text{--}60\text{ }\mu\text{m/s}$.^{276–279,281,282}

Thin film of poly(*p*-xylene tetrahydrothiophenium chloride), a soluble precursor of PPV (**3a**), can be patterned by local heating (Figure 12A).^{278,281} Temperature-controlled metal wires and an SPM tip have been used for scanning thermochemical lithography. Unconverted region of the thin film was washed out after patterning, and then the patterned polymer nanostructures were fully converted to PPV (**3a**) by further annealing if necessary.²⁷⁸ Clear nanowire features were observed from SPM and fluorescence microscopy images. Here, very small widths ($\sim 28\text{ nm}$) of PPV (**3a**) nanowires were synthesized from a relatively large tip with a diameter of $\sim 5\text{ }\mu\text{m}$.²⁷⁸ Tip translation speed and tip temperature largely affected the width of nanowires.

Scanning near-field optical lithography has also been used for patterning nanoarrays of PPV (**3a**).²⁸⁰ Thin film of precursor of PPV (**3a**) was exposed to HeCd laser light of 325 nm wavelength through an aperture with diameter of 40–80 nm. A substrate was dipped into methanol for short time to wash out unexposed precursor, and then

followed by thermal conversion. The procedure resulted in arrays of nanodots with diameter as small as 130 nm.²⁸⁰

Scanning electrochemical lithography is another kind of SPL that exploits the conversion of a precursor to synthesize organic semiconductor nanowires. Thin films of spin-coated precursor of PPV (**3a**)²⁷⁵ and an insulating polynorbornylene with oligothiophene pendants (PNP3T) (**19b**)²⁷⁷ were used for the proof of concept. Electrochemical decomposition of precursor, especially on the vinylene sites, through a conductive tip was involved in the case of PPV (**3a**), resulting in a nonluminescent lines with widths as small as $d \approx 20\text{ nm}$.²⁷⁵ In another study, oligothiophene pendants on an insulating polymer backbone (**19b**) were electrochemically cross-linked as local electric potential of 1.4 V was applied through a conductive tip (Figure 12B).²⁷⁷ Line width as narrow as $\sim 45\text{ nm}$ was obtained from tapping mode scanning, whereas the line width was $\sim 120\text{ nm}$ from contact mode. This technique showed a relatively high scanning speed of $\sim 60\text{ }\mu\text{m/s}$ compared to other SPL methods.²⁷⁷

Dip-pen nanolithography is an additive-type SPL, using the tip as a “pen” and a solution of the material to be patterned as an “ink” of the lithography. Both conjugated polymer semiconductors and their monomers can be used as ink. Since the ink is delivered to the substrate by tip, the amount of ink adsorbed to the tip defines the width, length, and height of the nanostructure. Humidity and scan speed are also factors that determine the resolution of nanopatterns. Nanowires based on MEHPPV (**3b**),²⁸² poly(aniline sulfonic acid) (SPAN) (**23**),²⁷⁹ PPy (**2**),²⁷⁹ and PEDOT (**5**)^{276,283} have been reported with widths of 30–300 nm. The scan rate of dip-pen nanolithography is less than $1\text{ }\mu\text{m/s}$, which is

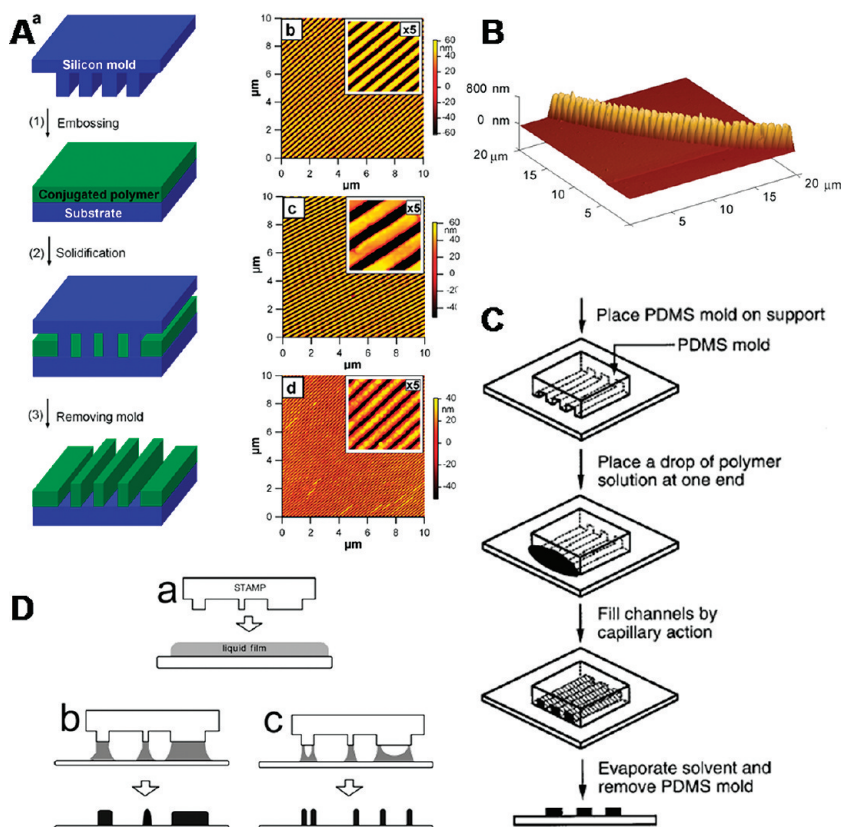


Figure 13. (A) Nanoimprinting lithography (NIL): (a) Schematic procedure and (b) atomic force microscopy (AFM) images of PFO (**6a**), (c) PQT12 (**12**), and (d) PPy (**2**) nanowires synthesized by NIL. Reprinted with permission from ref 264. Copyright 2007 American Chemical Society. (B) AFM image of an MEHPPV (**3b**) nanowire synthesized by electrospinning, and then patterned by RT-NIL. Reprinted with permission from ref 230. Copyright 2008 Nature Publishing Group. (C) Schematic procedure of micromolding in capillary (MIMIC). Reprinted with permission from ref 297. Copyright 1999 Wiley-VCH. (D) Schematic procedure of lithographically controlled wetting (LCW). Reprinted with permission from ref 299. Copyright 2003 American Chemical Society.

much lower than other SPL methods; this is because the process involves a transfer of material from the tip to the substrate. In the case of SPAN (**23**) and PPy (**2**) (Figure 12C), adhesion of the polymers on a substrates were caused by electrostatic interaction, resulting in features with a height of $t \approx 1.5\text{--}2\text{ nm}$.²⁷⁹ In addition to the direct synthesis of nanowires from a PEDOT (**5**) solution,²⁸³ electrochemistry has also been combined to dip-pen nanolithography to polymerize EDOT monomer ink at the substrate.²⁷⁶ Because a negative bias was applied between the tip and substrate, oxidative polymerization of EDOT occurred resulting in nanowires with width as small as 30 nm.²⁷⁶

Polydiacetylene (PDA) (**15i**) nanowires with widths of $d \approx 6\text{ nm}$ have been synthesized by chain polymerization of a monolayer of 10,12-nonacosadiynoic acid on a graphite surface.²⁷⁴ The polymerization was locally initiated by a pulsed electrical bias on a tip of a scanning tunneling microscope (STM). The reaction propagated along the direction defined by self-assembly of the monomers until the nanowire met a defect of the monolayer where termination occurred. Such a defect was also created by the tip of a STM with an opposite electrical bias.

2.3.3. Nanoimprinting and Soft Lithography. Nanoimprinting and soft lithography are often considered to be the most promising methods that may replace conventional

photolithography by virtue of the combination of high-resolution, cost-effectiveness, high-throughput, and a capability of large area patterning.^{256,259} Design of nanopatterns are transferred from a master (mold) to a substrate. Nanoimprint lithography, microtransfer molding, micromolding in capillary, and lithographically controlled wetting have been studied as means of preparing nanowires and nanopatterns of organic semiconductors (Figure 13). Feature sizes are mainly governed by the size of the masters. The reported typical widths (d) of nanowires and nanopatterns of organic semiconductors are on the order of $d \approx 100\text{ nm--}1\text{ }\mu\text{m}$, although feature sizes as small as $\sim 10\text{ nm}$ have been demonstrated in general soft lithography.^{256,259}

Nanoimprinting lithography (NIL), also called embossing, is the most widely investigated method among soft lithographic approaches (Figure 13A). It uses a rigid mold at high temperature ($120\text{--}250\text{ }^\circ\text{C}$; $\sim 10\text{--}20\text{ }^\circ\text{C}$ above the glass-transition temperature) and pressure ($5\text{--}140\text{ bar}$) to transfer features of the mold onto the pressed materials. Nanostructures of organic semiconductors, such as Alq₃ (**24**),²⁸⁴ MDMOPPV (**3e**),²⁸⁵ PFO (**6a**),²⁶⁴ F8BT (**6c**),²⁶³ and P3HT (**4f**)^{262,286,287} and other polythiophene derivatives (PQT12 (**12**)²⁶⁴ and TDPTD (**25a**)²⁸⁸) have been directly created by NIL. One of the major applications of such embossed organic nanostructures is in nanophotonics, given that the periodicity

is on the order of 100 nm.^{284,285} Molecular orientation of polymer semiconductor chains under confined nanostructures^{262–264} and the effects of nanopatterns on the device performance^{263,264,286–288} have been studied. Liquid crystalline π -conjugated polymers such as PFO (**6a**) and F8BT (**6c**) tend to have their backbones (*c*-axis) aligned along the grooves of the master mold, resulting in anisotropy of absorption and emission as well as charge transport.^{263,264} Another liquid crystalline polymer, PQT12 (**12**), was observed to have the π -stacking direction (*b*-axis) along the trenches.²⁶⁴ Arrays of well-isolated nanowires of PFO (**6a**) and PQT12 (**12**) with widths of 80–800 nm, heights of \sim 100 nm, and lengths of \sim 100 μ m have been produced from the precisely controlled thickness of polymer thin films and the dimensions of patterns in a mold.²⁶⁴ In this study, the absorption and emission of PFO (**6a**) nanowires showed anisotropy factors of 0.65 in excitation and 0.70 in emission.²⁶⁴ Field-effect charge-carrier mobility in the arrays of PQT12 (**12**) nanowires was 1.7 times larger than in the homogeneous thin films.²⁶⁴ However, when the PQT12 (**12**) nanowires were aligned parallel to the OFET source/drain electrodes no electrical conduction was observed, suggesting that the nanowires were isolated.²⁶⁴ Nanolithographically patterned PMMA has been used as a resist for the synthesis of high density PPy (**2**) and PANI (**1**) nanowires.²⁸⁹

The necessity of applying a high temperature for nanoimprinting may limit the versatility of the method for nanopatterning of organic semiconductors. Therefore, a room-temperature nanoimprinting version has been developed for the fabrication of 1D and 2D nanopatterns by applying a high pressure (\sim 100–2900 bar) without heating.^{230,290} Thin films of fluorescent conjugated polymers such as PFO derivatives (**6c,e,f**) and PPV derivatives (**3b,f**) have been successfully patterned by room-temperature NIL, forming photonic nanostructures such as distributed feedback lasers with a periodicity of 200–600 nm.^{290–292} In combination with electrospinning, room-temperature NIL has been used for printing nanograting patterns on a single electrospun nanofiber of various polymer semiconductors (Figure 13B).^{230,245} Electrospun nanofibers with diameters of \sim 100 nm–10 μ m were used for the study of effects of photonic nanostructures on waveguiding in fluorescent polymer nanofibers.^{230,245} From nanograting features that are parallel to the axis of the nanofiber, enhancement of polarization ratios of 2.4 was observed compared to the nanofiber without nanopatterns.²⁴⁵ Assistance of solvent, which swells and softens a polymer film, may offer an alternative route to embossing and eliminate the necessity of a high temperature. Well-isolated nanowires of PPy (**2**) have been imprinted at room temperature with the presence of residual solvent in the original film.²⁶⁴

Nanoimprinting can be modified and combined with microtransfer molding if required. After pressing a drop of polymer solution by a PDMS elastomeric stamp and drying, nanograting patterns on the polymer film can be made.^{293,294} A dried polymer thin film may be pressed by

PDMS at elevated temperature instead of a solution.²⁹⁴ From MEHPPV (**3b**) films with grating periodicities of 370 and 405 nm, distributed feedback lasers were fabricated.²⁹³ 1D and 2D structures with a periodicity of 278 nm have been patterned in polythiophene derivatives (POWT (**4m**) and POMEPT (**4q**)).²⁹⁴ In another study, nanoimprinting of a rigid mold was used to transfer nanopatterns onto a polymer semiconductor.²⁹⁵ Although the width of wires of the semiconducting polymer were in the micrometer scale, it is noteworthy that removal of residual layers between the wires was demonstrated.²⁹⁵ A polymer thin film was imprinted by a mold with nanopatterns, and then transferred to a mold. The mold filled with the polymer was treated with heat or solvent to remove the residual polymer on the protrusion of the mold patterns. In such a way, polymer nanowires that filled in the mold patterns were isolated from each other. The polymer nanowires were finally transferred from the mold to a substrate. This method has been applied to make nanopatterns of MEHPPV (**3b**) and P3HT (**4f**) with a periodicity of \sim 10 μ m and PMMA with a periodicity of 700 nm.²⁹⁵ Solvent-assisted microtransfer molding has been demonstrated to make nanopatterns of organic semiconductors.²⁹⁶ Patterned surface of a mold was covered with Alq₃ (**24**) solution, and then placed on a substrate. After drying the solvent, the mold was peeled away, resulting in linear features with a width of \sim 400 nm.²⁹⁶

Micromolding in capillary (MIMIC) has been commonly used for fabricating nanowires on a substrate (Figure 13C). Here, a solution of an organic semiconductor moves into the capillary formed by an elastomeric mold and a substrate. Nanowires of doped PANI (**1**),^{297,298} PEDOT (**5**),²⁹⁴ and water-soluble polythiophene derivative (POWT) (**4m**)²⁹⁴ have been produced by this method. Minimum widths of the nanowires were \sim 200–350 nm. OFETs consisting of P3HT (**4f**) thin film as a semiconductor and the doped PANI (**1**) nanowires as electrodes have been reported.²⁹⁷ In another study, nanowires of PANI (**1**) with a height of \sim 70–85 nm and a width of \sim 200–250 nm were produced.²⁹⁸

Lithographically controlled wetting (LCW) is an interesting nanofabrication strategy that utilizes the wetting of a solution in a narrow gap between a substrate and a stamp to create 1D nanostructures (Figure 13D).^{261,299} Nanowires of amorphous Alq₃ (**24**)²⁹⁹ and crystalline thiophene-fluorene oligomer (F-T3-F) (**26**)²⁶¹ have been prepared by this method. Dimensions of the nanowires are controlled by the concentration of the solution and the size of the gap.²⁹⁹ Nanowires with widths of 75–450 nm and heights of 5–60 nm were produced. Exploiting the spontaneous introduction of the semiconductor solution in MIMIC, OFETs based on such F-T3-F (**26**) nanowires have been demonstrated.²⁶¹

2.3.4. Other Nanolithographic Techniques. Edge lithography is an unconventional technique that utilize skiving of multilayer structures (Figure 14).³⁰⁰ Constituent materials have orthogonal solubility in solvents, i.e., mutually exclusive solubility in the same solvents, so that

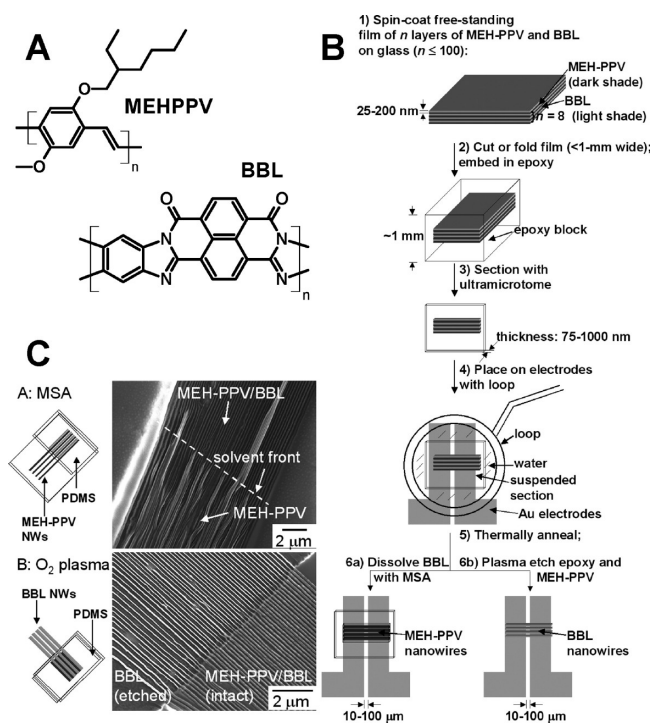


Figure 14. Edge lithography: (A) Chemical structures of MEHPPV (**3b**) and BBL (**27**). (B) Illustration of the procedure of edge lithography. (C) SEM images of produced nanowires of MEHPPV (**3b**) and BBL (**27**) after etching. Reprinted with permission from ref 300. Copyright 2008 American Chemical Society.

multilayered thin films (~25–200 nm) are formed by sequential spin-coating on top of each other. After embedding the stacks of thin films into epoxy block, the block is sectioned to have a thickness of ~75 nm–1 μm. By a selective etching process for one of the constituent materials, a set of a few hundred nanowires can be obtained. The removal of sacrificial layers can be done by wet chemistry or dry etching. Such an edge lithography has been used to produce nanowires of MEHPPV (**3b**) and BBL (**27**) as shown in Figure 14C.³⁰⁰ The sectioned stack of MEHPPV (**3b**)/BBL (**27**) bilayer thin films, before selective etching, has been used to make solar cells with laterally ordered nanostructures, although the performance was very poor (~0.02% PCE).³⁰¹

Holographic nanopatterning is another method for fabricating periodic nanopatterns.³⁰² A thin film of PPV (**3a**) was deposited from a precursor polymer followed by thermal conversion. On top of the PPV (**3a**) thin film a layer of photoresist was spin-coated. Nanograting patterns or an array of pillars were copied to a photoresist by interference of laser light. By using reactive ion etching, stripes and pillars of PPV (**3a**) were formed on a substrate. The periodicity of 1D and 2D nanostructures of PPV (**3a**) were ~200–250 nm.³⁰² Although the requirement of orthogonal solubility of the constituent materials of a bilayer is a limitation of both edge lithography and holographic nanopatterning; however, there are numerous π -conjugated polymer pairs^{303,304} and oligomer/polymer pairs³⁰⁵ that already meet this requirement in the context of solution-processed multilayer OLEDs. Depending on the intended application, such existing pairs of organic

semiconductors^{303–305} could be good candidates for the creation of nanowires and 1D nanopatterns using edge lithography and holographic nanopatterning.

2.4. Solution-Phase Self-Assembly. Self-assembly involves the spontaneous formation of ordered discrete aggregates or higher-order structures via the noncovalent interactions of molecular components.^{61,306} The various intermolecular interactions or forces that can contribute to and direct the self-assembly process include:^{58–62,306,307} π – π stacking; dipole–dipole; hydrophobic; van der Waals; electrostatic; hydrogen bonding; and ion–dipole. Well-defined aggregates of all dimensionalities (0D, 1D, 2D, and 3D) can be realized by self-assembly, depending on the molecular building blocks, the noncovalent interactions designed into them, and the medium or environment for the assembly process.^{58–62,306,307} The basic principles of supramolecular self-assembly are well established in supramolecular chemistry and are increasingly applied in the design and construction of nanostructures.^{58–62,306–310}

Self-assembly is potentially the ultimate and most powerful strategy for organizing π -conjugated molecular building blocks into 1D functional nanostructures and nanodevices. Because of their generally planar molecular framework and highly delocalized π -systems, intermolecular interactions among most π -conjugated small molecules, oligomers, or polymers in solution are dominated by π – π stacking while hydrophobic and other forces are substantially weaker. Such a large anisotropy in noncovalent intermolecular interactions leads to preferential self-assembly or aggregation in 1D.^{306,308} Asymmetric design of the molecular architecture, as in surfactants and block copolymers,^{311,312} can give rise to amphiphilicity that provides an additional way to control the competing intermolecular interactions and thus the self-assembly process. Among the many advantages of self-assembly as a route to 1D crystalline organic nanostructures are: (i) the methodology is simple in concept and implementation, requiring minimum equipment (beaker, solvents, heater); (ii) it is a facile bulk synthesis of large quantities of the nanostructure; (iii) it is easy to control and vary the nanoscale morphology by means of the assembly conditions (concentration, solvent/nonsolvent, temperature); (iv) it readily allows for assembly of multi-component nanostructures and hybrid nanocomposites with a variety of other building block materials (inorganic, biomolecular); and (v) the degree of reproducibility is very high. Studies of the self-assembly of 1D functional nanostructures from π -conjugated organic semiconductors in the past decade have documented its promise and versatility among diverse types of π -conjugated molecular architectures. Several previous articles have reviewed the supramolecular self-assembly of organic semiconductor nanostructures.^{307–310} In the following discussion, we first examine the self-assembly of crystalline 1D nanostructures in bulk solution, then at solvent/solvent interfaces, and last at surfaces.

2.4.1. Self-Assembly in Bulk Solution. Self-assembly that takes place in bulk solution commonly utilizes the

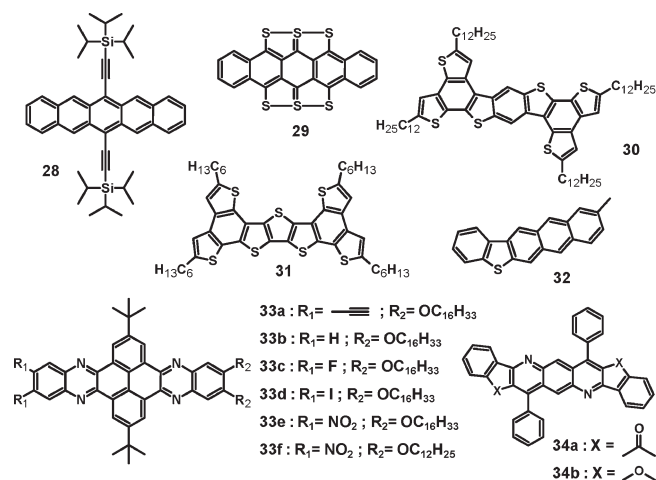
difference in solubility of the molecular building block in different environments, such as solution temperature, the solvent, or a mixture of solvents. Organic semiconductors that have limited solubility but are more soluble at elevated temperature in a certain solvent can crystallize into 1D nanocrystals upon cooling. The unique anisotropic interactions, such as π - π stacking and steric hindrance with assistance of hydrophilic/hydrophobic interactions, can allow the nanocrystals to grow into large aspect-ratio 1D nanostructures. If there is a solubility difference of an organic semiconductor in two solvents, nucleation and crystal growth of the organic semiconductor can take place when transferred from one solvent to another in this case.

2.4.1a. π -Conjugated Small Molecules and Oligomers. Planar π -conjugated small molecules and oligomers^{50,52} represent a class of organic semiconductor materials that are especially ideal for producing nanowires by π -stacking-driven assembly in solution. Nanowires and microwires of oligoacene derivatives and heteroaromatic oligomers have been produced by solution-phase self-assembly.^{313–349} Triisopropylsilyl ethynyl pentacene (TIPS-PEN) (**28**) microribbons, for example, were prepared by the solvent-exchange method, which transfers the molecule from a good solvent into a poor solvent in solution phase.³¹³ The single-crystalline microribbons were found to have typical dimensions of 4–13 μm in width, 100–600 nm in height, and 40–800 μm in length. In another example, hexathiapentacene (HTP) (**29**) self-organized into single-crystal nanowires upon cooling from a hot benzonitrile solution to room temperature.^{314,315} The HTP (**29**) nanowires precipitated from the solution and floated in the solution like a bundle of cotton. The length of wires ranges from about 50 μm to hundreds of micrometers and the height falls into 70–470 nm, whereas the width can be tuned from ~ 1 to ~ 150 μm by addition of methanol during the cooling process.³¹⁴ It was shown that the nanowires grow in the [100] direction, initiated by strong π - π interactions with a measured stacking distance of 0.38 nm.³¹⁴

Besides the pentacene-based π -systems, nanowires of thiophene-acene-based oligomers (**30,31,32**)^{316–319} and imine-nitrogen-containing bisphenazines (**33a–f**)^{320,321} have also been produced from solution phase and investigated (see Chart 9). Crystalline nanowires and microwires were produced from benzothiophenes (**30,31,32**) rich in sulfur atoms, following the procedure of cooling a hot solution in a poor solvent or the precipitation by solvent-exchange.^{316–319} The extended π -system of these molecules favored strong π - π interaction, resulting in bulk quantity of crystalline nanowires.^{316–319} These oligomer nanowires were 200 nm–8 μm in width and 30–100 μm in length depending on the chemical structure and crystallization process. Bisphenazine (**33a–f**) nanowires synthesized by recrystallization had widths of 15 nm to several μm depending on the functional groups and synthesis conditions.^{320,321}

Electron-transporting (n-type) conjugated molecules based on ladder-type bisindenoanthrazolines (**34a,b**)

Chart 9. Chemical Structures of 28–34



were shown to readily self-assemble into single-crystal nanowires from a solution-phase route.³²² The molecular structure of bisindenoanthrazolines (**34a**) is exemplified by DADK (**34a**) in Figure 15A. Single-crystal X-ray diffraction showed that the heptacyclic π -framework is planar and leads to a slipped face-to-face π -stacking with short intermolecular distances of 3.4 Å (Figure 15B).³²² This optimum molecular packing enables the facile solution-phase self-assembly of nanowires. SEM images show that DADK (**34a**) NWs have widths of 200–250 nm and lengths of several hundred micrometers (Figure 15C). Figure 15D shows the TEM image of a DADK (**34a**) nanowire and the corresponding electron diffraction (inset) which demonstrated that the nanowires are single-crystalline. Electron mobility in evaporated thin films of DADK (**34a**) was as high as $3.84 \times 10^{-4} \text{ cm}^2/(\text{V s})$ as measured by the SCLC method under ambient air conditions.³²²

The solution-phase assembly of nanowires and nanoribbons of perylene tetracarboxylic diimides (PTCDIs) (**35a–j,l–o**) (see Chart 10) has been extensively investigated.^{323–334} PTCDI (**35a–j,l–o**) nanowires and nanobelts were produced by rapid mixing of a solution in a good solvent (e.g., chloroform) into a poor solvent (e.g., methanol) thereby inducing the aggregation of the molecules into 1D nanostructures.^{325,327,328} These crystalline PTCDI (**35a–j,l–o**) nanobelts self-assembled via strong π - π interactions with widths ranging from 80 nm to 1.5 μm , depending on the solubilizing chains on imide-nitrogens and the processing conditions.^{325–329,334} An asymmetric PTCDI (**35j**) was employed to grow ultralong nanobelts ($L > 0.3 \text{ mm}$, $d = 1\text{--}2 \mu\text{m}$) through seeded self-assembly.³³⁰ The hydrophilic polyoxyethylene side-chains facilitated the tuning of solubility of this PTCDI (**35j**) molecule in water/ethanol mixture. An increase in the water fraction increased the solvent polarity and forced the solvophobic association between the alkyl side-chains.

Single-crystalline nanoribbons and nanorods of 9,10-diphenylanthracene (DPA) (**36b**) have been assembled in solution in the presence of a surfactant, CTAB.³³⁵

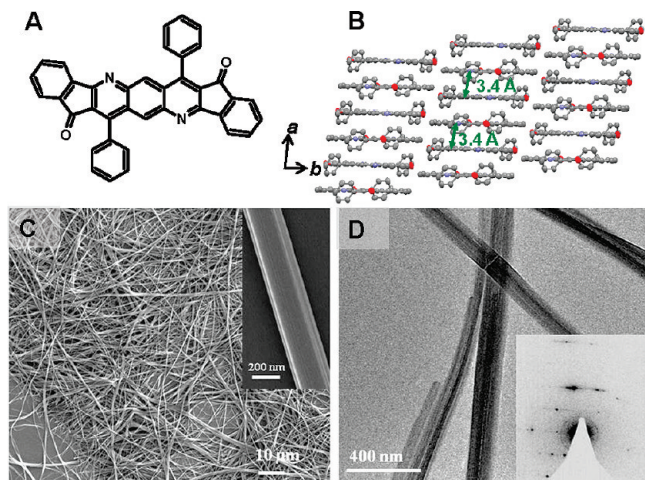
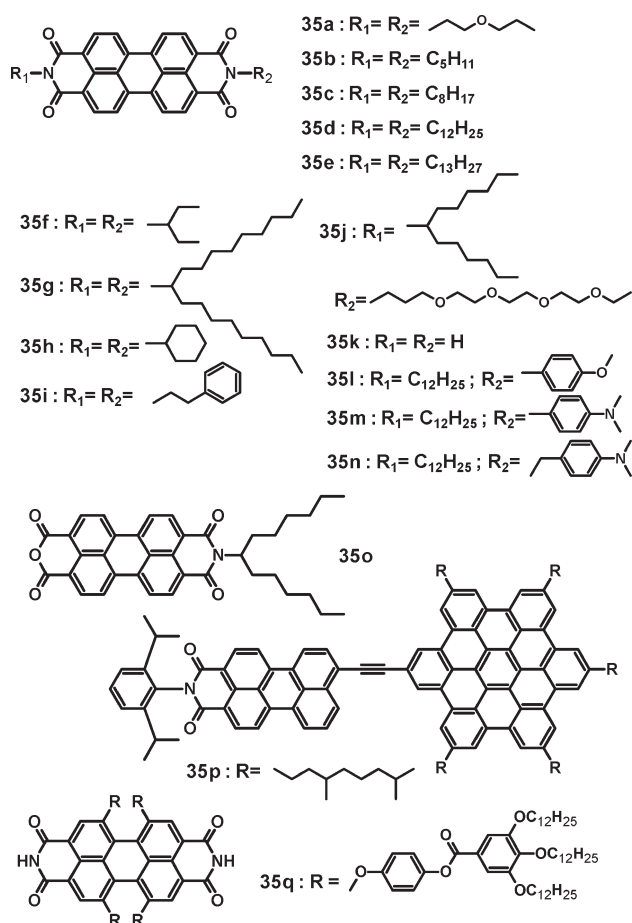


Figure 15. (A) Molecular structure of DADK (**34a**). (B) Molecular packing of DADK (**34a**) illustrating π -stacking direction, view down the c -axis. (C) SEM image of DADK (**34a**) nanowires. (D) TEM image of DADK (**34a**) nanowires with corresponding electron diffraction (inset). Reprinted with permission from ref 322. Copyright 2010 American Chemical Society.

Chart 10. Chemical Structures of 35



Nanostructures of various shapes were produced by varying the concentration of DPA (**36b**) in solution with the surfactant. Only nanoribbons were produced in the absence of the surfactant and regardless of the DPA (**36b**) concentration in the solution.³³⁵ The dimensions of the nanoribbons and nanorods were $d = 500 \text{ nm} - 5 \mu\text{m}$,

$t = 20 - 80 \text{ nm}$, and $L = 5 - 20 \mu\text{m}$, depending on the assembly conditions.

Functionalized oligophenylenevinyls (**37a-f**)³³⁶⁻³³⁸ and oligothiophenevinyls (**38a-e**)³³⁹ tend to self-assemble into 1D nanostructures (see Chart 11). Because of the strong π - π interactions and hydrogen bonding in the oligomers, organogels that undergo thermoreversible gelation can form in solution. Entangled nanowires and nanobelts with widths of 20–200 nm and heights of 10–20 nm were observed from a dried gel of oligophenylenevinyls (**37a-f**) in nonpolar hydrocarbon solvents, such as hexane, decane, dodecane, cyclohexane, benzene, and toluene, as imaged by SEM, TEM, and AFM.³³⁶⁻³³⁸ Nanobelts of oligothiophenevinyls (**38a-e**) showed widths of 50–200 nm, heights of 4–15 nm, and lengths of 500 nm–5 μm .³³⁹

Oligophenylene-based π -conjugated molecules of various rigid-flexible molecular architectures (**39a-i**), including dumbbell-shaped, T-shaped, H-shaped, and other shapes, self-assemble into nanowires and networks of nanowires in aqueous solutions^{340,350-352} and in organic solutions.³⁵³ The width of an individual nanowire revealed by TEM was about 5–16 nm.^{340,350-353} Similarly, asymmetrically functionalized oligophenylenevinyls (**40a,b**), that can form dimers or multimers, have been shown to self-assemble into helical nanowires.^{336,341-345} The rod segments of the assembly stack on top of each other with mutual rotation to avoid steric hindrance of the bulky end groups.^{336,340-343} Additional details on the self-assembly of various molecules containing π -conjugated aromatic rod blocks can be found in prior reviews.^{307,336,354}

Arylene ethynylene macrocycles (**41a,b**) (see Chart 12) were used to demonstrate the sol-gel processing in fabricating nanowires.^{346,347} It was shown that certain solvents (like cyclohexane) can induce gelation of the macrocycle (**41a**), resulting in a high degree of supramolecular organization driven by π - π stacking.³⁴⁶ The cross section size of a single nanowire is about 4–5 nm, corresponding to the size of two laterally assembled, fully side chain-interdigitated molecules.³⁴⁶ In another example, a dye molecule, 3-ethyl-2-[(3-ethyl-2(3H)-benzothiazolylidene)-methyl]benzothiazolium iodide (thiacyanine, TC) (**42**), was self-assembled into nanowires from an aqueous solution.³⁴⁸ The length of nanowires was controllable from submicrometers to $\sim 300 \mu\text{m}$ by varying the growth time. These nanowires were demonstrated as optical waveguides.³⁴⁸ Nano- and microwires of pyrazino[2,3-g]quinoxalines (PyQs) (**43a-e**) have been produced by diffusion of ethanol vapor into toluene solutions and also studied as waveguides.³⁴⁹

Porphyrins (**44a-c**) represent another class of π -conjugated small molecules that have been shown to form 1D nanostructures. Diacid form of tetrakis(4-sulfonatophenyl)porphyrin (TPPS) (**44a**) in an acidic solution (pH 0.9–1) self-assembled into nanowires with heights of $\sim 3.8 - 4.5 \text{ nm}$ and bundles with diameters up to 40 nm.³⁵⁶⁻³⁵⁸ A mixture of two porphyrin derivatives (**44a,b**) were shown to self-assemble into well-defined nanotubes in an acidic solution (pH 2), as shown in Figure 16.^{355,359}

Chart 11. Chemical Structures of 36–40

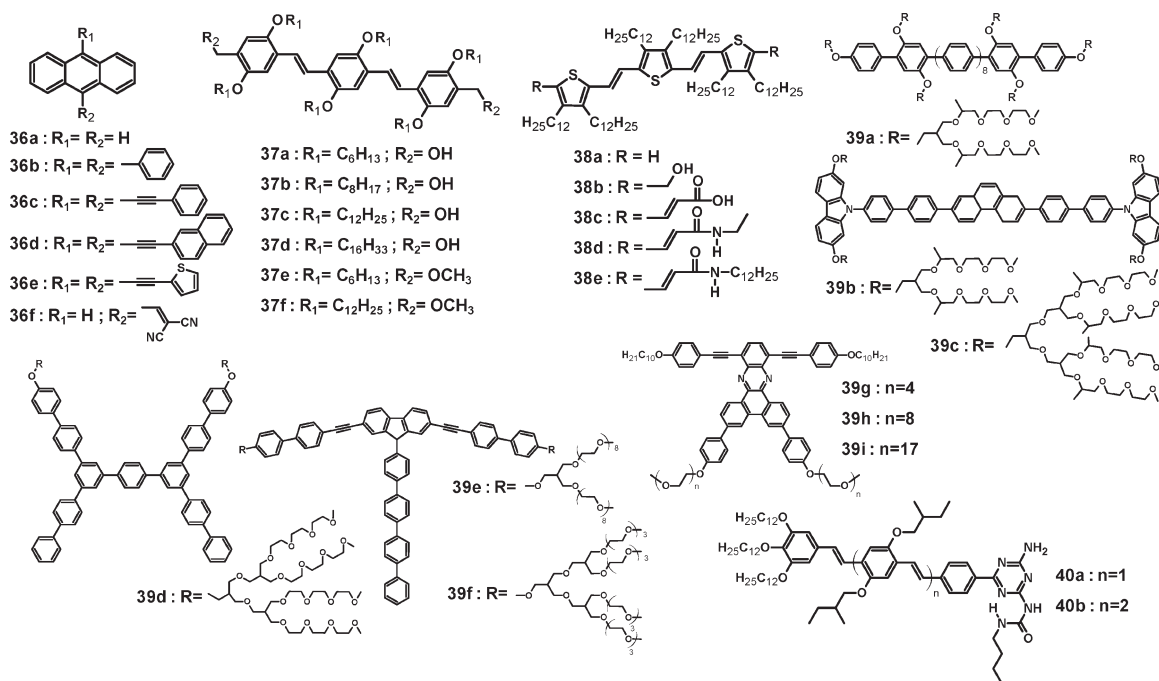


Chart 12. Chemical Structures of 41–44

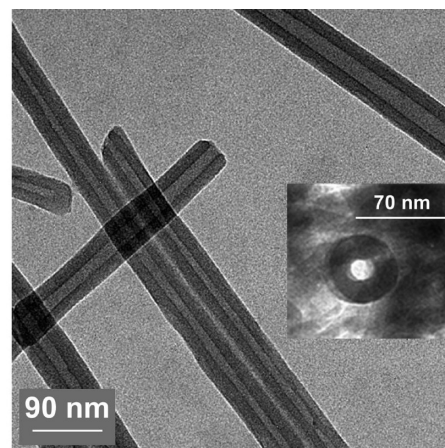
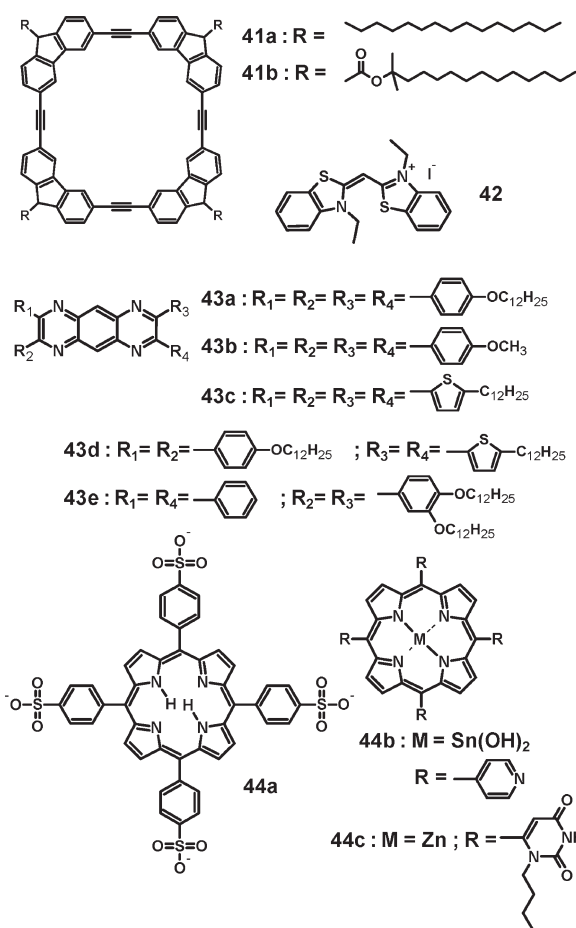


Figure 16. TEM image of porphyrin (**44a,b**) nanotubes produced by ionic self-assembly. Inset shows a nanotube trapped in vertical direction. Reprinted with permission from ref 355. Copyright 2004 American Chemical Society.

By ionic self-assembly, nanotubes of 50–70 nm in outer diameter with 20 nm thick wall were obtained.³⁵⁵ Nanowires of 5,10,15,20-tetrakis(1-butyl-6-uracil)porphyrinato

zinc(II) (**44c**) were reported to have diameters of 2–50 nm.³⁶⁰

2.4.1b. π -Conjugated Polymers. Although the self-assembly of 1D nanostructures of well-defined dimensions from π -conjugated polymers would seem to be a difficult proposition in view of their large molar mass, polydispersity of their molecular weight, extremely rigid backbones, and potentially disordering flexible side chains, however, it turns out that nanowires with large aspect ratios and well-controlled lateral dimensions (d , t) can readily self-assemble from solutions of various π -conjugated polymers. The most extensive interest in the growth of crystalline nanowires from π -conjugated polymers has been focused on the regioregular poly-(3-alkylthiophene)s (P3AT)s (**4b–k**) due to their great promise as p-type semiconductors for solution-processable,

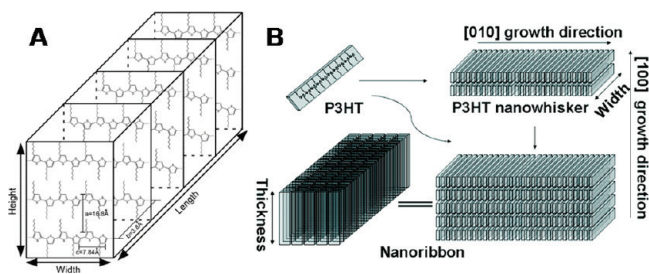


Figure 17. (A) Molecular packing of poly(3-hexylthiophene) nanowires. Reprinted with permission from ref 379 Copyright 2004 American Chemical Society. (B) Schematic illustration of the formation of P3HT nanoribbons. Reprinted with permission from ref 380. Copyright 2009 American Chemical Society.

low-cost organic field-effect transistors (OFETs)^{34,361–364} and solar cells.^{39–41} Enormous research efforts have been put to understanding the molecular packing, crystallization, charge transport, and photovoltaic properties of thin films of P3ATs (**4b–k**), especially poly(3-hexylthiophene) (P3HT) (**4f**), which was once a leading high-mobility p-channel material in polymer-based OFETs^{363,365,366} and solar cells.^{367,368}

Nanowires of P3ATs (**4c,d,f,h,k**) were first reported to self-assemble from dilute solutions in poor solvents in 1993.³⁶⁹ Typically, a dilute P3AT (**4c,d,f,h,k**) solution (0.05–1%) is prepared in a poor solvent (such as cyclohexanone and n-decane) at elevated temperatures (50–90 °C) and allowed to cool slowly to room temperature, inducing the assembly of the polymer chains into nanowires. This method of growing nanowires is sometimes called the whisker method. It was found that the width (*d*) of these P3AT (**4c,d,f,h,k**) nanowires was ~15 nm, and it was independent of the alkyl-side chain length, whereas the thickness (*t*) scaled with the side-chain length as revealed by transmission electron microscopy (TEM).³⁶⁹

Investigation of the morphology of P3AT (**4b–k**) nanowires showed that they were highly crystalline as evidenced by electron diffraction^{369–371} and X-ray diffraction.^{366,369–374} The crystalline structure of P3AT (**4b–k**) nanowires is found to be of Type I (with the exception of poly(3-heptylthiophene) (**4g**)),^{369,370,374} which is the commonly observed bulk crystal structure of P3ATs (**4b–k**) crystallized from solution.^{369,370,374–376} In Type I crystal structure, the unit cell is orthorhombic as shown in Figure 17A for a P3HT nanowire (**4f**) (*a* = 1.68 nm, *b* = 0.38 nm, *c* = 0.784 nm).^{370,374,377–379} Electron diffraction showed that the backbones of P3ATs (**4b–k**) are oriented perpendicular to long axis of the nanowires (*b*-axis), forming a lamellar structure driven by the efficient π – π stacking between thiophene rings, corresponding to a (020) spacing of 0.38 nm.³⁶⁹ XRD investigation shows crystalline diffraction patterns, and the weakened amorphous halo diffraction around 20° compared with solution-cast P3ATs (**4b–k**) films indicated high crystallinity within the nanowires.³⁷⁰ Both small-angle and wide-angle XRD showed that the [200] direction normal to the [020] direction laid parallel to the substrate, and a long period of 3–7 nm was observed in the [200] direction (*a*-axis), which corresponded to 2–4 times the lattice dimension of

P3HT (**4f**) (*a*/2 = 1.74 nm).^{369,374,378} This value also represents the thickness of nanowires, and confirmed the thickness (~5 nm) estimated from the TEM images of the shadowed samples.³⁶⁹ Taking into account the contour length of P3HT (**4f**) (~65 nm, calculated from the number-average molecular weight (*M_n*)) and the width of the nanowires (~15 nm, corresponding to ~40 thiophene units),³⁷⁸ it becomes clear that the polymer chains must fold in the (200) plane to accommodate the molecular packing within the nanowire. These nanowires were reported to have lengths exceeding 10 μm, with aspect ratios (*L/d*) larger than 670. Overall, the nanowire formation can be attributed to the quasi-one-dimensional crystallization of P3ATs (**4b–k**) induced by both an attractive π – π^* interaction between polymer backbones and the crystallization of alkyl side chains.³⁷⁴

In the case of poly(3-heptylthiophene) (**4g**) nanowires, a crystal structure that slightly deviated from Type I was observed. Briefly, the lattice constant *a* contracts but *b* expands; however, these slight deviations from Type I are not significant enough to be distinguished from Type I in XRD. Type II crystal structure, which resembles the structure of Type I but has a 30% reduction in the *a*-axis dimension because of side-chain interdigitation,^{376,381} while the lattice constant *b* is increased.³⁷⁶ Therefore, the crystal structure for poly(3-heptylthiophene) (**4g**) nanowires was referred as Type I'.³⁷⁴ Further investigation revealed that the Type I' nanowires could be converted to Type I nanowires in the solid state at 70 °C and in solution at 50 °C.³⁷⁴

The morphology of P3AT (**4b–k**) nanowires has been reported to depend on factors such as length of alkyl side-chains,^{369,370,382} regioregularity,³⁸² molecular weight (including polydispersity),^{374,380} polymer concentration in solution,^{380,382,383} crystallization temperature,^{380,384} solvent quality,³⁸² and cooling rate.³⁸² In a given solvent, because the solubility of P3ATs (**4b–k**) increases with the side-chain length, P3ATs (**4b–k**) with relatively shorter side-chain length form nanowires more easily than those with longer side-chain length.³⁶⁹ It is also reported that the alkyl side-chains enhance the crystallinity of nanofibers, as evidenced from the increasing domains (crystallite) of the (100) and (020) peaks with increasing side-chain length as characterized from XRD.³⁷⁴ Similar study of crystalline nanowires based on TEM, AFM, XRD, and UV–vis suggested significant improvement in order when the alkyl side-chain length increased from poly(3-propylthiophene) (**4c**) to poly(3-pentylthiophene) (**4e**), but only marginal improvement in going from poly(3-pentylthiophene) (**4e**) to poly(3-nonylthiophene) (**4i**).³⁷⁰

The regioregularity of P3ATs (**4b–k**) is considered critical for the growth of nanowires, because the assembly of nanowires in solution is influenced by the partial crystallization of side-chains; regiorandom P3ATs (**4b–k**) do not form nanowires under the same condition as that of regioregular P3ATs (**4b–k**).³⁸²

The molecular weight (*M_n*) of conjugated polymers has a significant impact on the assembly of nanowires. Polymer backbones with 60–70 monomer units are

considered the threshold for nanowire formation in the case of P3ATs (**4b–k**). It was observed that due to the lower saturation concentration, P3AT (**4b–k**) with a high M_n forms nanowires more rapidly.³⁷⁴ Molecular weight also affects the dimensions of the nanowires, especially the width. An investigation of the morphology of P3HT (**4f**) nanowires assembled from known M_n and contour length of polymer chains suggested that there is a M_n -dependent chain folding during crystallization.^{385,386} The width (d) of P3HT (**4f**) nanowires equals the polymer contour length for P3HT (**4f**) with GPC-determined M_n less than 10 kDa, but remained constant ($d \sim 15$ nm) for P3HT (**4f**) with M_n higher than 10 kDa.³⁸⁰ The M_n -independent nanowire width above the critical M_n is made possible by the ability of P3AT (**4b–k**) chains to form U-turn type folding, when several thiophene units adopt a continuous *cis* conformation with alkyl side-chains pointing outward.^{384,387,388}

The polymer concentration in solution also influences the assembly of nanowires. For example, P3HT (**4f**) nanowires can only form from *p*-xylene at concentrations higher than 0.05 wt %, which is attributed to the need to exceed a minimum strength of intermolecular interaction between P3HT (**4f**) chains.³⁷⁴ Interestingly, for P3HTs (**4f**) with less than critical M_n , increased polymer concentration (0.2–0.5 mg/mL) changes the 1D nanowires into 2D thin films.³⁸⁰ The molecular packing in P3HT (**4f**) nanoribbons and the formation of the nanoribbons are shown in Figure 17B. In contrast, P3HT (**4f**) with higher than critical M_n only forms nanowire aggregates instead of nanoribbons, which is explained in terms of the poorly defined surfaces similar to crystal defects that prohibit further growth. A concentration higher than 1.5 mg/mL results in gelation regardless of M_n , and the gels are composed of nanowires and nanoribbons for the respective M_n ranges. The concentration dependence of nanowire morphology was also reported for P3PT (**4e**).³⁸³ It was found that P3PT (**4e**) nanowires prepared from 6 mg/mL 1,2-dichlorobenzene solution had the largest aspect ratios and higher flexibility, compared with those made from higher concentrations.

According to traditional crystallization theory, the morphology of nanowires can be affected by the crystallization temperature (T_c), because a higher T_c leads to longer folding length in lamellar crystals, resulting in increased width.³⁸⁰ For P3HT (**4f**) nanowires, the average width increased from 12.0 to 17.0 nm when the crystallization temperature was increased from 0 to 35 °C, for 33.5 kDa (M_n) P3HT (**4f**); when a 15.6 kDa P3HT (**4f**) is used, the trend persists but the width increased more rapidly with temperature, which is attributed to a lower dissolution temperature. Thus, the crystallization temperature may represent a way to control the dimension of P3AT (**4b–k**) nanowires.³⁸⁰

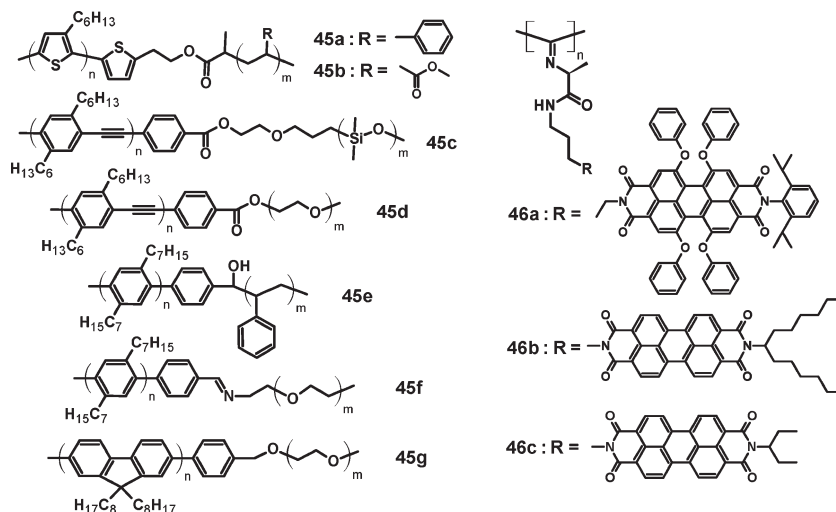
The thermodynamic quality of a solvent plays an important role in the self-assembly of π -conjugated polymer nanowires and their morphology. Taking P3HT (**4f**) as an example, chloroform and chlorobenzene are good solvents, whereas *p*-xylene and cyclohexanone are poor

solvents.^{369,389} If a polymer can only dissolve in a solvent at an elevated temperature, the solvent is a marginal one (for example, anisole for high M_n P3HT (**4f**)).³⁸⁰ One semiquantitative way to select a good solvent for a given polymer is via the Hildebrand solubility parameter δ ,^{370,374,390–392} a given polymer with solubility parameter (δ_p) is likely to be dissolved in a solvent with a similar solubility parameters (δ_s), i.e., $\delta_p - \delta_s \leq 1 \text{ cal}^{1/2} \text{ cm}^{3/2}$. The solubility parameter of a polymer can be calculated, or measured using solvent–nonsolvent titration, inverse gas chromatography, and so on.³⁹⁰ Another method to direct the nanowire growth is proposed based on the solvent refractive index n_D , which appears to work well for aliphatic hydrocarbon and (chlorinated) aromatic hydrocarbon solvents.³⁷⁰ The quality of solvent also affects the morphology of nanowires. A comparison of P3HT (**4f**) nanowires made from cyclohexanone and *p*-xylene reveals that although the nanowires have a similar thickness (3–8 nm), nanowires from *p*-xylene were relatively straight fibers that are well-isolated, whereas nanowires from cyclohexanone were rather curved and entangled at one end, forming large aggregated nanowire network.³⁸² This difference is attributed to the quality of solvent, because cyclohexanone is considered a poorer solvent than *p*-xylene for P3HT (**4f**). However, only entrapped solvent molecules in nanowires may also play a role on the morphology.^{382,393}

P3AT (**4b–k**) nanorods have been demonstrated by solvent-induced aggregation.³⁹⁴ These nanorods were prepared by addition of hexane (a good solvent for alkyl side-chains but poor solvent for polymer backbones) into P3AT (**4b–k**)/chloroform solution, and the self-assembly process is driven by solvophobic interaction. The nanorods adopt a helical conformation of the main chain with 12 thiophene rings per helical turn, and the morphology can be tuned by adjusting the solvent composition or concentration of P3AT (**4b–k**) in solution. Besides, P3HT (**4f**) nanowires were grown from a solvent mixture containing a dipolar solvent (acetonitrile) and a nonpolar good solvent (chlorobenzene), assisted by ultrasonication.³⁹⁵ It is believed that the formation of polymer aggregates was induced by the increasing polymer chain interactions as a more polar solvent was added. Ultrasonication was used to change the random aggregates into ordered nanowires having a width of 20–25 nm.

Block copolymers represent another class of polymer semiconductors that have the ability to self-assemble into nanowires from solution. Diblock and triblock copolymers composed of P3HT (**4f**), polystyrene and polymethylacrylate segments with different block compositions (**45a,b**) (see Chart 13) self-assembled into well-defined nanowires having widths of 30–40 nm and lengths of a few micrometer upon solvent evaporation.³⁹⁶ Further investigation of one of the diblock copolymers, polystyrene-*b*-polyhexylthiophene (PS-*b*-P3HT) (**45a**) using atomic force microscopy (AFM) revealed that the nanowires were composed of P3HT core and PS sheath.³⁹⁶ Other rod–coil diblock copolymers based on polyphenyleneethynylene, poly(*p*-phenylene), and polyfluorene blocks as the

Chart 13. Chemical Structures of 45–46



rigid-rod segments (**45c–g**) have also been found to form nanowires and nanofibers with widths of 8–60 nm, and molecular packing in the assemblies has been studied by computational modeling.^{397–399} Nanowires of block copoly(3-alkylthiophene)s composed of multiple sized side-chains, e.g. poly(3-butylthiophene)-*b*-poly(3-octylthiophene) (P3BT-*b*-P3OT) (**4r**),⁴⁰⁰ poly(3-butylthiophene)-*b*-poly(3-hexylthiophene) (P3BT-*b*-P3HT) (**4s**),⁴⁰¹ poly(3-hexylthiophene)-*b*-poly(3-cyclohexylthiophene) (P3HT-*b*-P3cHT) (**4t**),⁴⁰² have been self-assembled from solution phase. The formation of nanowires in the block copolymers was found to be both by π -stacking of the polythiophene backbones and the segregation of the blocks according to length of side-chains.⁴⁰⁰ These nanowires have widths in the range of 8–13 nm and lengths in the several micrometers range. Interestingly, the aspect ratio of nanowires,⁴⁰⁰ as well as the nanoscale morphology,⁴⁰² could be tuned by means of block composition. By adjusting the good/poor solvent ratio, nanowires and nanorings were obtained from P3BT-*b*-P3HT.⁴⁰¹ Amphiphilic rod-coil block copolymers containing a rodlike π -conjugated polymer block and a flexible coil block (e.g., polystyrene) in solution self-assembled into various ordered aggregates including fluorescent microtubes.^{403,404}

Poly(phenylene vinylene) (PPV) with crown ether substituents (C-PPV) (**3g**) has been reported to self-assemble into nanorods, and further to nanoribbons with 15 nm width, 3 nm thickness and micrometer-sized length, induced by K^+ complexation in a chloroform solution.^{405,406} It was proposed that the formation of a 2:1 sandwich complex between K^+ and the crown ether substituents enabled the closer interaction between two polymer chains, through creation of interpolymer bridges to form C-PPV (**3g**) aggregates in solution.⁴⁰⁷ In addition, aggregation is also promoted by the attractive π - π interactions among the aromatic rings. Nanorods with an average length of less than 100 nm formed in 30 min after the addition of K^+ ions. The counteranions (PF_6^-) diffuse and accumulate at the positively charged backbones, producing an electrostatic shield along the nanorods to

enable the anisotropic 1D growth, and the formation of more bridges between K^+ ions and nanorods leads to connection of nanorods at their ends to produce nanoribbons. The length of nanoribbons exceeded 400 nm over 20 days of growth.

Large quantities of nanobelts of BBL (**27**), an n-type polymer semiconductor, have been produced by solution-phase assembly.⁴⁰⁸ The solvent-dispersible nanobelts were produced by adding a solution of protonated BBL (**27**) dropwise into a rapidly stirring solvent mixture (chloroform and methanol, 4:1). The self-assembly process is mainly initiated by methanol which serves as a base to deprotonate the BBL (**27**) chains, while chloroform only serves as weakly interacting solvent to disperse the nanobelts. The BBL (**27**) nanobelts have a thickness of 10–50 nm, width of 200–1000 nm, and length in the range of 20 μm to over 150 μm . The molecular packing of BBL (**27**) chains in the nanobelts was found to be unlike traditional molecular packing in π -stacked P3AT (**4b–k**) nanowires.⁴⁰⁸ A schematic illustration of the structure and molecular packing in these nanobelts is shown in Figure 18, which indicates that BBL (**27**) polymer chains pack face-to-face perpendicular to the long axis (*c*-axis) of the nanobelts. The striking difference between BBL (**27**) and other polymer semiconductor nanowires is likely from the extraordinary strength of intermolecular interactions, which originate from the rigid and planar molecular backbone of BBL (**27**), as well as the large shear force caused by stirring of solution during the synthesis of BBL (**27**) nanowires.

Crystalline nanowires of a polydiacetylene, poly(1,6-di(N-carbazolyl)-2,4-hexadiyne (PDCHD) (**15j**), have been prepared by the reprecipitation method in the presence of an anionic surfactant, sodium dodecyl sulfate (SDS), at 25 and 60 °C. A solution of the diacetylene (DCHD) monomer in acetone was reprecipitated by injecting 200 μL of solution (5.0 mM) into 10 mL of water containing SDS at 25 or 60 °C. After UV-irradiation of the resulting DCHD monomer crystals, nanowires of PDCHD (**15j**) were obtained with a diameter of 50 nm

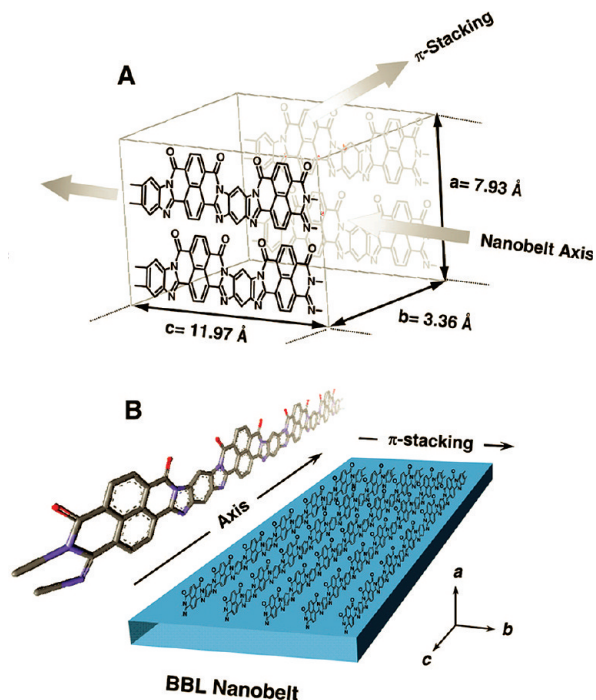


Figure 18. (A) Schematic representation of the molecular arrangement of BBL (27) polymer chains in the orthorhombic unit cell with indicated crystallographic axis directions. (B) Perspective illustration of the molecular packing of BBL (27) polymer chains within a nanobelt. Reprinted with permission from ref 408. Copyright 2008 American Chemical Society.

and lengths of 5–10 μm .⁴⁰⁹ The molecular packing in the nanowires inferred from high-resolution TEM imaging and electron diffraction is that the polymer chains are aligned parallel to the long axis of the wires,⁴⁰⁹ similar to that observed in BBL (27) nanoribbons.⁴⁰⁸

Polyisocyanopeptides decorated with perylene diimide chromophores as pendants (46a–c) are known to form nanowires.^{410–412} From AFM images, the widths and heights of the nanowires were determined to be 5.5 and 2.5 nm, respectively, which were preserved over their entire length ($\sim 1 \mu\text{m}$).⁴¹⁰ It turned out that a single polymer chain formed a coiled structure with a pitch of about 1.5 nm, caused by strong hydrogen-bonding of amide units and strong π – π interactions from the bulky perylene diimides.⁴¹⁰

2.4.2. Self-Assembly at Interfaces and Surfaces. Self-assembly at solvent/solvent interfaces usually takes advantages of the solubility difference of molecules in two different solvents. To maintain an interface where the solute can transfer between, the solvents are usually immiscible or different in nature. For self-assembly that occurs at solvent/substrate interface, the process usually involves solvent evaporation, when the solution is oversaturated and nanocrystals of solutes will form.

2.4.2a. π -Conjugated Small Molecules and Oligomers. Nanowires of π -conjugated small molecules and oligomers have been demonstrated to form at both solvent/solvent interfaces and solvent/substrate interfaces. Assembly of 1D nanostructures at solvent/solvent interfaces is exemplified by nanowires of squaraine dye and organometallic complexes synthesized at the interface of water

and dichloromethane (DCM).⁴¹³ A small amount of water was added on top of a solution of 2,4-bis[4-(*N,N*-dimethylamino)phenyl]squaraine (47a) in DCM to partially cover the surface of DCM solution. During the evaporation of DCM through the exposed air/DCM interface, squaraine dye (47a) aggregated to form nanowires. The single-crystalline squaraine (47a) nanowires had widths of $d \approx 300$ –500 nm, tunable by the initial concentration of squaraine (47a) in solution.⁴¹³ Although nanowires could also be obtained by evaporation of DCM solution without the water layer, nanowires produced from the DCM/water interface were more uniform and well aligned in one direction.⁴¹³ Nanowires of organometallic complexes, Zn(salophen) (47b) and Ni(dimethylglyoximate) (47c) have also been produced by this method (see Chart 14).⁴¹³

Organic semiconductor nanowires have also been synthesized at solvent/substrate interfaces.^{414–425} For example, a propeller-shaped perylene diimide trimer (48) was demonstrated to grow into fluorescent nanowires following a simple evaporation on a glass substrate.⁴¹⁴ Nanowires of high aspect ratio ($L/d = 500$) and diameters in the range of 4–150 nm, which can be controlled by adjusting the concentration of the initial solution, were obtained.⁴¹⁴ An anthracene derivative (36f) was recently shown to self-assemble into micro- and nanowires upon solvent evaporation on a substrate.⁴¹⁵ Various patterns, including ordered microwires, nanowire network, and firework-structured nanowires, were obtained and demonstrated to exhibit superhydrophobic surfaces.⁴¹⁵ Helical nanowires of hexaazatrinaphthylene (HATNA) (49)⁴¹⁶ were produced following the surface-assisted assembly at the solvent/substrate interface. Typically, a 1 mg/mL HATNA (49)/dichloromethane solution was allowed to slowly evaporate over an extended period (24 h) on a silicon substrate. The π -stacked oligomers in the form of coiled-coil helical superstructures with a diameter $d \approx 290$ nm and an average pitch of 600 nm were observed. It was proposed that the growth started with formation of multilayered nanoribbons with a width of over 300 nm, followed by further assembly of ribbons through interdigitation and intercalation of side-chains to reduce the surface energy, during which process the occurrence of twisting turned the nanostructures into a helix.⁴¹⁶

Nanowires of oligophenylenevinylenes and oligothiophenevinylenes (50a–i) have been produced by solvent evaporation after drop casting of solutions in various organic solvents onto substrates.^{417,418} The widths and lengths of the nanowires were about 100 nm and tens of micrometers, respectively. According to the structural analysis done by the X-ray diffraction and multiscale simulations, various interactions, such as dipole–dipole interaction, $-\text{CF}_3/-\text{CF}_3$ repulsion, $-\text{CF}/-\text{CH}$ interaction, and π – π stacking, are responsible for the crystallization of the molecules into 1D nanostructures. By systematically varying the functional group ($-\text{CN}$ or $-\text{CF}_3$) of the oligophenylenevinylenes (50a–e), the resulting nanostructures were tuned from 1D nanowires to 2D films to 3D crystals (Figure 19).⁴¹⁸

Chart 14. Chemical Structures of 47–50

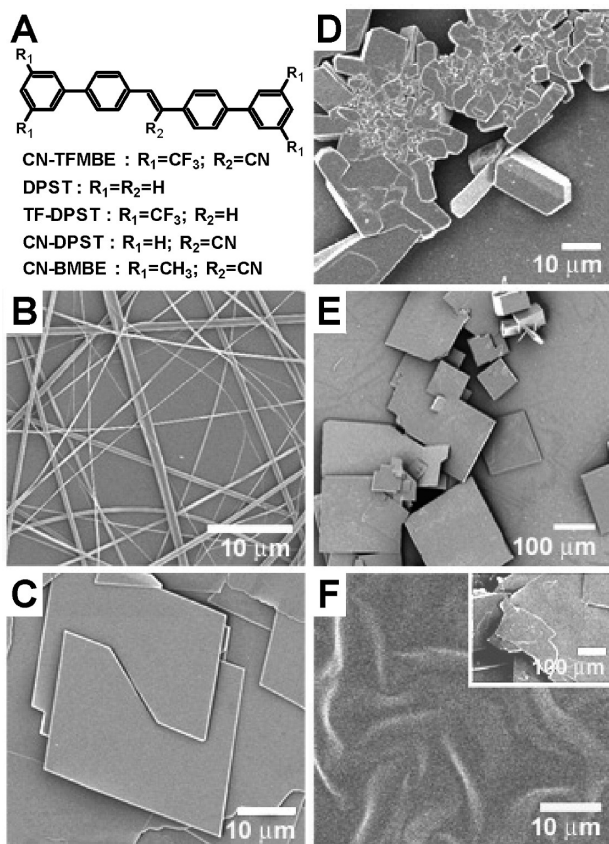
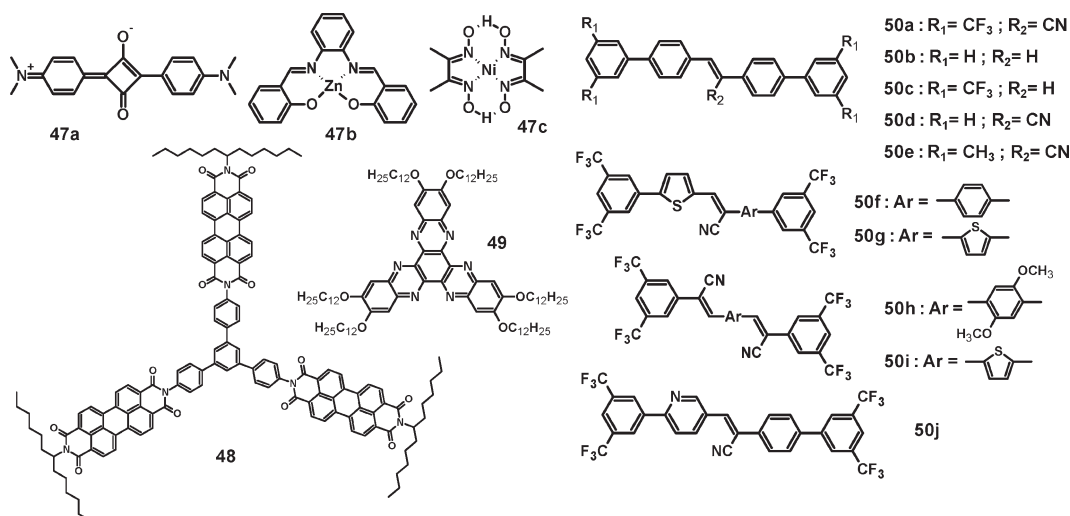
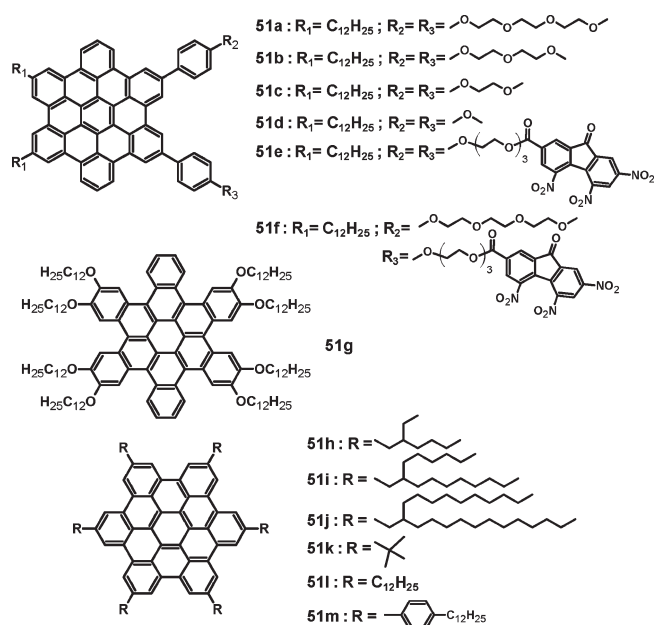


Figure 19. (A) Chemical structures of various oligophenylenevinylenes. (B–F) SEM images of solution-phase self-assembled nanostructures of the oligophenylenevinylenes: (B) CN-TFMBE (50a); (C) DPST (50b); (D) TF-DPST (50c); (E) CN-DPST (50d); and (F) CN-BMBE (50e). Depending on the chemical structures, the resulted nanostructures are tuned from (B) 1D nanowires to (F) 2D amorphous films to (C–E) 3D crystals. Reprinted with permission from ref 418. Copyright 2009 American Chemical Society.

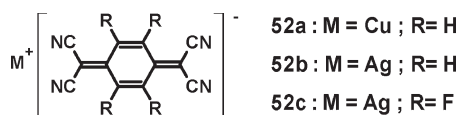
Well-defined nanotubes can also be assembled from π -conjugated molecular building blocks in a facile way. An exquisite example of this is demonstrated by hexa-peri-hexabenzocoronene (HBC) derivatives (51a), which self-assemble into graphitic nanotubes that exhibit

Chart 15. Chemical Structures of 51



semiconductor properties.^{419–421} A slow cooling of heated HBC (51a)/THF solution resulted in the assembly of nanotubes driven by π - π stacking.⁴¹⁹ The graphitic nanotubes are 1 order of magnitude larger in diameter than single-walled carbon nanotubes (SWCNTs), and they are straight and discrete with a diameter of 20 nm, a wall thickness of 3 nm, and an internal diameter of 14 nm. Octa-substituted HBC (51g) molecules were also able to assemble into long nanowires with ~ 200 nm width.⁴²⁰ Influence of the alky side-chain substituents of HBC (51 h–l) on the morphology was also investigated (see Chart 15).⁴²¹ A similar evaporation of a drop cast solution was utilized to produce nanobelts of oligoarene derivative (30).⁴²² The resulting nanobelts featured micrometers in length, several hundred nanometers in width, and 50 nm in thickness. Replacing the solvent resulted in flower-shaped supernanostructures.

Chart 16. Chemical structures of 52



In addition to the above-mentioned planar molecules, spherical fullerene (C_{60}) (**20a**)^{423,424} and metal-tetracyanoquinodimethane (TCNQ) complexes (**52a**)⁴²⁵ (see Chart 16) have also been grown into nanowires. C_{60} (**20a**) nanorods with face-centered cubic (fcc) crystal structure were obtained following a simple evaporation method using *m*-xylene as a shape-controller.⁴²³ These nanorods have widths of 100–450 nm, and lengths of 100 μ m, and average ratio of thickness to width of ~ 0.45 . The solvent *m*-xylene was believed to be trapped into the crystal to form the hexagonal solvated C_{60} (**20a**) nanorods during the initial stage of evaporation, but it was removed by heat treatment under vacuum, during which the hexagonal structure was transformed into the fcc structure.⁴²³ Exceptionally long C_{60} (**20a**) nanowires, each composed of two nanobelts joined along the growth direction to form a V-shaped cross-section, were synthesized by the slow evaporation of a 1,2,4-trimethylbenzene solution.⁴²⁴ The aspect ratio of these nanowires reached 3000, and the crystal structure was identified as orthorhombic. Upon high-temperature treatment, these nanowires were transformed into graphitic carbon nanowires. The growth of these nanowires was attributed to anisotropic solvent- C_{60} (**20a**) interactions that enabled the preferential growth.⁴²⁴ Cu-TCNQ (**52a**) nanowires with widths of 500 nm and lengths of 5 μ m were grown by immersing metallic copper into a solution of TCNQ in acetonitrile.⁴²⁵ Spontaneous redox reaction between copper and TCNQ resulted in a nanostructured film on a copper substrate. The morphology of Cu-TCNQ (**52a**) were strongly dependent on the reaction conditions, such as concentration, temperature, and reaction time.⁴²⁵

2.4.2b. π -Conjugated Polymers. Polymer semiconductor nanowires have been assembled at solvent/substrate interfaces. Many polymer semiconductors have a strong tendency to crystallize with a nanofibrillar morphology during common solution thin-film processing, such as spin-coating^{36,372,426–428} and drop-casting^{366,372,377} followed by postdeposition thermal annealing.^{36,429,430} However, the 1D nanostructures formed in this way are usually embedded in an amorphous thin film and lack precise control in the dimensions and properties. This limits their potential applications in discrete nanoelectronics but they could still be profitably used in thin-film-based devices such as thin film transistors, solar cells, and photodetectors.

Poly(phenylene ethynylene)s (PPEs) (**7**)^{49,431–436} are highly rigid and crystalline macromolecules that can self-assemble into discrete nanowires when deposited on a substrate from solution. Nanowires of PPEs (**7i,j**) were deposited from a dilute solution onto a substrate for a prolonged period of 2–3 days.^{434,435} Typical widths, heights, and lengths of the nanowires were 5–16 nm,

3–10 nm, and several micrometers, respectively.^{431,432,435} Molecular weight of the polymer,⁴³² solvent,^{431,435} solution casting method,^{431,435} and deposition time⁴³⁵ affected the morphology and dimensions of the nanowires. Although the concentration of the solution affected the quantity of nanowires produced, it had little influence on the nanowire width.⁴³⁵ The PPE nanowires were highly crystalline as characterized by X-ray and electron diffractions.⁴³⁵

2.4.3. Solvent-Vapor Annealing. Nanowires of PTCDI derivatives (**35d,f,g,p**)^{328,437,438} and oligophenylenevinyls (**50a,j**)⁴³⁹ have been synthesized by solvent-vapor annealing of thin films. When thin films of a small-molecule organic semiconductor are exposed to the vapor of a good solvent in a closed environment, the molecules can move and crystallize into nanowires. Nanowires produced in this method have diameters of 50 nm–1 μ m and heights of 10–250 nm depending on the material, solvent, and processing time.^{328,437–439} By masking thin films of oligophenylenevinyls (**50a,j**), selective growth of nanowires in the area exposed to a solvent vapor was also demonstrated.⁴³⁹

2.5. Physical Vapor Transport and Deposition. Physical vapor transport method has been extensively studied as a way to grow high-quality single crystals of small-molecule organic semiconductors.^{440–451} Single crystals of oligothiophenes,^{442–444} oligoacenes,^{442,448} and copper phthalocyanines^{442,451} have been grown from this method, with dimensions ranging from nanometers to centimeters.^{442–444,448,451} Because single crystals are free of any morphological defect, this method has been employed to fabricate high-mobility organic field-effect transistors (OFETs).^{445–450} To fabricate nanostructures, the molecules have to sublime under low pressure and heating conditions.

The experimental setup is very simple, as shown in Figure 20.^{440,442} Typically, a two-zone furnace tube made of quartz with a temperature gradient is employed. Low pressure inside the tube may be required to sublime the oligomer semiconductor. The organic material is placed at the high-temperature end of the tube where sublimation slowly occurs. The vapor of the molecules is then carried by a flow of inert gas (i.e., Ar, He, H₂, or N₂), which flows through the tube. A substrate is placed at the low-temperature region where the molecules crystallize. High-purity single crystal can be collected on a substrate, whereas impurities are deposited before and after the crystallization region. The resulting single crystals can be in a bulk form (3D),^{444–446} flexible films (2D),⁴⁴⁹ or nanowires and nanobelts (1D)^{450,452–455} depending on the nature of the molecular packing in the crystal and the conditions of the process, such as temperature and deposition time.

Nanowires of various materials, including metal phthalocyanines and their derivatives (i.e., CuPc and F₁₆CuPc) (**53a–f**),^{450,452–454,456} tris(8-hydroxyquinoline) aluminum (Alq₃) (**24**),⁴⁵⁷ peryloothiophene (PET) (**54b**),⁴⁵⁸ 1,5-diaminoanthraquinone (DAAQ) (**55**),^{455,459} and metal-TCNQs (**52a–c**)^{425,460–462} (see Chart 17) have been produced via

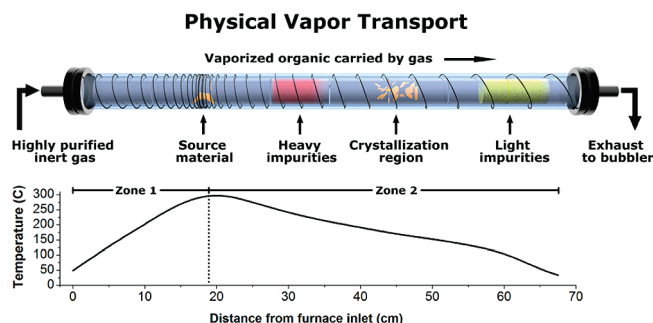
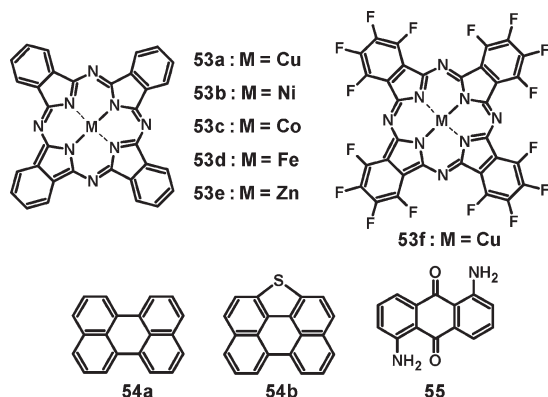


Figure 20. Experimental setup of a physical vapor transport method to grow single crystals and nanowires of small-molecule and oligomer semiconductors. Reprinted with permission from ref 440. Copyright 2007 Elsevier.

Chart 17. Chemical Structures of 53–55



this method. Nanowires made by physical vapor transport and deposition feature several advantages: (1) ready production of wires because of the simple experimental setup; (2) a high crystallinity without impurities; and (3) a controllability of morphology and dimensions by changing process conditions. However, there are also drawbacks: the synthesis of nanowires is limited to small molecules and oligomers that are sublimable, and the fabrication of devices is a low-throughput process.

2.5.1. Metal Phthalocyanine (MPc) and Its Derivatives.

Metal phthalocyanines (MPcs) are a class of p-type organic semiconductors that are attractive for growth of nanowires due to their ruggedness, commercial availability, and diversified potential applications in OFETs, chemical sensors, nonlinear optics, and photovoltaic cells.^{463,464} Various MPcs with different metal cores, such as CuPc (**53a**),^{451,465,466} NiPc (**53b**),^{465,466} CoPc (**53c**),⁴⁶⁶ FePc (**53d**),⁴⁶⁶ and ZnPc (**53e**)⁴⁶⁶ have been reported. However, due to their limited solubility in common organic solvents, nanowires of MPc are usually made through physical vapor transport and deposition. Among all the MPcs, copper phthalocyanine (CuPc) (**53a**) is most commonly studied because of its excellent charge-transport properties along with its high thermal and chemical stability.^{451,467} By making nanowires of CuPc (**53a**), its charge-transport properties and stability can be enhanced because of the enhanced crystallinity and controllable morphology.

CuPc (**53a**) nanowires were discovered during CuPc (**53a**) thin film deposition by physical vapor transport.⁴⁶⁸

It turned out that both the substrate material and substrate temperature had great impact on the morphology of thin films deposited.⁴⁶⁸ Both a clean glass substrate with a contact angle 0° to water and a glass modified by a thin layer of gold yield a thin film of CuPc (**53a**) with a fine grainlike morphology at low temperature (28–100 °C). However, CuPc (**53a**) film deposited at a high substrate temperature (150–200 °C) showed nanowires with a typical dimension of 150 nm in diameter and 1–2 μm in length. The direction of the nanowires is drastically different depending on the substrate. Nanowires with a horizontal orientation on a glass substrate were obtained whereas a gold-coated substrate resulted in nanowires grown perpendicular to the substrate plane. Further investigation showed that CuPc (**53a**) nanowires can grow from glass, silicon, indium tin oxide (ITO), and fluorine-doped tin oxide (FTO).⁴⁶⁹ At a substrate temperature above ~210 °C, β-CuPc nanowires were found instead of α-phase, and these β-CuPc nanowires had higher absorbance at longer wavelengths, which is potentially beneficial for photovoltaic applications.⁴⁶⁹ Studies of five metal phthalocyanine nanostructures, CuPc (**53a**), NiPc (**53b**), CoPc (**53c**), FePc (**53d**), and ZnPc (**53e**), also showed the substrate temperature dependence of crystal-phase and morphology.⁴⁶⁶

Nanoribbons of pure CuPc (**53a**) can be obtained by using physical vapor transport from β-CuPc powder as the precursor.⁴⁵⁰ These single-crystalline CuPc (**53a**) nanoribbons have a typical dimension of tens to hundreds of nanometers in width, and 20–50 μm in length.⁴⁵⁰ The growth of CuPc (**53a**) nanoribbons was found to be along the [010] direction (*b*-axis), formed by the stacking of planar CuPc (**53a**) molecules and driven by the π–π interactions (Figure 21A). Patterned β-CuPc nanoribbons could also be realized using vapor deposition on pretreated substrates.⁴⁵³ Vapor deposited nanoribbons of CuPc (**53a**) could be dispersed in ethanol and sonicated to make a suspension of CuPc (**53a**) nanocrystals.⁴⁵³ A cleaned Si wafer was dipped into the suspension to deposit the CuPc (**53a**) nanocrystals and was then transferred to a physical vapor transport system for further growth. The nanocrystals acted as nuclei for growth of nanoribbons, which extended along the *b*-axis of the nanocrystals, driven by the π–π stacking of β-CuPc, resulting in horizontally grown nanoribbons.⁴⁵³

Copper hexadecafluorophthalocyanine (F₁₆CuPc) (**53f**) is known to be an air-stable n-type organic semiconductor with high electron mobility in OFETs.⁴⁷⁰ The growth of single-crystalline F₁₆CuPc (**53f**) nanowires has thus been of interest.^{452,466} Temperature dependent morphology was observed as the size of F₁₆CuPc (**53f**) nanowires decreases with reduced substrate temperature. Unlike CuPc nanowires which grow along the [010] direction, despite the similarity of the molecular structure, the growth of F₁₆CuPc (**53f**) nanowires is along the [100] direction (Figure 21B).^{452,456} OFET devices fabricated with F₁₆CuPc (**53f**) nanowires showed electron mobility of ~0.2–0.6 cm²/(V s) with on/off ratios of 10³–10⁴.^{452,454} Growth of F₁₆CuPc (**53f**) crystals on

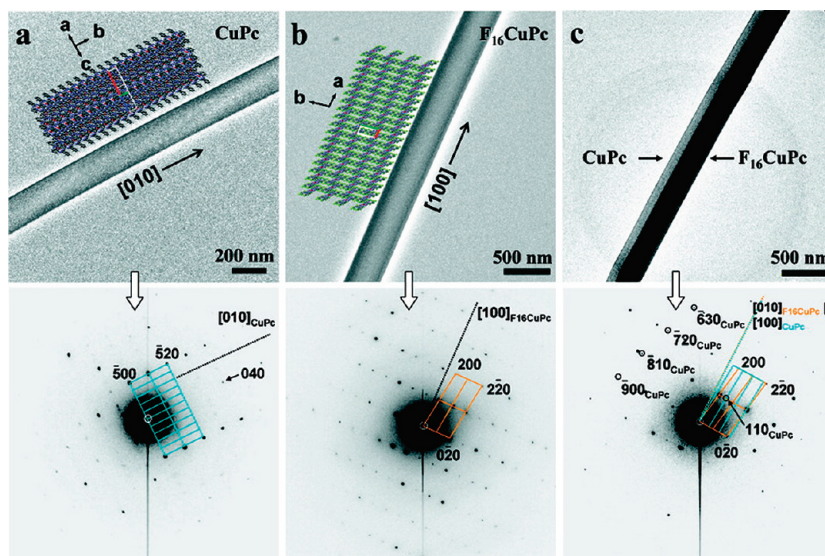


Figure 21. (A–C) TEM images and corresponding SAED patterns of nanoribbons produced via physical vapor transport: (A) CuPc (**53a**); (B) F_{16} CuPc (**53f**); and (C) CuPc (**53a**)/ F_{16} CuPc (**53f**) heterojunction. Reprinted with permission from ref 456. Copyright 2010 American Chemical Society.

CuPc (**53a**) nanowires was demonstrated to form p–n heterojunction nanoribbons (Figure 21C). Integration of CuPc (**53a**) and F_{16} CuPc (**53f**) nanowires grown from physical vapor transport have been performed to fabricate complementary logic circuits,⁴⁵⁴ heterojunction ambipolar transistors,⁴⁵⁶ and p–n heterojunction photovoltaic devices.⁴⁵⁶ In addition to nanowires, nanotubes of F_{16} CuPc (**53f**) were grown using vapor-phase transport and template-directed deposition.⁴⁷¹ Silicon oxide wafers functionalized with gold nanoparticles arrays were used as the substrates. F_{16} CuPc (**53f**) film was then deposited onto the Au nanoparticles by vapor phase deposition under ultrahigh vacuum of 1×10^{-9} mbar. High-resolution TEM showed that multiwall nanotubes were obtained, with a wall-to-wall distance of 0.35 nm, a wall thickness of 10–37 concentric layers, and a channel diameter of 3–80 nm.⁴⁷¹ These nanotubes were believed to assemble by wrapping the lamellar sheets into cylinders, with π -stacking in the radial direction.⁴⁷¹

2.5.2. Tris(8-hydroxyquinoline) Aluminum (Alq_3). Tris(8-hydroxyquinoline) aluminum (Alq_3) (**24**), one of the most widely used electron transport materials and green fluorescent emitters in organic light emitting diodes (OLEDs),²⁴ has been used to synthesize nanostructures, including nanoparticles, nanorods, and nanowires, via vapor condensation.^{457,472,473} The synthesis followed the usual vapor transport and deposition procedure except that the substrate was cooled with liquid nitrogen. The dimensions and morphology of the nanostructures turned out to be dependent on pressure of the chamber, temperature of sublimation boat, and distance between the boat and a substrate.⁴⁷³ Amorphous nanoparticles (diameters \approx 50–500 nm)⁴⁷³ and nanowires (\sim 30–50 nm wide and several μ m long)⁴⁵⁷ as well as crystalline nanorods (\sim 100 nm wide and \sim 1 μ m long)⁴⁷² were synthesized by varying such conditions. In another study using low-temperature sublimation without cooling of the substrate, the effects of substrate temperature and

carrier-gas flow rate on the morphology of Alq_3 (**24**) nanowires have been reported.⁴⁷⁴ Alq_3 (**24**) nanowires with diameters of 50–500 nm have also been synthesized by sublimation of Alq_3 (**24**) from mixture of Alq_3 (**24**) and inorganic adsorbent (alumina or silica gel).⁴⁷⁵ The presence of the adsorbent reduced the sublimation temperature of Alq_3 (**24**) and resulted in uniform nanowires.⁴⁷⁵ Arrays of helical rods of Alq_3 (**24**) have grown on silicon and glass substrates by a deposition method called glancing angle deposition (GLAD) which can generate helical, polygonal spiral, and various columnar morphologies.^{476,477} The substrates were mounted on a rotating substrate chuck and tilted to have a deposition angle. The resulting nanorods were uniform and had a width of 40–75 nm. The arrays of nanorods with chiral morphology had selective transmission of polarized light and generated circularly polarized PL emission.^{476,477}

2.5.3. Other Small Molecules and Oligomers. A peryloethiophene (PET) (**54b**) was demonstrated to form crystalline nanowires, in which the planar PET (**54b**) molecules packed along the *b*-axis with a distance of 0.347 nm.⁴⁵⁸ In addition to π – π stacking of planar PET (**54b**) molecules, strong interactions between adjacent sulfur atoms are considered to be the reasons for the directional growth of PET (**54b**) nanowires. These nanowires showed good p-channel characteristics in OFETs, and a hole mobility in the range of 0.3–0.8 $\text{cm}^2/(\text{V s})$ was obtained. By using a modified experimental setup, arrays of vertically aligned nanowires of 1,5-diaminoanthraquinone (DAAQ) (**55**) have been grown.^{455,459} The vapor deposition process took place in a round-bottom flask coated with a thin layer of DAAQ (**55**), instead of a quartz tube, to ensure uniform heating over the entire sample during sublimation. The diameters of the DAAQ (**55**) nanowires are 80–500 nm depending on the heating temperature, and the lengths of nanowires are from 500 nm to over 10 μ m depending on the deposition time (Figure 22). The mechanism of vertical growth relative to

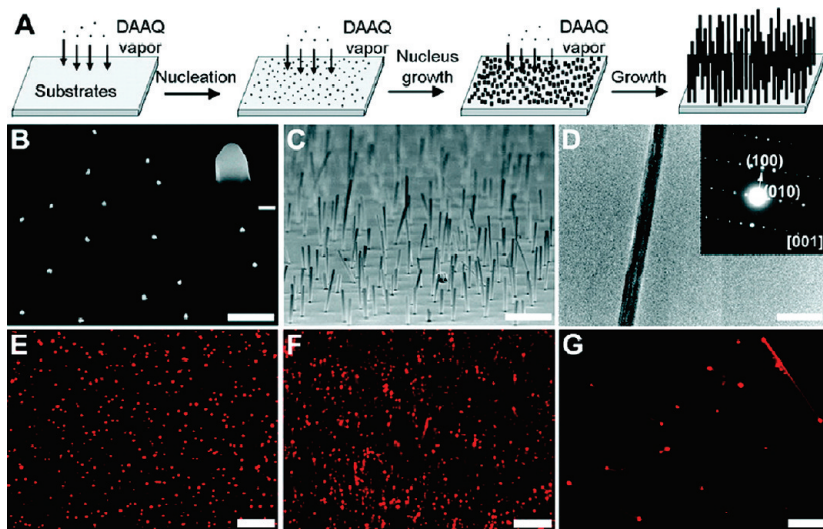


Figure 22. (A) Schematic illustration for the growth of the vertical DAAQ (**55**) nanowire arrays via vapor transport. (B–C) SEM images of the DAAQ (**55**) seeds (B) and nanowire arrays (C). (D) TEM image of a single nanowire and the corresponding SAED patterns. (E, F) Plane view (E) and tilt view (F) PL microscope image of the vertical DAAQ (**55**) nanowire arrays. (G) PL microscope image of isolated wires on glass. Scale bars: (B) $2\ \mu\text{m}$ (Inset $100\ \text{nm}$); (C) $1\ \mu\text{m}$; (D) $500\ \text{nm}$; (E, F) $10\ \mu\text{m}$; and (G) $20\ \mu\text{m}$. Reprinted with permission from ref 459. Copyright 2010 American Chemical Society.

a substrate is believed to be a vapor-solid condensation process on DAAQ (**55**) nanoparticles seeds as the nanoparticles are seen on the substrate at early stage of growth. Growth of nanowires was built upon the seeding nanoparticles along the [100] direction. The DAAQ (**55**) nanowires were tested as an acid sensor⁴⁵⁵ and a waveguide.⁴⁵⁹ Single-crystalline Cu-TCNQ (**52a**)^{425,460} and Ag-TCNQ derivatives (**52b,c**)^{461,462} nanowires with widths of 30–500 nm were also vertically grown on a metal substrate by the reaction of TCNQ vapor with the metal in a physical vapor transport system.

2.6. Other Techniques. **2.6.1. Langmuir–Blodgett (LB).** Modified amphiphilic polythiophene (**4u**), which has alternating hydrophilic and hydrophobic side-chains attached to the backbone, was found to self-assemble into nanowires of 60 nm width and 10–15 nm thick using the Langmuir–Blodgett (LB) technique.^{478,479} These nanowires were formed by the isothermic compression and the π -stacking of the polymer chains. The monolayer films and nanowires formed by this method had anisotropic orientation of ordered domains as seen from the polarized optical characterization.^{478,479} AFM revealed that the nanowires have lengths of micrometers, widths of 60 nm, and heights of 10–15 nm.⁴⁷⁹

2.6.2. Directional Epitaxial Crystallization. Highly oriented nanofibers of P3ATs (**4d,f,j**) with a shish-kebab-like morphology were prepared by oriented epitaxial crystallization.⁴⁸⁰ The epitaxial growth of P3ATs (**4d,f,j**) took place on the surface of a molecular material, 1,3,5-trichlorobenzene, in liquid pyridine. These fibers consisted of an oriented fiber core several hundreds of micrometers long, called the “shish,” along with the lateral crystalline fibers of folded polymer chains (the “kebabs”) placed periodically 18–30 nm apart.⁴⁸⁰ A unique alignment of the P3AT (**4d,f,j**) chains in the nanostructures was confirmed by selected-area electron diffraction. The shish-kebab nanowires showed polarized

photoluminescence excitation and emission, supporting that polythiophene chains are highly oriented.⁴⁸⁰

2.6.3. Controlled Polymerization. Several polymerization techniques, including chemical oxidative polymerization, electrochemical polymerization, interfacial polymerization, and dilute solution polymerization, have been used to synthesize various conducting polymer nanowires. Chemically polymerized PA (**10**) exhibited nanofibrillar morphology with a fiber diameter of 20 nm.^{153,195} Chemical oxidative polymerization of aniline is one of the traditional methods for the synthesis of PANI (**1**) in bulk quantity.^{481,482} Nanofibers of PANI (**1**) are formed during the oxidative polymerization of aniline.^{481–483} The diameters of nanowires are strongly dependent on the acid⁴⁸¹ and the oxidant⁴⁸² used in the polymerization. For example, the average diameters of nanofibers produced with hydrochloric acid, camphorsulfonic acid, and perchloric acid are about 30, 50, and 120 nm, respectively.⁴⁸¹ The diameters are found to be from 12 to 130 nm depending on the redox potential of the oxidant.⁴⁸² In the case of PANI (**1**) nanowires synthesized by chemical oxidative polymerization of aniline using an ammonium peroxydisulfate oxidant, the morphology was believed to be controlled by the anilinium-peroxydisulfate ion clusters.⁴⁸³ Chemical oxidation of aniline at the liquid/liquid interface of two immiscible solvents also resulted in PANI (**1**) nanowires.^{484–487} The nanowires have diameters of 30–200 nm and lengths ranging from 300 nm to several μm .^{485–487} This interfacial polymerization was further developed to synthesize nanostructures of other conducting polymers such as PPy (**2**) and PEDOT (**5**).⁴⁸⁸ A dilute solution polymerization, chemical oxidation of aniline in an aqueous solution with substantially low concentrations of aniline ($\sim 8\ \text{mM}$) and oxidant (aniline:oxidant = 2:1) compared to conventional oxidative polymerization

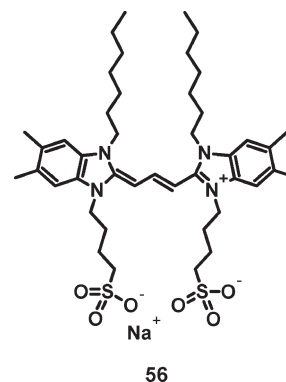
(~ 400 mM aniline with aniline:oxidant = 4:1), was later developed to produce a large quantity of interconnected PANI (**1**) nanowires in the bulk solution.^{489–491} Electrochemical polymerization has also been employed to produce 1D nanostructures of PANI (**1**).⁴⁹² The PANI (**1**) nanowire networks produced in the electrochemical polymerization between two parallel electrodes has nanowire diameters of 40–80 nm, and sensing properties toward acid/base and ethanol vapors.⁴⁹² The synthesis and applications of PANI (**1**) nanowires can be found from dedicated review papers.^{76,481}

2.6.4. Solid-Phase Reaction. Anthracene (**36a**) nanowires and perylene (**54a**) nanorods were synthesized by the so-called solid-phase synthesis.⁴⁹³ The reaction takes place in a horizontal tube furnace with controlled temperature and time under flow of argon gas. For synthesis of anthracene (**36a**) nanowires, the precursor 9-anthracenecarboxylic acid (ACA) reacted with CaO in the solid-state at 340 °C for 2 h. The diameters and lengths are in the range of 40 nm–1.5 μ m and 9–20 μ m for the anthracene (**36a**) nanowires, respectively.⁴⁹³ Perylene (**54a**) nanorods were produced by the reaction of 3,4,9,10-perylenetetracarboxylic dianhydride (PTCDA) with BaO at 280 °C for 2 h, yielding 1D nanostructures that are 30–110 nm wide and 160–500 nm long.⁴⁹³

3. Properties and Applications

3.1. Optical Properties. One-dimensional nanostructures of organic semiconductors have a range of tunable, and novel or enhanced, linear optical, nonlinear optical, and optoelectronic properties beyond those of the building blocks (π -conjugated small molecules, oligomers, and polymers) and those of thin films or the bulk solid. Such properties of organic nanostructures do not originate from quantum confinement size effects, which are well-established in inorganic semiconductor nanostructures,^{1–3,9} because of the rather small exciton Bohr radii (< 1 –2 nm) of π -conjugated molecular systems (Figure 3). Instead, it is the nature, geometry, and dynamics of excitons in the 1D nanostructures of organic semiconductors that are crucial to the tunable and novel optical and optoelectronic properties.^{494–503} The extent of exciton delocalization within the self-assemblies of π -molecular building blocks in 1D organic semiconductor nanostructures and the detailed geometrical arrangement of the building blocks within the assemblies control their absorption, photoluminescence (PL), and other photophysical properties.^{494–500} Examples of these supramolecular and mesoscopic effects in 1D nanostructures of π -conjugated molecules include the formation of J- and H-aggregates and consequent spectral red- and blue-shift,^{494–500} respectively, narrowing or broadening of the absorption band,^{494,504,505} increase or decrease in PL quantum yield relative to the isolated molecules in solution,^{494,506,507} superradiance,^{494,496,497} enhancement of charge photogeneration and thus photoconductivity,^{504,505,508–510} self-waveguiding of fluorescence,^{349,511–516} among others. In the case of multicomponent systems, involving two or

Chart 18. Chemical Structures of **56**



more π -conjugated molecular building blocks with different electronic structures (HOMO/LUMO levels) or multiple assemblies with different exciton energies, additional supramolecular and mesoscopic phenomena such as resonance energy transfer,⁵⁰¹ exciplex formation,⁵⁰⁹ and photoinduced charge transfer⁵¹⁷ can lead to various photophysical and optoelectronic properties in the organic semiconductor nanostructures. In the following, we provide a few recent examples of these supramolecular and mesoscopic excitons in 1D organic semiconductor nanostructures.

Highly ordered, self-assembled, nanotubes of π -conjugated molecules provide excellent model systems for investigation of their optical properties by nanoscale spectroscopic/microscopic probes. Double-walled nanotubes ($d \approx 10$ nm, $L > 1$ μ m) of amphiphilic cyanine dye 3,3'-bis(2-sulphopropyl)-5,5',6,6'-tetrachloro-1,1'-diocetylbenzimidacarbocyanine (C8S3) (**56**) (see Chart 18) assembled in solution were deposited on quartz substrates via a drop-flow technique (Figure 23).⁵⁰² The J-aggregates within the nanotubes were investigated by means of polarization-resolved fluorescence near-field scanning optical microscopy (NSOM), revealing uniform exciton fluorescence along the long axis of an individual nanotube and between nanotubes.⁵⁰² Exciton diffusion length in these nanotubes was estimated to be about 100 nm and possibly much longer.⁵⁰² Similar long-distance exciton migration distance of 70 nm has been measured in J-aggregates of perylene tetracarboxylic diimide (PTCDI) derivative (**35q**) via fluorescence blinking experiments.⁵⁰³ Extensive earlier theoretical and experimental studies of J-aggregates in 1D assemblies of diverse π -conjugated molecules have established the excitonic nature of their diverse optical properties.^{494–500} For example, the enhanced red-shifted or broadened absorption spectra of such assemblies in the solid state can lead to orders of magnitude enhancement in charge photogeneration efficiency in photoconductive systems.^{504,505,508–510}

The propagation of exciton polaritons, formed by the strong coupling of photons and excitons, over long distances (~ 250 μ m) at room temperature was recently demonstrated in self-assembled, crystalline nanofibers of thiacyanine (TC) dye (**42**).⁵¹¹ Defect-free rectangular nanofibers with heights of 100–200 nm, widths of

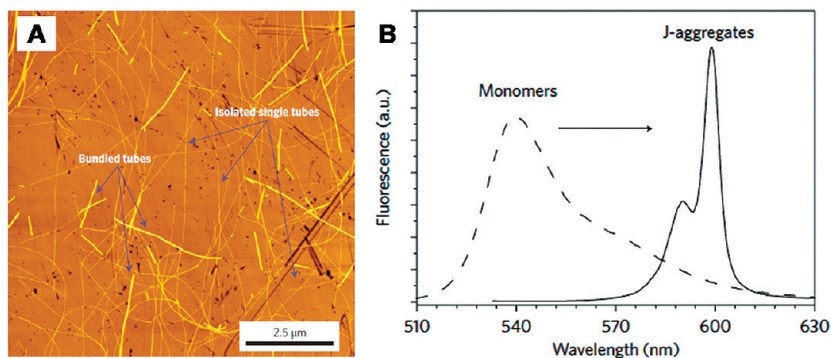
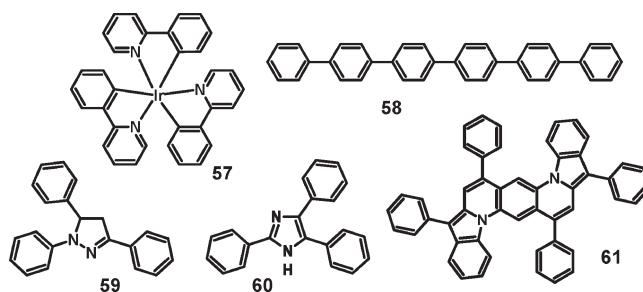


Figure 23. (A) AFM image of tubular aggregates of C8S3 (**56**) on a quartz substrate. (B) Fluorescence spectra of C8S3 (**56**) monomers and the aggregates in solution. Reprinted with permission from ref 502. Copyright 2009 Nature Publishing Group.

400–700 nm, and lengths of about 250 μm were self-assembled in aqueous solution of the TC dye (**42**) and were transferred onto a glass substrate (refractive index = 1.526) by drop-casting and solvent evaporation.^{348,511,518,519} The photoexcited nanofibers self-waveguided the fluorescence over their entire length of 250 μm.^{348,511,518} The mechanism of the self-waveguiding or “active” waveguiding was shown to be fluorescence propagation in the form of exciton polaritons.⁵¹¹ It is suggested from these studies and results that nanofibers of fluorescent organic semiconductors are promising for developing exciton polariton-based integrated optoelectronic circuits which could be more highly integrated than waveguide optical circuits.⁵¹¹

The phenomenon of active waveguiding of emitted fluorescence in self-assembled organic semiconductor nanowires has also been observed in several other π -conjugated molecular systems, including pyrazino-[2,3-g]quinoxaline derivatives (PyQs) (**43a,c**),³⁴⁹ cyclohexyl-substituted PTCDI (CH-PTCDI) (**35h**),³²⁹ 9,10-bis-(phenylethynylene)anthracene (BPEA) (**36c**),⁵¹³ fac-tris(2-phenylpyridine)iridium (Ir(ppy)₃) (**57**),⁵¹⁴ para-hexaphenyl (p-6P) (**58**),^{515,516} 1,3,5-triphenyl-2-pyrazoline (TPP) (**59**),⁵²⁰ TPP (**59**)/rubrene (**9**),⁵²⁰ 2,4,5-triphenylimidazole (TPI) (**60**),⁵¹² and TPI (**60**)/perylene (**54a**) (see Chart 19).⁵²¹ In the case of the PyQs (**43a,c**), crystalline microwires with widths d = 500 nm–5 μm and lengths L = 100–1000 μm were shown to exhibit low-loss active waveguide of fluorescence emission in the green to yellow (502–543 nm) region.³⁴⁹ The single-crystalline nanoribbons of CH-PTCDI (**35h**) (250–1500 nm widths, 100 nm thickness, and > 100 μm lengths) self-waveguided a highly polarized fluorescence over their lengths without a significant emission loss (Figure 24A); however, an optical loss coefficient (α) was not determined.³²⁹ Flexibility of the nanoribbons facilitated the active waveguiding of the fluorescence even in the bent state. Size-dependent active waveguiding of fluorescence was observed in microrods ($d \approx 1$ μm, $L > 1000$ μm) and nanowires ($d \approx 100$ nm, $L > 100$ μm) of Ir(ppy)₃,⁵¹⁴ the single-crystalline microrods self-waveguided green fluorescence whereas the less crystalline nanowires waveguided yellow-green emission (Figure 24B,C). Nanorods and nanowires of the binary TPP (**59**)/rubrene (**9**) and TPI (**60**)/perylene (**54a**) systems self-waveguided fluorescence that

Chart 19. Chemical Structures of 57–61



resulted from energy transfer between the two chromophores.^{520,521} In the former case, self-waveguided white fluorescence was observed at an optimum composition of the blue-emitting TPP (**59**) and orange-emitting rubrene (**9**) incorporated into the nanowires.⁵²⁰ The similarity of all these observations of self-waveguiding of fluorescence in 1D nanostructures of diverse π -conjugated small molecules and polymers strongly suggest that the basic underlying mechanism must be the same. In this respect, Takazawa's recently proposed mechanism, i.e., that active waveguiding of fluorescence is due to the propagation of exciton polaritons in the photoexcited nanofibers, appears to account for all observations to date.⁵¹¹

The photoluminescence (PL) emission in organic semiconductor nanowires has been investigated and exploited in various other ways. Subwavelength multicolor PL emission from multicomponent single nanofibers of organic semiconductors have been investigated and explored in novel applications. Figure 5 shows light-emitting barcode nanowires based on P3BT (**4d**) and PEDOT (**5**) as the emissive materials.¹²⁹ High contrast PL emissions of the compartments, which can be further amplified by a thin layer of metal coating, make the nanowires a good candidate for developing nanoscale barcodes.¹²⁹ PL emission of rubrene (**9**) nanowires synthesized by vapor transport and deposition in AAO templates was studied and compared with bulk rubrene (**9**) single crystals prepared under the same conditions without the template.¹²⁸ Nanometer-scale laser confocal microscope (LCM) PL spectra obtained from both nanowires and bulk single crystals showed that their respective emissions are greenish-yellow and yellowish-orange. The full-width-at-half-maximum (fwhm) of the LCM PL of a single rubrene (**9**) nanowire was much

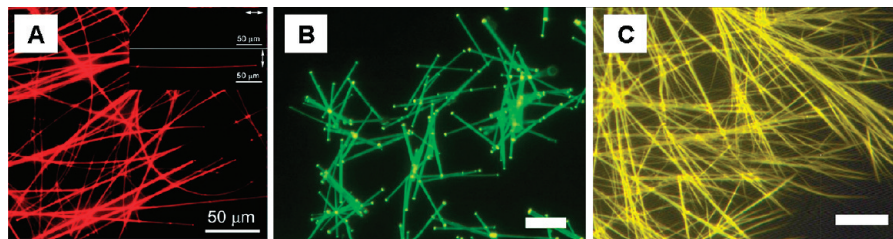


Figure 24. (A–C) PL microscopy images of nano- and microrods. (A) PTCDI (**35h**). Reprinted with permission from ref 329. Copyright 2009 American Chemical Society. (B) Ir(ppy)₃ (**57**) microrods and (C) nanorods. Scale bar 50 μm . Reprinted with permission from ref 514. Copyright 2009 Royal Society of Chemistry.

broader than the PL of the rubrene single crystal. This was attributed to the emission of mixed polarized bands due to different crystal growth characteristics in the nanowire.¹²⁸ The PL emission from nanowires tends to be polarized when the organic semiconductor molecules are oriented in the nanowires as exemplified by nanowires of PTCDI (**35a**),³²³ F8BT (**6c**),^{230,245,263} and PTMSDPA (**16**).²³³ Alignment of the nanowires also resulted in the polarized emission, as seen in electrospun nanofibers of MEHPPV (**3b**),²¹⁷ PFO (**6a**),²¹⁶ PF+ (**6d**),²¹⁶ and PFO (**6a**)/DBPPV (**3c**) blend.²¹⁵

As described in section 2.2 (Electrospinning), the morphology and composition of nanowires play an important role in their photophysical properties. For example, the PL spectra of nanofibers of PFO derivative (**6a,g–i**)/PMMA blends^{216,235} and MEHPPV (**3b**)/PEO blends²²⁰ were blue-shifted from the PL spectra of the blend thin films. The shifts of PL emission peaks came from the fact that the dilution effect of the insulating component in the polymer semiconductor/insulating polymer blends is more significant in nanofibers of the blends than in thin films of the blends.^{216,220,235} The morphology and composition also significantly affect energy transfer in binary blends of conjugated polymers, such as MEHPPV (**3b**)/P3HT (**4f**) and MEHPPV (**3b**)/PFO (**6a**).^{215,218,219,238,244,246} Small-scale phase separation results in enhanced energy transfer with large interfacial area between the component conjugated polymers, whereas large-scale phase separation reduces the degree of the energy transfer.^{215,219}

3.2. Charge-Transport and Electrical Properties. The charge-transport properties of organic semiconductor nanowires are of great interest for both scientific and practical reasons.^{307,333,522} Because of their superior, often single-crystalline, morphology compared to polycrystalline or amorphous thin films, studies of charge transport in 1D organic nanostructures can provide a fundamental understanding of the nature of charge transport, its limits, and structure–charge-transport relationships in organic semiconductors. Furthermore, organic semiconductor nanowires represent a promising alternative route to low-cost and high-performance organic electronics and nanoelectronics. Intrinsic charge-transport properties of organic nanowires and factors that govern the transport have been widely studied and we provide a brief overview of those studies in this section. In general, charge-carrier mobility and dc conductivity are the typically reported

figures of merit of charge transport in organic 1D nanostructures.

3.2.1. Conducting Polymer Nanowires. Electronically conducting organic nanowires that have been extensively studied can be classified into two types: conducting polymers and organic/polymer semiconductors. Conducting polymers are conjugated polymers that are chemically or electrochemically doped to maximize the density of charge-carriers and thus their electrical conductivity.^{210,523,524} In contrast, organic/polymer semiconductors are π -conjugated small molecules, oligomers, or polymers that exhibit intrinsic electronic properties. PANI (**1**),^{151,184,209–212,225,297,525} PPy (**2**),^{85,86,143,150,253,265,269,526,527} MEHPPV (**3b**),³⁰⁰ and PEDOT (**5**) and polythiophene derivatives (**4a,b,d,f,h,j,w**, **5,25b**)^{85,86,100,101,185,269,271,374,396,479,526,527} are the most widely studied examples of doped conducting polymer nanowires with the reported dc conductivity (σ_{dc}) of $\sim 1 \times 10^{-3}$ to 1×10^3 S/cm. The conductivity depends on the type and concentration of dopants and reagents,^{109,225,485,487,526,528} size of nanowires,^{100,101,209,526} and composition in the case of blends.^{212,253} It has been found that a film composed of the conducting polymer nanowires filled in nanopores (diameters less than 1 μm) exhibited a higher dc conductivity than a homogeneous thin film (Figure 25).^{86,526} The ratio of the conductivity of a mat of nanowires with diameters of ~ 10 nm to the conductivity of a homogeneous film was higher than 10 for PEDOT (**5**) and a polythiophene derivative (**25b**), and reached 90 for PPy (**2**) as shown in Figure 25A.⁵²⁶ The origin of the diameter dependence of the conductivity has been explained as a consequence of an extended conjugation length and a better ordering of the molecules in the more confined nanostructures, which were revealed from infrared spectroscopy and X-ray diffraction.⁵²⁶

The conductivity of electrospun nanofibers of CSA-doped PANI (**1**)/PEO decreased from 1×10^{-1} S/cm to 1×10^{-3} S/cm as the diameter of the nanofiber got smaller from ~ 500 to 20 nm, and this has been attributed to the effect of Schottky barrier at the metal contact.²⁰⁹ However, it may also be that the effect of phase separation is more severe for the smaller nanofibers, resulting in the poorer charge transport. Vertically oriented PPy (**2**) nanowires after removal of a template showed a high conductivity, as characterized by AFM and related techniques (Figure 25B).¹⁴³ Although further studies in the synthesis and properties of conducting polymer nanowires are

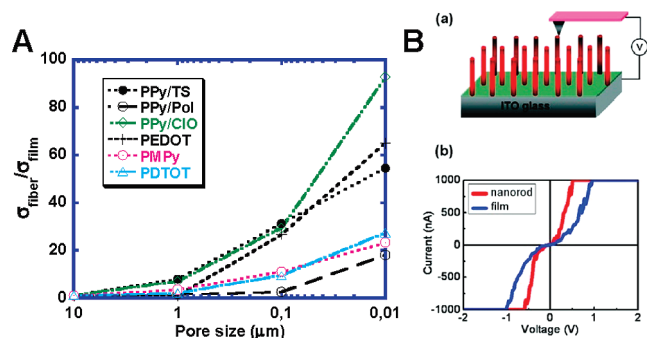


Figure 25. (A) Conductivity of conducting polymer fibers as a function of the pore size of the template and counterion. Reprinted with permission from ref 526. Copyright 1995 Elsevier Science. (C) Current-sensing AFM results of PPy (2) film and vertical nanorods. Reprinted with permission from ref 143. Copyright 2008 American Chemical Society.

required to realize reliable performance with little nanowire-to-nanowire variations in real applications, the highly conductive nanowires have potential for use as electrodes and interconnecting elements in organic/flexible electronics. The modulation of the conductivity caused by environmental and external factors also make these nanowires promising for sensor applications in which the output electrical signals can be directly processed by conventional semiconductor devices.

3.2.2. Nanowires of Semiconducting Small Molecules and Oligomers. Nanowires of organic semiconductors are of growing broad interest in part because of their potential as active materials in electronic, optoelectronic, and sensor devices. Consequently, organic semiconductor nanowires are often characterized by using an organic field-effect transistor (OFET) as a platform to investigate their charge-transport properties, although other techniques such as space-charge-limited current (SCLC)^{121,322} and time-resolved microwave conductivity (TRMC)^{339,529} measurements have also been applied as well.

Small-molecule organic semiconductors have strong π - π interactions between the relatively planar molecules in most cases. Nanostructures preferably grow in one direction governed by the most favorable interaction, especially when nanowires are synthesized by self-assembly in solution or vapor phase, and steric hindrance or other types of interactions are not severe. The nanowires have a high crystallinity with less defects, resulting in high carrier mobility. Figure 26 shows the results of OFETs based on single-crystalline, self-assembled TIPS-PEN (28) grown from a solution.³¹³ The molecules are packed in such a way that the direction of π -stacking lies along the wire axis, as revealed by selected area electron diffraction (SAED). An average hole mobility of $0.75 \text{ cm}^2/(\text{V s})$ and a maximum mobility of $1.42 \text{ cm}^2/(\text{V s})$ were observed, which are higher than the mobility from thin films ($0.17 \text{ cm}^2/(\text{V s})$).³¹³

Single-crystal nanowires of HTP (29), grown in the [100] direction via recrystallization from a solution, showed a hole mobility as high as $0.27 \text{ cm}^2/(\text{V s})$ with an average of $0.11 \text{ cm}^2/(\text{V s})$. The mobility of a single nanowire is higher than in a network of nanowires

($0.042 \text{ cm}^2/(\text{V s})$) as well as in a thin film ($0.04 \text{ cm}^2/(\text{V s})$).³¹⁴ The effect of boundaries between crystalline domains has been implicated for the lower mobilities in thin films as well as in networks or bundles of nanowires.^{261,314,458} Such comparisons between OFETs based on nanowires and thin films have been made from other materials as well, showing that the nanowire devices generally have a higher carrier mobility. Peryloothiophene (PET) (54b) is a planar molecule that form crystalline nanowires via physical vapor transport.⁴⁵⁸ The PET (54b) showed a hole mobility of $0.3\text{--}0.8 \text{ cm}^2/(\text{V s})$ in a nanowire, whereas the value is $0.05 \text{ cm}^2/(\text{V s})$ in a thin film.⁴⁵⁸ Nanowires of another thiophene-acene oligomer Me-ABT (32) prepared by self-assembly had an average hole mobility of $0.85 \text{ cm}^2/(\text{V s})$ (maximum of $1.66 \text{ cm}^2/(\text{V s})$), which is about 4.7 times higher than in a thin film ($0.18 \text{ cm}^2/(\text{V s})$).³¹⁹ Crystalline nanowires of thiophene-fluorene oligomer F-T3-F (26) synthesized by nanolithography have a field-effect hole mobility of $5 \times 10^{-5} \text{ cm}^2/(\text{V s})$, which is ~ 10 and ~ 100 times higher than the mobilities in evaporated and spin-coated films, respectively.²⁶¹ F_{16}CuPc (53f) ($\mu_e = 0.2\text{--}0.6 \text{ cm}^2/(\text{V s})$) and CuPc (53a) ($\mu_h = 0.5\text{--}0.6 \text{ cm}^2/(\text{V s})$), nanoribbons grown by physical vapor transport^{450,452-454} were reported to have higher mobilities than thin films studied by others, whereas electron mobilities in PTCDI (35c) nanowires ($\mu_e = 0.027 \text{ cm}^2/(\text{V s})$) were lower than reported values in thin films.³²⁵

p-Type conjugated ladder oligomers exemplified by the tetra-phenyl bisindoloquinolines (TPBIQ) (61) is shown in Figure 27A.⁴⁴⁷ Single-crystals of TPBIQ (61) were initially grown by the physical vapor transport method. Charge transport properties of TPBIQ (61) microwires were investigated by directly growing the single crystals onto a substrate with source-drain electrodes by physical vapor transport as shown in Figure 27B. A field-effect hole mobility of $1.0 \text{ cm}^2/(\text{V s})$ in the saturation region was observed (Figure 27C). The growth of the single crystal was determined to be along the [001] direction which coincides with the short π - π stacking direction. Therefore, the measured carrier mobility was along c -axis direction which coincides with the long axis of the microwires.⁴⁴⁷ Similar carrier mobilities have been obtained in solution-phase grown nanowires of TPBIQ (61).

Nanoribbons of an anthracene derivative DPA (36b) have been studied in an OFET geometry, revealing a high field-effect hole mobility of $0.16 \text{ cm}^2/(\text{V s})$.³³⁵ Studies of molecular structures and charge transport properties in the 1D nanostructures of related anthracene derivatives with phenyl-ethynyl (BPEA) (36c), naphthalenyl-ethynyl (BNEA) (36d), and thiophenyl-ethynyl groups (BTEA) (36e) showed that small variations in molecular structure resulted in the change of molecular packing, and therefore the field-effect carrier mobility ($\mu_{h,\text{BPEA}(36c)} = 0.03\text{--}0.73 \text{ cm}^2/(\text{V s})$; $\mu_{h,\text{BNEA}(36d)} = 0.01\text{--}0.52 \text{ cm}^2/(\text{V s})$; and $\mu_{h,\text{BTEA}(36e)} = 1 \times 10^{-4} \text{ cm}^2/(\text{V s})$).⁵³⁰ Nano/microribbons of thiophene-based oligoacenes (30,31,32) assembled from solution were found to exhibit hole mobilities of $0.34\text{--}2.1 \text{ cm}^2/(\text{V s})$.³¹⁷⁻³¹⁹ Charge transport

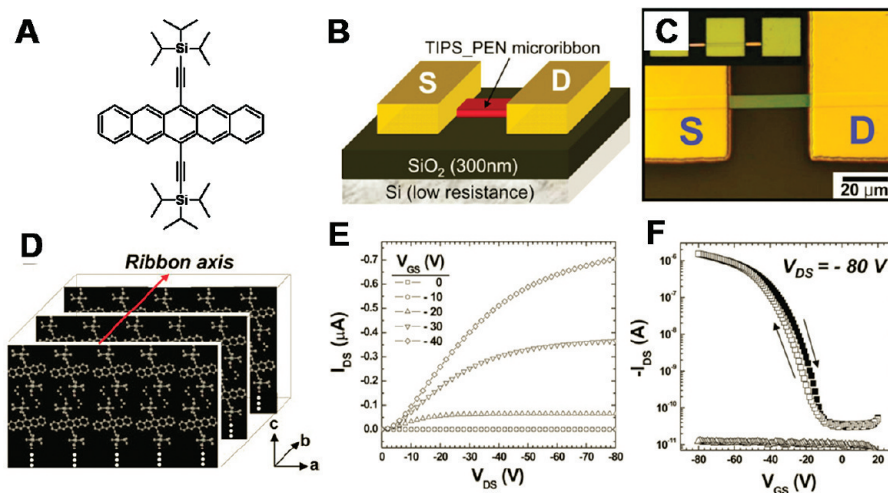


Figure 26. (A) Chemical structure of TIPS-PEN (**28**). (B, C) Schematic (B) and optical images (C) of microribbon transistor based on self-assembled TIPS-PEN (**28**). (D) Molecular packing motif of TIPS-PEN (**28**). (E, F) Output (E) and transfer (F) characteristics of a single microribbon transistor. Reprinted with permission from ref 313. Copyright 2007 Wiley-VCH.

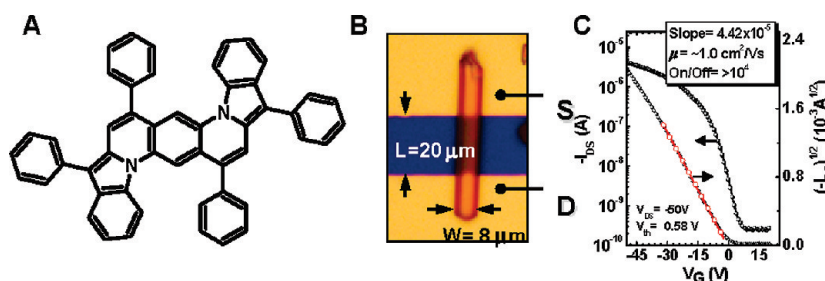


Figure 27. (A) Molecular structure of TPBIQ (**61**). (B) Optical micrograph image showing a single crystal bridging source-drain electrodes. (C) Transfer characteristic of TPBIQ (**61**) single crystal. Reprinted with permission from ref 447. Copyright 2008 American Chemical Society.

in a network of nanowires of thiophene-acene-vinylene oligomer (**50g**) showed an SCLC hole mobility of $3.1 \text{ cm}^2/(\text{V s})$ when nanowires were produced by drop-casting from a chlorobenzene solution and devices were tested in OFET geometry with a grounded gate voltage.⁴¹⁷ However, films of nanowires spin-casted from a solution gave a mobility of $0.11 \text{ cm}^2/(\text{V s})$ because of the less-ordered morphology.⁴¹⁷

Nanotubes of asymmetric hexa-peri-hexabenzocoronene (HBC) (**51a–f**) have interesting morphology of molecular self-assembly: nanotubes consist of a double-layer of closely packed HBC (**51a–f**) as a tube wall.^{529,531} The field-effect hole mobility in randomly oriented bundles of HBC (**51a–d**) nanotubes was 1.3×10^{-4} – $2.3 \times 10^{-4} \text{ cm}^2/(\text{V s})$ (higher with a shorter side-chain), whereas that in a thin film of unassembled HBC (**51a–d**) was $2.8 \times 10^{-6} \text{ cm}^2/(\text{V s})$. The low mobility in a network of nanotubes may be caused by short HBC (**51a–d**) nanotubes that resulted in frequent charge-carrier hopping across long side-chains of HBC (**51a–d**) molecules. In order to investigate the intrinsic mobility, time-resolved microwave conductivity (TRMC) measurements were also performed. The maximum mobility ($\phi\Sigma\mu$) was 9×10^{-4} – $2.4 \times 10^{-3} \text{ cm}^2/(\text{V s})$ (higher with longer side-chain).⁵²⁹ These results imply that the intratube charge transport is better in the HBC (**51a–d**) with longer side-chain, presumably due to the better packing of HBC (**51a–d**)

molecules. However, the intertube charge transport is limited by long side-chains on the HBC (**51a–d**) molecules.⁵²⁹ Balancing intra- and internanostructure transport is therefore critical to achieving a high carrier mobility.

3.2.3. Polymer Semiconductor Nanowires. The process of molecular ordering/crystallization is more complicated for conjugated polymers due to their long backbone chains and additional interactions caused by solubilizing side-chains. Nevertheless, polymer semiconductor nanowires suitable for charge transport studies have been prepared by solution-phase self-assembly, template-assisted synthesis, electrospinning, and nanolithography. Vapor-phase growth of nanowires, which tends to lead to more crystalline structures in small-molecules, is almost impossible for conjugated polymers. Among many polymer semiconductors, nanowires of P3HT and polythiophene derivatives (**4d–i,12**),^{46,121,219,228,229,248,264,378,379,383,532–535} PPE (**7j**),⁴³⁵ F8BT (**6c**),²⁶³ polyisocyanopeptides with PTCDI pendants (**46a–c**),^{411,412} and BBL (**27**)⁴⁰⁸ have been synthesized and their charge-transport properties have been investigated.

The charge-transport properties of solution-phase self-assembled P3AT (**4d–i**) nanowires have been intensively studied.^{46,369,370,378,379,383,532–534} Figure 28 shows a single-nanowire P3HT transistor and its OFET characteristics.³⁷⁹ Single nanowires of P3HT (**4f**) exhibit a field-effect hole mobility of 0.02 – $0.06 \text{ cm}^2/(\text{V s})$.^{378,379} Studies of the temperature dependence of the mobility in P3HT

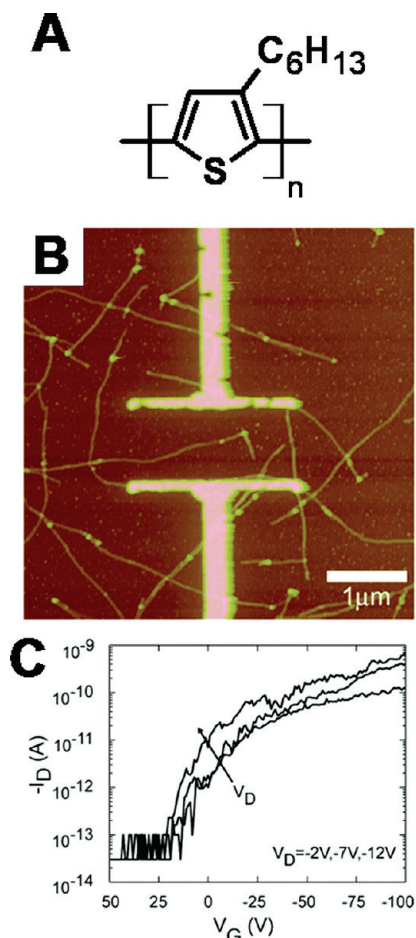


Figure 28. (A) Chemical structure of P3HT (**4f**). (B) AFM image of a single-nanowire P3HT (**4f**) transistor. (C) OFET transfer curves of the single-nanowire transistor. Reprinted with permission from ref 379. Copyright 2004 American Chemical Society.

(**4f**) nanowires showed that the charge transport mechanism could be interpreted from both multiple trap and release (MTR) and variable range hopping (VRH) models.³⁷⁹ Carrier mobilities in nanowires of P3ATs (**4d–i**) with various alkyl side-chain lengths have also been studied.⁵³⁴ The field-effect mobilities in the P3AT (**4d–i**) nanowires ($2\text{--}3 \times 10^{-3} \text{ cm}^2/(\text{V s})$) were found to be higher than those in corresponding thin films ($10^{-4}\text{--}10^{-3} \text{ cm}^2/(\text{V s})$). The field-effect mobilities in a network of P3AT (**4d–i**) nanowires (alkyl side-chain from butyl to nonyl) were independent of the length of side-chain, whereas the carrier mobility varied significantly in homogeneous thin films.⁵³⁴ However, SCLC measurements showed that the P3AT (**4d–i**) nanowires had lower carrier mobilities in the vertical direction than spin-coated thin films from solution. Similar to the field-effect mobilities, the SCLC mobilities were also independent of the length of side-chain.⁵³⁴ Compared with the field-effect mobility in a thin film, higher mobility in a network of nanowires was also observed from a PPE (**7j**) derivative.⁴³⁵ The nanowire network showed typical p-type field-effect charge transport with mobility as high as $0.1 \text{ cm}^2/(\text{V s})$, whereas a thin film of PPE (**7j**) showed a hole mobility of $1 \times 10^{-5} \text{ cm}^2/(\text{V s})$.⁴³⁵

In other studies, films of P3HT (**4f**) nanoribbons were found to have higher mobility ($0.012 \text{ cm}^2/(\text{V s})$) than films

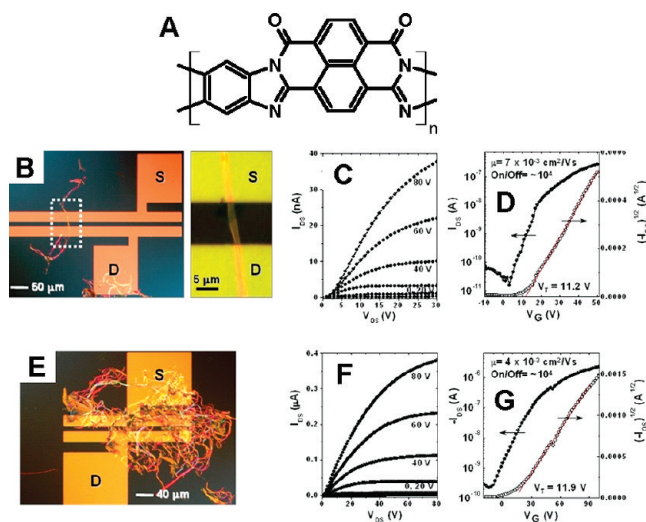


Figure 29. (A) Chemical structure of BBL (**27**). (B–D) Single-nanowire BBL (**27**) transistor: (B) optical images and the corresponding (C) output and (D) transfer characteristics of the single-nanowire transistor. (E–G) BBL (**27**) nanowire-network transistor: (E) an optical image, (F) output curves, and (G) transfer curves. Reprinted with permission from ref 408. Copyright 2008 American Chemical Society.

from solution ($1.7 \times 10^{-3} \text{ cm}^2/(\text{V s})$).³⁸⁰ The self-assembled P3HT (**4f**) nanowires were embedded into an insulating matrix by blending, again showed a higher field-effect mobility ($4\text{--}6 \times 10^{-3} \text{ cm}^2/(\text{V s})$) than blend thin films of P3HT (**4f**) and polystyrene ($7 \times 10^{-4} \text{ cm}^2/(\text{V s})$).⁵³⁵ It should be noted that single-crystalline nano/microwires based on P3HT (**4f**) have been synthesized from solution, however, the charge-carrier mobility was not reported.⁵³⁶

BBL (**27**) is one of few air-stable n-type polymer semiconductors.⁵³⁷ Charge transport of BBL (**27**) nanowires synthesized by self-assembly have been studied by fabricating and testing OFET devices from a single nanowire as well as a network of nanowires (Figure 29).⁴⁰⁸ BBL (**27**) has also shown higher mobilities in nanowires than in thin films. A single nanowire and a network of nanowires have an electron mobility of $7 \times 10^{-3} \text{ cm}^2/(\text{V s})$ and $4 \times 10^{-3} \text{ cm}^2/(\text{V s})$, respectively, whereas the mobility of BBL (**27**) film is $1\text{--}2 \times 10^{-3} \text{ cm}^2/(\text{V s})$. Unlike the self-assembled P3HT (**4f**) nanowires, the BBL (**27**) molecules were aligned along the nanowire revealed by electron diffraction.⁴⁰⁸

Polyisocyanopeptides with perylene diimide (PTCDI) as a pendant (**46a–c**) are known to self-assemble into nanowires.^{410–412} As expected from the PTCDI pendants stacked to each other along the nanowire, this polymer also transport electrons.^{411,412} The field-effect mobility of electrons in the nanowires are on the order of $1 \times 10^{-4} \text{ cm}^2/(\text{V s})$.⁴¹¹ When blended with molecular PTCDI the polymer nanowires have shown to bridge crystalline domains of PTCDI molecules, enhancing the charge transport properties compared with homogeneous PTCDI films.⁴¹²

The charge-transport properties of polymer semiconductor nanowires synthesized by electrospinning, template-assisted methods, and nanolithography have also been investigated. Field-effect hole mobilities of $0.017\text{--}0.03 \text{ cm}^2/(\text{V s})$ are reported for electrospun nanofibers of pure P3HT (**4f**)^{228,229,248} deposited on silicon dioxide as

a dielectric layer, whereas 4.7×10^{-4} – 2×10^{-3} cm²/(V s) was seen in a nanofiber from P3HT (**4f**) blends with polyethylene oxide (PEO) or poly(ϵ -caprolactone) (PCL).^{228,248} From nanofibers of P3HT (**4f**) and PCL blends, very high hole mobility (2 cm²/(V s)) was also reported when deposited on an ion-gel gate dielectric.⁵³⁸ Similarly, a field-effect mobility of 5×10^{-6} to 5×10^{-4} cm²/(V s) was observed in a mat of P3HT (**4f**)/MEHPPV (**3b**) blend nanofibers on an inorganic substrate.²¹⁹ The P3HT (**4f**)/MEHPPV (**3b**) blend nanofibers showed an exponential dependence of hole mobility on blend composition, having higher mobility with more P3HT (**4f**). The OFET channels were not fully covered by the mat of nanofibers and thus the actual mobility of the nanofibers can be $\sim 1 \times 10^{-3}$ cm²/(V s) after correction of the channel area.²¹⁹ A diode based on electrospun P3HT (**4f**) and SnO₂ nanofibers has exhibited rectification ratios of ~ 25 , demonstrating feasibility of electrospun nanofibers for a hybrid p-n junction diode.²²⁸ P3HT (**4f**) nanowires synthesized in anodic aluminum oxide (AAO) templates were a subject of SCLC studies.¹²¹ The highest hole mobility of 6×10^{-3} cm²/(V s) which is 20 times higher than that of a neat film was observed from nanowires synthesized through a template with a pore size of 75 nm. Alignment of long P3HT (**4f**) chains in the confined structures and the screening effect of the dielectric have been attributed for the increase in mobility.¹²¹

Nanoimprinted polymer semiconductors have periodic one-dimensional nanostructures. A liquid crystalline (LC), ambipolar charge-transport polymer, F8BT (**6c**), tends to have their backbones (*c*-axis) aligned along the grooves of the master, resulting in anisotropy of absorption and emission as well as charge transport.²⁶³ The field-effect mobilities of electrons and holes along the nanowire directions are ~ 2 times larger than those in homogeneous thin films, whereas those in perpendicular direction are an order of magnitude lower, resulting in anisotropic ratio of 5–15.²⁶³ Another LC conjugated polymer, PQT12 (**12**), had the π -stacking direction (*b*-axis) along the trenches.²⁶⁴ Charge-carrier mobility in the arrays of PQT12 (**12**) nanowires was 1.7 times larger than in homogeneous thin films. The PQT12 (**12**) nanowires aligned in parallel to the OFET source/drain electrodes showed no electrical conduction, suggesting that the nanowires were isolated.²⁶⁴

These studies of charge-transport properties in polymer nanowires imply that organic nanowires are very effective approaches to high charge-carrier mobility that is hardly achieved from thin film processing of organic molecules. Increased charge-carrier mobility in polymer semiconductor nanowires is considered one of the reasons for the reported enhanced performance in nanowire-based bulk heterojunction polymer solar cells as exemplified by studies of P3BT (**4d**) nanowires.^{46,532,533} The combination of high carrier mobility in organic semiconductor nanowires with the unique optoelectronic properties of organic semiconductors may also offer realization of building

blocks for nanoelectronic devices. Furthermore, the intrinsic properties and mechanism of charge transport in organic semiconductors can be revealed by the in-depth studies based on such well-ordered molecular solids.

3.3. Photoconductivity. Photoconductivity in a material arises if the electrical conductivity under illumination is enhanced relative to the dark conductivity. It can be an important platform for investigating various photoelectronic phenomena such as charge photogeneration mechanisms, carrier dynamics, and nature of electrical contacts as well as a basis for developing photodetectors, phototransistors, and photovoltaic devices.^{539,540} We defer a discussion of the photovoltaic properties and applications of organic semiconductor nanowires to section 3.6. Here, we briefly discuss the photoconductive properties of a few selected 1D organic semiconductor nanostructures, including the demonstration of promising nanowire photodetectors and phototransistors. The organic semiconductor nanowires investigated include assemblies of F8T2 (**6b**),¹²⁷ F₁₆CuPc (**53f**),⁵⁴¹ TPPS (**44a**),³⁵⁷ PTCDI derivatives (**35l,m**),³³¹ a thiophene-acene oligomer Me-ABT (**32**),³¹⁹ and HBC derivatives (**51a,e,f**).⁵³¹

The photoconductivity of a single nanowire of F8T2 (**6b**), with diameters of 200 nm produced by AAO templated synthesis, has been studied by illuminating with a 40 W/cm² of 405 nm light through a near-field scanning optical microscope.¹²⁷ Current–voltage measurement with and without continuous illumination as well as with periodic switching of the light showed that photoresponse of the current is reversible. The photocurrent (I_{ph}) and dark current (I_{dark}) were about 200 pA and 50 pA, respectively, at a bias of -40 V. The measured responsivity ($R_{\text{res}} = I_{\text{ph}}/[\text{radiant flux}]$) of the single F8T2 (**6b**) nanowire was 0.4 mA/W, which is comparable to the published values for inorganic semiconductor nanowires (InP and ZnO) at low voltage bias.¹²⁷ Nanoribbons of F₁₆CuPc (**53f**) grown by vapor transport have been studied as photoswitches and phototransistors under illumination of white light (0.37–5.76 mW/cm²), taking advantages of the photoconductivity of F₁₆CuPc (**53f**).⁵⁴¹ Simple photoswitches in which voltages were applied between source and drain showed a photoconductivity gain ($I_{\text{ph}}/I_{\text{dark}}$) of 10–100 with good reversibility. As the gate voltage was applied, turning the devices into phototransistors, the photoconductivity gain became as high as 1×10^5 at $V_{\text{gs}} = -6$ V. The photoconductive gain of the phototransistors varied from 1×10^2 to 1×10^5 depending on the width, length, and thickness of the conductive channel. Nevertheless, the phototransistors had a higher photoconductive gain than the photoswitches, because of the efficient dissociation of photogenerated excitons under the applied gate field.⁵⁴¹ Phototransistors of Me-ABT (**32**) microribbons exhibited a responsivity of 1.2×10^4 A/W and $I_{\text{ph}}/I_{\text{dark}}$ of 6×10^3 at illumination power density of 30 $\mu\text{W}/\text{cm}^2$, $V_{\text{ds}} = -80$ V, and $V_{\text{gs}} = -18$ V.³¹⁹ For comparison, a thin film phototransistor of Me-ABT (**32**) exhibited an R_{res} of 477 A/W and $I_{\text{ph}}/I_{\text{dark}}$ of 4×10^3 at $V_{\text{ds}} = -100$ V, and $V_{\text{gs}} = 12$ V.³¹⁹

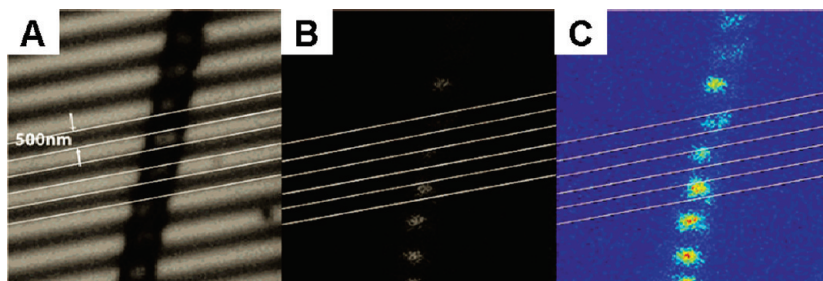


Figure 30. (A–C) Electroluminescence from a single electrospun nanofiber of $[\text{Ru}(\text{bpy})_3]^{2+}(\text{PF}_6^-)_2$ (**21**) embedded in PEO: (A) Bright-field image of a nanofiber crossing multiple electrodes with 500 nm gaps. (B) Emission from the fiber imaged under driving voltage of 4 V. (C) Pseudocolored image of B. Reprinted with permission from ref 227. Copyright 2007 American Chemical Society.

The photoconductivity of self-assembled nanotubes and nanofibers of asymmetric HBCs (**51a–f**) decorated with an electron accepting unit has been studied.⁵³¹ Attachment of the trinitrofluorenone (TNF) group to HBC resulted in a donor–acceptor (D–A) architecture (**51e,f**), which facilitated photoinduced charge separation. Monosubstituted HBC (**51f**) assembled into nanotubes with a diameter of 16 nm and a wall thickness of 3 nm, whereas the disubstituted HBC (**51e**) showed aggregates under the same conditions. Under illumination (wavelength = 300–650 nm), the monosubstituted HBC (**51f**) nanotubes exhibited a linear dependence of photocurrent on the power density of the irradiation from 0.55 to 15 W/cm². Under 7 W/cm² of power density and 2 V applied bias, a photocurrent (I_{ph}) of 4.2 nA and dark current (I_{dark}) of 0.07 pA were observed, resulting in a large photoconductivity gain of 6×10^4 .⁵³¹ The charge photogeneration follows an extrinsic mechanism, involving D and A moieties of the molecule. Unlike the nanotubes of D–A HBC (**51e,f**), nanofibers of the D–A HBC (**51e,f**) and nanotubes of non-D–A HBC (**51a**) did not show any significant photocurrent under illumination, suggesting that the electron transfer between D and A moieties in the modified HBC (**51f**) facilitates the photocurrent generation and the spatially separated D and A domains in the nanotubes prevents rapid recombination of photogenerated charge carriers.⁵³¹

3.4. Organic Light-Emitting and Field-Emission Devices.

Current organic light-emitting diodes (OLEDs) for large-area display and solid-state lighting applications are essentially 2D homogeneous thin film devices.²⁴ Efficient exciton fluorescence and phosphorescence in amorphous thin films of organic/polymer semiconductors have been extensively investigated and exploited in such OLEDs.^{26–28} There has been only limited studies of OLEDs based on organic semiconductor nanowires.^{475,542} It is not clear that there are potential benefits for incorporating fluorescent or phosphorescent nanowires or nanoribbons of organic semiconductors into conventional large-area OLEDs. Indeed, there may be drawbacks of inhomogeneous charge injection and emission. However, heterostructured nanowires of organic semiconductors could be excellent building blocks toward the realization of novel nanoscale light sources for potential applications in subwavelength near-field optical microscopy, nanolithography, and optical data storage.^{543,544}

OLEDs fabricated from an emissive layer of Alq_3 (**24**) nanowires made via a physical vapor transport have shown that the current density and electroluminescent (EL) intensity of the devices are dependent on the width of nanowires.⁴⁷⁵ Light-emitting diodes based on PTCDI (**35k**) nanoclusters grown by vapor deposition on ZnO nanorods with a nonconventional geometry have been demonstrated to achieve white EL emission, which is different from the photoluminescence (PL) of the parent materials ZnO and PTCDI (**35k**).⁵⁴² Brightness and efficiency of the device were not reported. Electrically driven light-emitting nanofibers have been synthesized by electrospinning of ruthenium complex ions embedded in poly(ethylene oxide) (PEO) (Figure 30). The nanofibers of $[\text{Ru}(\text{bpy})_3]^{2+}(\text{PF}_6^-)_2$ (**21**)/PEO blends with a diameter ranging from 150 nm to 5 μm deposited onto interdigitated gold electrodes emitted visible light under applied electric potential.²²⁷ Detectable emission from a cross-sectional area of $240 \times 325 \text{ nm}^2$ was observed through a charge-coupled device (CCD) at 3.2 V and naked eyes at 4 V. The maximum emission wavelength was 600 nm from such a small area, suggesting that the nanofibers can be used as a subwavelength point source.²²⁷

Nanopatterned OLEDs based on F8BT (**6c**) have also been reported.²⁶³ By using nanoimprinting, 1D grooves with a periodicity of 100 nm were formed. The liquid crystalline nature of F8BT (**6c**) made the polymer backbones aligned along the grooves. The F8BT (**6c**) films showed not only polarized PL, but also polarized EL when sandwiched between PEDOT/ITO and Ca/Al electrodes. The polarization ratio of EL was 11.²⁶³

Conducting polymer nanowires, such as PEDOT (**5**), PPV (**3a**), and PPy (**2**), synthesized by AAO templates have been demonstrated as the nanotip emitters of field-emission.¹¹⁰ For example, a turn-on field of 3.5–4 V/ μm was observed in PPy (**2**) nanowires.¹¹⁰ Alq_3 (**24**) nanowires synthesized by the vapor transport method were also shown to exhibit efficient field-emission.^{472,475} The Alq_3 (**24**) nanowire field-emitters (with diameters of 40–80 nm) were shown to have a turn-on electric field of 8.5–10.3 V/ μm .^{472,475} Stability test showed that the emission current density degraded drastically in the initial 1000 s and then remained steady at $\sim 3 \text{ mA/cm}^2$, demonstrating their ability to maintain a stable emission from Alq_3 (**24**) nanowires.⁴⁷²

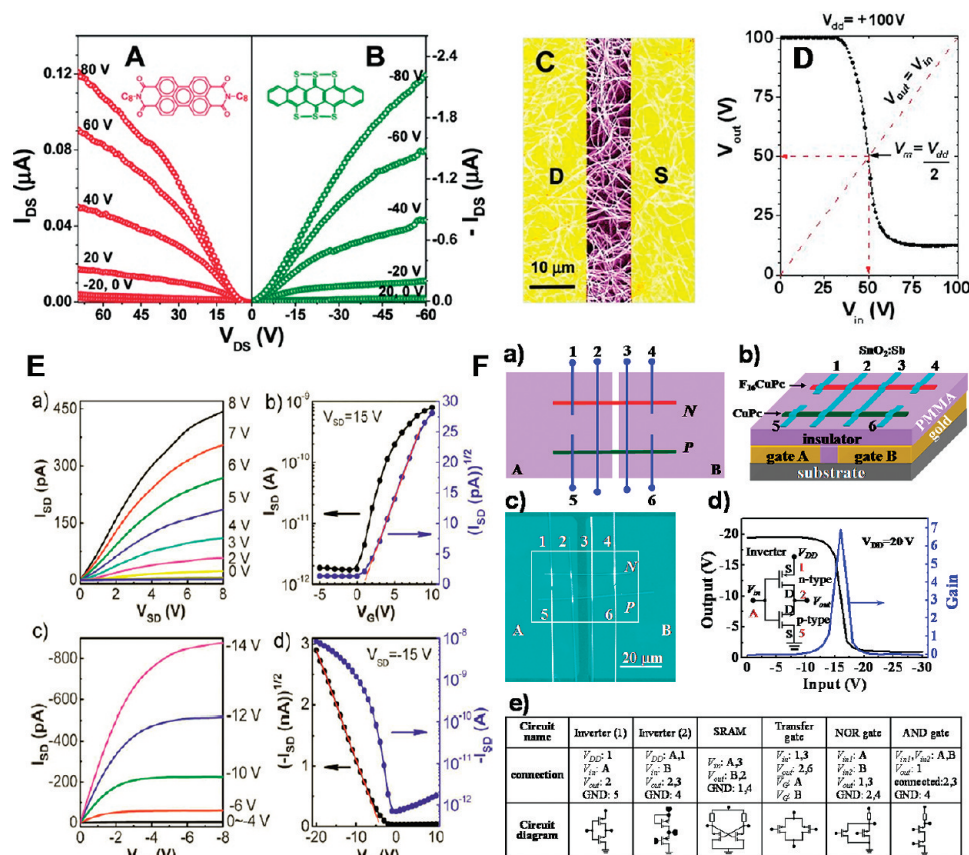


Figure 31. (A–D) Nanowire transistors and complementary circuits based on PTCDI (35c) and HTP (29): output characteristics of (A) PTCDI (35c) and (B) HTP (29) nanowire transistors; (C) a colorized SEM images of a PTCDI (35c) transistor; and (D) a voltage transfer characteristic of a complementary inverter. Reprinted with permission from ref 325. Copyright 2007 American Chemical Society. (E, F) Nanowire transistors and complementary circuits based on F₁₆CuPc (53f) and CuPc (53a): (E) output and transfer characteristics of (a, b) F₁₆CuPc (53f) and (c, d) CuPc (53a); and (F) (a, b) schematic diagrams, (c) a colorized SEM image, (d) voltage transfer characteristics of an inverter, and (e) circuit diagrams of complementary circuits. Reprinted with permission from ref 454. Copyright 2009 Wiley-VCH.

3.5. Nanoscale Field-Effect Transistors and Nanoelectronics. The field-effect transistor is one of the most basic building blocks in electronics and nanoelectronics. Among the desirable properties of organic field-effect transistors (OFETs) for practical applications include high charge-carrier mobilities, large on/off current ratios, and threshold voltages close to zero. As previously discussed in section 3.2, charge-carrier mobilities in organic semiconductor nanowires can be one to 3 orders of magnitude larger compared to 2D polycrystalline thin films. There has thus been a growing interest in developing high performance field-effect transistors and electronic circuits from highly crystalline organic semiconductor nanowires.³³³ For small-molecule organic semiconductors, p-channel nanowire OFETs have been produced from TIPS-PEN (28) (Figure 26),³¹³ HTP (29),^{314,325} F-T3-F (26),²⁶¹ PET (54b),⁴⁵⁸ HBC (51a–d,g),^{420,529} thiophene-based oligoacenes (30,31,32),^{316–319} CuPc (53a),^{450,453,454} and TPBIQ (61),⁴⁴⁷ and n-channel nanowire OFETs were realized with PTCDI (35b,c,e)³²⁵ and F₁₆CuPc (53f).^{452,454} In the case of polymer semiconductors, nanowires of p-type P3HT (4f) (Figure 28) and P3ATs (4d–i),^{46,219,228,229,248,378,379,383,402,532,534,535} PQT12 (12),²⁶⁴ PANI (1),^{211,266} and PPY (2),²⁶⁶ ambipolar F8BT (6c),²⁶³ and n-type BBL (27) (Figure 29)⁴⁰⁸ and PTCDI-containing

polymers (46a–c)^{411,412} have been synthesized and utilized to construct nanowire OFETs.

Complementary inverters were successfully demonstrated by incorporating p-channel HTP (29) and n-channel PTCDI (35b,c,e) nanowire OFETs in a circuit (Figure 31A–D).³²⁵ Single nanowires of n-type F₁₆CuPc (53f) and p-type CuPc (53a) in combination with conductive nanoelectrodes have also been used to demonstrate complementary inverter circuits.⁴⁵⁴ In this case, more complicated logic gates, such as SRAM, transfer gates, and NOR and AND gates, were also demonstrated by changing voltages at the terminals, as shown in Figure 31E,F. The balanced and high mobilities of electrons and holes in such complementary inverters thus allowed digital logic circuits with good switching characteristics to be observed.

Although these are exciting developments in nanoscale organic semiconductor devices, there are important challenges to address in order to fully realize the potential of organic nanoelectronics. First, facile and high-throughput methods for aligning, positioning, and addressing an individual nanowire and bundles of nanowires have to be developed for producing the nanodevices and assembling them into circuits. Only limited methods have been applied to the alignment and addressing of nanowires

without manual positioning.^{160,215,216,267,268,326} Second, it is also very important to have reliable performance from the single-nanowire devices. With these challenges tackled, organic semiconductor nanowires with high charge-carrier mobility have a great potential to lead to low-cost, high-performance nanoelectronic devices and other nanotechnologies.

3.6. Organic Photovoltaics. Organic photovoltaics (OPVs) based on conjugated small-molecule, oligomer, and polymer semiconductors are emerging as very promising low-cost, large-area, and lightweight approaches to efficient solar energy conversion.^{39–45,53} Numerous recent reviews have been published on the large, exponentially growing, literature on OPVs.^{39–45,53} Our objective here is to focus on recent work exploring 1D organic semiconductor nanostructures in OPVs and thereby to highlight the potential advantages of such nanomaterials both for fundamental studies of photon-to-electric conversion processes in organic semiconductors and for developing more efficient solar cells.

Light absorption in organic semiconductors creates excitons with large binding energies (ca. 0.4–1.0 eV)^{545–548} unlike silicon and other bulk inorganic semiconductors in which photoexcitation essentially produces free charge carriers directly.⁵⁴⁹ In organic solar cells, efficient photogeneration of free charge carriers thus requires dissociation of excitons at a heterojunction or an interface between a p-type organic semiconductor and an n-type one with a sufficient energy band offset (e.g., difference in electron affinities and/or ionization potentials). A major consequence of the requirement of such a p/n interface or heterojunction for efficient photoconversion in OPV cells, dye-sensitized solar cells (DSSCs), and in general all excitonic solar cells,⁵⁵⁰ is that they are intrinsically nanostructured systems defined by the exciton diffusion length. The bulk heterojunction (BHJ) OPV cell, consisting of a binary blend or composite of a p-type (donor) polymer and an n-type material (acceptor), was introduced in 1995 as a way to address the problem of small exciton diffusion lengths ($L_d = 5–20$ nm) in thin films of organic/polymer semiconductors.^{551,552} The photovoltaic efficiency of the best BHJ OPV cells now stands at 5–8% PCE as a result of progress in developing new organic semiconductor light absorbers and device fabrication processes since then.^{553–555} Fiber-based OPV devices,^{556–559} which were recently introduced as an alternative to the planar BHJ solar cell, represent a unique 1D device architecture that could also benefit from advances in organic semiconductor nanostructures.

Further advances in increasing the power conversion efficiency (PCE) of OPV cells toward 10–15% requires both innovations in p-type and n-type organic semiconductors and device architectures at the nanoscale as well as a better understanding of the underlying photoconversion processes, balanced charge transport, and energy transfer also at the nanoscale. In this respect, 1D nanostructures of p-type and n-type organic semiconductors are attractive candidates for OPV basic studies and applications. The substantially larger exciton diffusion

length in crystalline organic semiconductor nanowires (up to 100–1000 nm)^{498,502,503,511} compared to thin films could improve light-harvesting and charge-photogeneration processes. The many other potential advantages of organic semiconductor nanowires for BHJ solar cells and other OPV applications include (i) a rational control of the BHJ morphology; (ii) the polymer nanowires with widths of 10–50 nm and lengths of micrometers have sizes that are perfectly matched to the exciton diffusion lengths; (iii) ultralarge donor/acceptor interfacial area for efficient exciton dissociation; (iv) an electrically bicontinuous morphology is achieved a priori; (v) high carrier mobilities and high absorption coefficient are achievable because of the high crystallinity of the self-assembled nanowires; (vi) ease of production of devices on plastic substrates and scalability to large areas; and (vii) avoids the difficulties of blend phase-separation phenomena, including domain coarsening and time-dependent instability. Moreover, organic/polymer nanowires could be combined with inorganic nanowires and/or nanoparticles to create various hybrid BHJ solar cells.

Our group and others have used nanowires of p-type polymer semiconductors in conjunction with fullerene derivatives as acceptors to construct efficient BHJ solar cells.^{46,383,389,395,532,533,560–562} Because of the ready solution-phase assembly of poly(3-alkylthiophene)s (P3ATs) nanowires, which combine ideal dimensions (ca. 10–50 nm widths and 1–10 μ m lengths) with high crystallinity, high carrier mobilities, good dispersibility in organic solvents, and favorable optical absorption spectra, they have been the most widely studied. P3BT (**4d**) nanowires have been successfully used to demonstrate an order of magnitude enhancement in photovoltaic efficiency (up to 3.5% PCE) compared to conventional P3BT thin film BHJ devices.^{46,532,533} The highly crystalline P3BT (**4d**) nanowires have average widths of 10–15 nm, length of 5–10 μ m, and therefore an aspect ratio (length/width) of 333–1000. The nanowires can be either “preformed” separately and then blended with PCBM (**20b**)⁴⁶ or grown in situ in P3BT (**4d**)/PCBM (**20b**) blends⁵³² to make the active layers in BHJ solar cells. Nanowires prepared by either method have an interconnected network surrounded by a continuous PCBM (**20b**) phase, and this quasi-bicontinuous nanoscale morphology is beneficial to the charge photogeneration and transport. The mobility of holes in the blend thin films of P3BT (**4d**) nanowires and PCBM (**20b**) was 2 orders of magnitude higher than that of P3BT (**4d**)/PCBM (**20b**) blend thin films as measured from OFET.⁴⁶

Solution-phase assembled nanowires of other P3ATs have similarly been used to prepare nanostructured BHJ OPV cells with good control of the nanoscale morphology.^{383,389,395,560,561} In the case of P3HT (**4f**) nanowires/PCBM (**20b**) devices,^{389,395,560} the performance was comparable to but did not exceed conventional P3HT (**4f**)/PCBM (**20b**) blend thin-film solar cells. Similar results were obtained in BHJ devices constructed from P3PT (**4e**) nanowires and conventional blend thin films. Preassembled P3HT (**4f**) nanowires were blended with F8BT

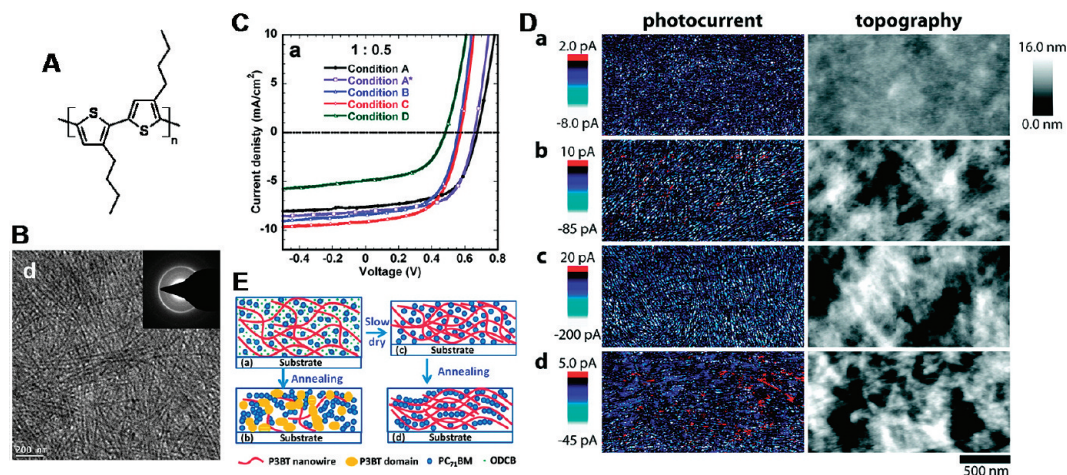


Figure 32. (A) Chemical structure of P3BT (**4d**). (B) Bright-field TEM and corresponding electron diffraction images of P3BT (**4d**) nanowires. (C–E) Solar cells based on P3BT (**4d**) nanowires blended with PC₇₁BM (**20c**): (C) Photovoltaic properties of the solar cells fabricated from different conditions. (D) Photoconductive AFM images of the film processed under same conditions in panel C. (E) Illustration of drying process of blend of P3BT (**4d**) nanowires and PC₇₁BM (**20c**). Reprinted with permission from ref 533. Copyright 2010 American Chemical Society.

(**6c**) to investigate the role of polymer nanowires in the control of morphology in all-polymer blend solar cells.⁵⁶¹ In this case, the nanowire-based devices were more efficient than the optimized thin film devices, predominantly because of the 10 times improvement in short circuit current density, which in turn originated from enhancement in optical absorption and charge transport.

The well-controlled morphology of polymer semiconductor nanowire-based BHJ solar cells has allowed a detailed systematic characterization of the film morphology, charge transport and photovoltaic properties of such OPV cells at the bulk and at the nanoscale.^{533,562} The latter measurements, including conductive and photoconductive atomic force microscopy (cAFM and pcAFM) imaging of P3BT (**4d**) nanowires/PCBM (**20b**) (Figure 32), have allowed the mapping of photocurrent distributions in the nanostructured solar cells.⁵³³ The results show direct correlations between the evolution of the nanowire network and the device performance. In addition, the changing local photovoltage (V_{oc}) measured via pcAFM provided evidence of how nanostructure determines the intensity-dependent open-circuit voltage in OPV cells.

Nanowires of p-type polymer semiconductors fabricated by means of other techniques, such as AAO templates⁵⁶³ and lithography,^{286–288} have also been explored in bulk heterojunction (BHJ)-OPV cells. Ordered P3HT (**4f**)-PCBM (**20b**) core-shell nanorods arrays were fabricated using AAO templates and used in solar cells.⁵⁶³ These composite nanorods were synthesized by melt-assisted wetting of the AAO templates, and a photovoltaic efficiency of up to 2.0% PCE was reported.⁵⁶³ Nanostructured solar cells with interdigitated donor/acceptor domains were fabricated by nanoimprint lithography.²⁸⁸ The devices were built on flexible ITO-coated plastic substrates, where a polythiophene derivative (**25a**) was spin-coated. After an imprinting process using a preformed stamp followed by thermal conversion to insoluble form, the PCBM (**20b**) electron acceptor was

spin-coated to complete the active layer. Two different grating molds with a depth of 200 nm and a periodicity of 510 and 700 nm were used as stamps to fabricate two sets of solar cells, and a planar-junction bilayer device was also made as the control cell. Enhancement of 2.64–3.20 times PCE was observed in the nanostructured solar cells compared with the control cell.²⁸⁸ The increment seen was attributed to the increase in short-circuit current density (J_{sc}) and fill factor (FF) because of the enlarged donor/acceptor interfacial area. A highest of 0.80% PCE was achieved.²⁸⁸

Organic BHJ solar cells comprising nanostructured P3HT (**4f**) and PTCDI (**35e**) were fabricated with features as small as 50 nm and aspect ratios of up to 2, leading a 2.5 times enhancement in efficiency compared with planar junction devices.²⁸⁶ Large-scale high-density (10^{10} /cm²) polymer nanopillars, fabricated using a combination of AAO template method and nanoimprint lithography, have been demonstrated for solar cell applications.²⁸⁷ To achieve this, an AAO membrane was first prepared and used as a mask for a two-step plasma etching process to produce a silicon mold with patterned pores that are 50–80 nm wide and 100–900 nm deep.²⁸⁷ Ordered P3HT (**4f**) nanopillars were fabricated by nanoimprint lithography using the mold, and PCBM (**20b**) was deposited on top of the P3HT (**4f**) to make the BHJ active layer. An efficiency of 2.57% was obtained in the nanoimprinted solar cells, which represented an almost 2 fold increase compared with the bilayer devices (1.44%).²⁸⁷

Although highly crystalline 1D nanostructures of several classes of n-type organic semiconductors have been grown and their optical and charge transport properties widely investigated,^{324–331,408,412,414,452} few have so far been explored in OPV applications. Blends of n-type PTCDI (**35f**) and p-type HBC (**51m**) showed nanorod-like thin film morphology and as the active layer in BHJ solar cells under 0.47 mW/cm² illumination of a single wavelength (490 nm) gave a photovoltaic efficiency of 1.95% PCE.⁵⁶⁴ Nanoribbons (width = 100–200 nm,

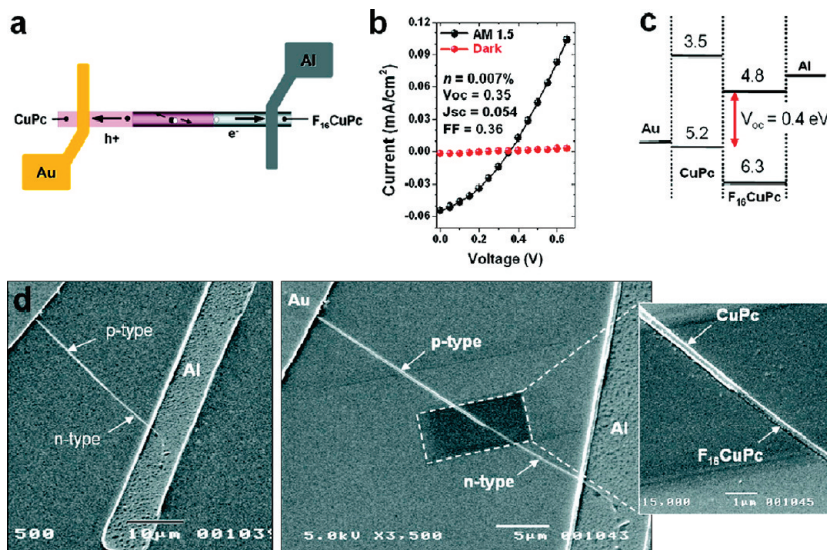


Figure 33. Organic nanowire solar cell based on single-crystalline CuPc (**53a**) and F₁₆CuPc (**53f**). CuPc (**53a**) and F₁₆CuPc (**53f**) were deposited by physical vapor transport and deposition. Reprinted with permission from ref 456. Copyright 2010 American Chemical Society.

length = several micrometers) of PTCDI-C8 (**35c**), prepared by solution-phase self-assembly in chloroform/methanol, were recently used in place of fullerene derivatives to make bulk heterojunction (BHJ) solar cells with the p-type conjugated polymers MDMOPPV (**3e**) and P3HT (**4f**).⁵⁶⁵ Quenching of photoluminescence (PL) in the n-type nanowire/p-type polymer composite thin films suggested photoinduced charge transfer. The PTCDI-C8 (**35c**)/MDMOPPV (**3e**) and PTCDI-C8 (**35c**)/P3HT (**4f**) BHJ solar cells had a photovoltaic efficiency of 0.92% PCE and 1.03% PCE, respectively, with photovoltages of 0.50–0.65 V and photocurrents of 3.75–4.60 mA/cm².⁵⁶⁵ The performance of these PTCDI-C8 (**35c**) nanowire-based OPV cells is modest probably because of the still much larger lateral sizes of the nanoribbons compared to the exciton diffusion length.

Recently, an OPV cell consisting of a single-nanowire p/n heterojunction based on CuPc (**53a**) and F₁₆CuPc (**53f**) was demonstrated (Figure 33).⁴⁵⁶ The p/n heterojunction nanowires were produced by using physical vapor transport and deposition of CuPc (**53a**), followed by the deposition of F₁₆CuPc (**53f**) from the same technique. Pregrown single-crystalline CuPc (**53a**) nanowires acted as epitaxial crystallization sites of F₁₆CuPc (**53f**).⁴⁵⁶ The p/n heterojunction nanowire solar cell, finished with gold and aluminum electrodes to collect charges, showed a J_{sc} of 0.054 mA/cm², V_{oc} of 0.35 V, and FF of 0.36, yielding a PCE of 0.007%.⁴⁵⁶ Although the photovoltaic efficiency is low, the p/n heterojunction nanowires constitute an interesting model system for fundamental studies of the photovoltaic properties of nanostructured organic semiconductors.

It is obvious that nanowires of poly(3-alkylthiophene)s (P3ATs) of various alkyl side chain lengths have been the most investigated in OPV cells so far. There is clearly a need to explore nanowires of other classes of p-type polymer semiconductors especially the emerging small band gap donor–acceptor copolymers^{553,554} which have

known improved thin-film photovoltaic properties compared to P3ATs. Because very little has been done so far, even greater opportunities exist in investigating the preparation, properties, and OPV applications of n-type organic/polymer semiconductors.

3.7. Sensors and Biosensors. There is a large and growing literature on the use of π -conjugated semiconducting and conducting polymers, as isolated molecules, assemblies, or thin films, in developing diverse sensors for chemical and biochemical analytes ranging from simple gases, organic vapors, explosives, ions in solution, glucose, DNAs, and proteins to viruses.^{485,566–570} Different aspects of this literature have been covered in several reviews.^{481,566–568} Our objective here is to briefly review aspects of chemical- and biosensors based on 1D nanostructures of π -conjugated molecules and polymers, and thereby to highlight the great potential of this class of 1D nanostructures for creating new sensor concepts and technologies.

1D nanostructured semiconductors, in general, are thought to offer great opportunities for developing ultra-sensitive and fast-responding chemical-/biosensor technologies by virtue of their large surface-area-to-volume ratios.^{225,334,485,568–570} However, the primary research focus has been on silicon/inorganic nanowires and carbon nanotubes (CNTs).^{568–570} We believe that organic semiconductor nanowires merit increasing interest in this area given that: (i) their conductivity can be modulated over 10–15 orders of magnitude; (ii) the dramatically increased exciton and charge carrier diffusion lengths and mobilities in 1D nanostructures compared to thin films; (iii) their ready chemical- or biochemical functionalization with receptors to impart selectivity; (iv) the huge potential for tunability of their optical, electronic, optoelectronic, and mechanical properties, which are essential for optimizing the sensors; and (v) the potential low cost in developing and deploying sensors based on this platform.

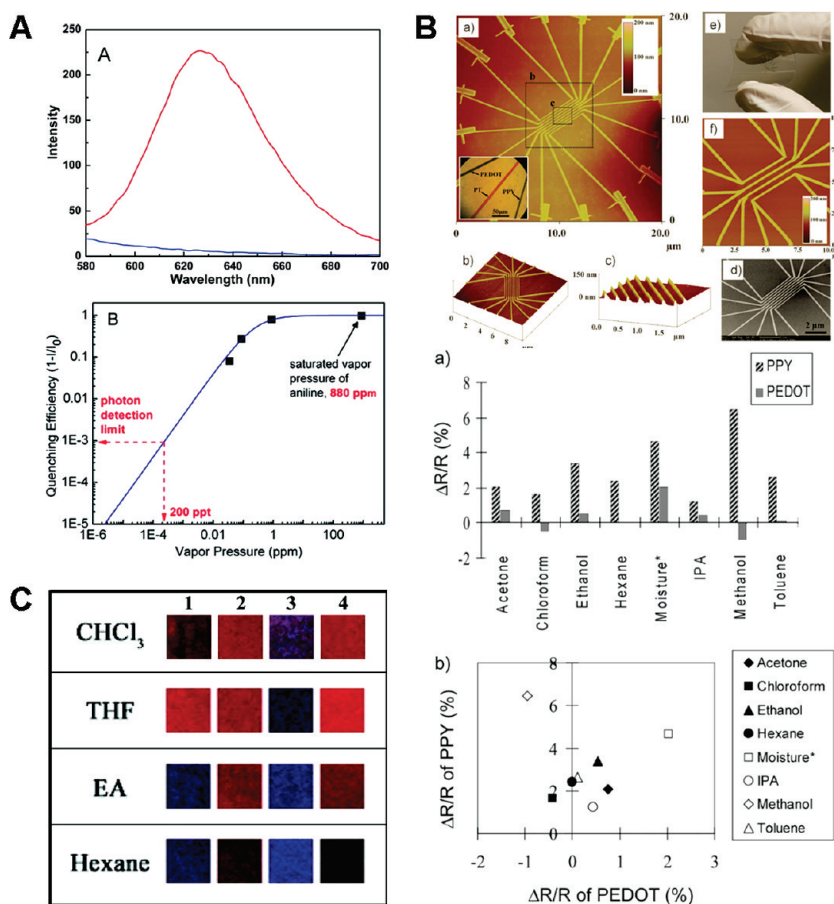


Figure 34. (A) Fluorescent spectra of self-assembled nanowires based on PTCDI derivative (**35o**) before and after the exposure to the aniline vapor (880 ppm) and the projected quenching efficiency as a function of vapor pressure of aniline. Reprinted with permission from ref 334. Copyright 2008 American Chemical Society. (B) Conjugated polymer nanowires for sensors: AFM and SEM images of the nanowires synthesized by template-assisted electrochemical polymerization, and the change of resistance of PPY (**2**) and PEDOT (**5**) nanowires upon exposure to various volatile organic compounds (1000 ppm). Reprinted with permission from ref 269. Copyright 2009 Wiley-VCH. (C) Colorimetric response of electrospun different PDA (**15a,b,f,h**)-embedded fibers to various organic solvents. Reprinted with permission from ref 252. Copyright 2007 American Chemical Society.

Among the benefits of the large surface-area-to-volume ratio of organic nanowires is that the sensing element/analyte encounter probability increases with the active area and hence the signal-to-noise ratio increases. An array or a network of nanowires may be more desirable than a single nanowire for high reliability. Signals representing the nanowire/analyte interactions must be in processable forms, such as current, color, or light, as produced by a transduction mechanism.^{566–568} Among the various transduction mechanisms, quenching of fluorescence and change of conductivity have been the most widely used in organic semiconductor nanowire sensors for various applications.

Optical sensors based on organic semiconductor nanowires exploit the exciton fluorescence of the materials and its susceptibility to modulation by interaction with the environment. When an analyte comes close to an organic nanowire, charge or energy transfer between the nanowire and the analyte occurs, resulting in quenching of the fluorescence. Such a detection mechanism is known to be very sensitive, especially when it comes to highly porous nanostructures such as a network of nanowires.³³⁴ The limit of detection based on fluorescence quenching has been estimated to be less than one part per billion in the

case of nanowires of a PTCDI derivative (**35o**) and the analyte is aniline (Figure 34A).³³⁴ Nanowires synthesized by electrospinning have been demonstrated to detect Fe³⁺,²²⁶ Hg²⁺,²²⁶ DNT,²²⁶ cytochrome-*c*,¹⁸⁶ methyl viologen,¹⁸⁶ and plasmid DNA.²¹⁶ A porous morphology formed by nanofibrils in thin film of ACTC (**41b**) have been shown to function as sensors for explosives such as DNT and TNT.³⁴⁷

Another type of signal that a nanowire sensor can generate is the change of conductivity upon exposure to an analyte. An electrical signal is preferred for easy integration of the sensors into electronic circuits. Organic semiconductor nanowires, such as CuPc (**53a**),^{468,571} PTCDI derivatives (**35a,j,l-n**),^{330,572} and DAAQ (**55**),⁴⁵⁵ and conducting polymer nanowires, such as PPY (**2**),^{109,265,267–269,289,573} PANI (**1**),^{225,266–268,485,487,528,574} and PEDOT (**5**),^{148,269,283,573,575,576} have been widely studied for sensor applications. Conducting polymer nanowires in particular are very promising for this mode of detection since their conductivity is greatly modulated by doping and dedoping processes.⁴⁸⁵ Reduction, swelling, and conformational change of chain have also been reported as mechanisms for the conductivity changes.⁴⁸⁵ Detections of pH^{266–268} and acidic/basic compounds

(HCl, NH_3),^{109,225,265,289,485,487,528,573,574} volatile organic compounds (acetone, chloroform, ethanol, hexane, moisture, isopropanol, methanol, and toluene),^{269,485,573,575,576} reducing agents (N_2H_4),^{330,485,572} explosives (DNT),³³¹ and toxic NO_x ^{283,468,571} have been reported. Specific degrees of responses of different active materials on various chemicals may offer multipurpose sensors with pattern-matching analysis (Figure 34B),^{269,485,573,575} although achieving selectivity and sensitivity at the same time is quite challenging.

Besides the above-mentioned transduction mechanisms, colorimetric response²⁵² and evolution of fluorescence²⁵¹ of nanowires of polydiacetylenes (PDAs) (**15a**, **b,f,h**) have also been shown to be promising for sensor applications. Upon exposure of PDA (**15a**, **b,f,h**)-based nanowires to volatile organic compounds such as chloroform, tetrahydrofuran, ethyl acetate, and hexane, different PDAs (**15a**, **b,f,h**) turned into different specific colors providing fingerprint-type selectivity (Figure 34C).²⁵² Nanowires based on PDA (**15a**) become highly fluorescent upon exposure to α -cyclodextrin (α -CD) but not β -CD nor γ -CD, forming a basis for selective detection of α -CD.²⁵¹

3.8. Lasers and Nanophotonics. Organic semiconductor nanowires and nanopatterns are of increasing interest for developing optically pumped lasers⁵⁷⁷ and nanophotonic devices.⁵⁷⁸ Microcavity effects in nanowires of organic semiconductors have enabled the achievement of optically pumped lasers and related laser action,^{126,579} whereas distributed feedback (DFB) lasers have been realized in thin films with nanograting patterns,^{273,291,293} both based on the highly fluorescent PFO (**6a**) and MEHPPV (**3b**). Emission from the laser has an extremely narrow full-width-at-half-maximum (fwhm; typically a few nanometers) and high directionality when the excitation fluence is above the lasing threshold (Figure 35).^{126,273,293} Amplified spontaneous emission (ASE), which is incoherent, may be seen in some cases.²⁹³ In the distributed feedback laser, the wavelength of emission is closely related to the periodicity of grating, the effective refractive index of the polymer medium, and the order of diffraction. DFB lasers made from MEHPPV (**3b**) exhibited optically pumped emission wavelength in the range of 607–645 nm with a pump threshold of $25 \mu\text{J}/\text{cm}^2$ to $250 \text{ mJ}/\text{cm}^2$.^{273,291,293}

The narrow width and large aspect ratio of organic semiconductor nanowires make them good candidates for developing nanoscale light sources as well as subwavelength waveguides in nanophotonic devices.^{230,329,348,349,459,519,580,581}

Having a higher refractive index in the organic semiconductor than the surrounding (air and substrates) allows luminescent emission from within the semiconductor to propagate along it. One of the key properties required for the use of the organic nanowires as a waveguide is that the emissive material has a large Stokes shift to minimize light loss caused by self-absorption.^{329,348,349,519,580} Another feature of a nanofiber or nanowire that enables low optical loss is having smooth surfaces and distinct flat facets to minimize

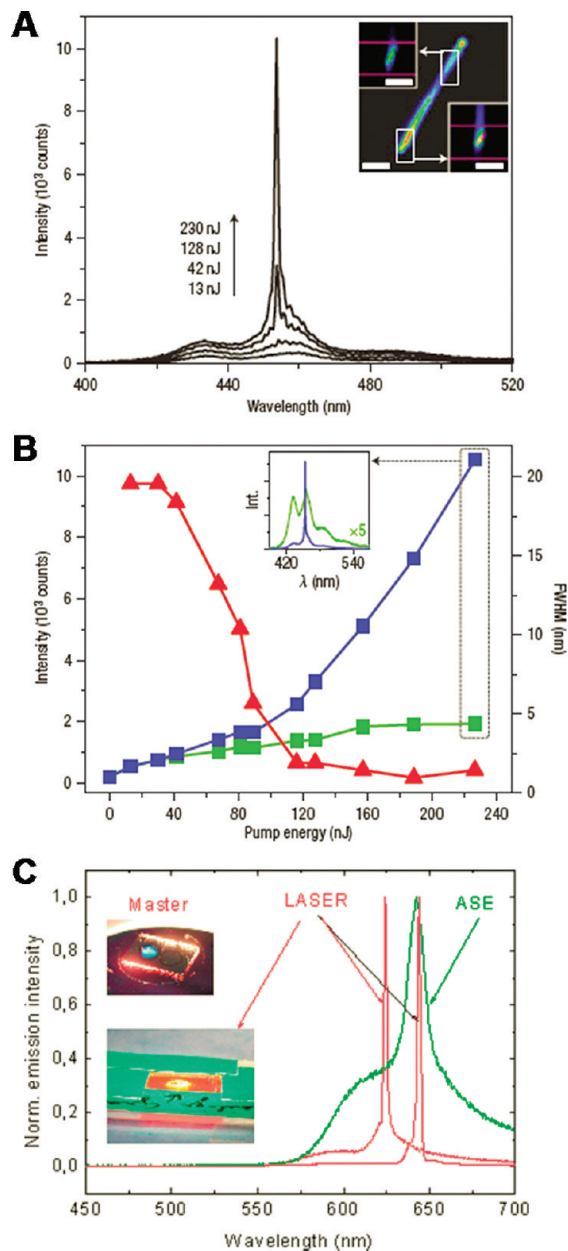


Figure 35. (A, B) Optically pumped single PFO (**6a**) nanowire laser: (A) Emission spectra from optically pumped single PFO (**6a**) nanowire laser. Inset shows emission of the single nanowire pumped at 1.3 nJ. Scale bars represent $2 \mu\text{m}$. (B) Tip emission intensity (blue square), fwhm of the tip emission spectra (red triangle), and body emission intensity (green square) as a function of pump energy for the PFO (**6a**) nanowire shown in A. Inset shows emission spectra from the nanowire tip and body under pump energy of 230 nJ. Reprinted with permission from ref 126. Copyright 2007 Nature Publishing Group. (C) Emission spectra from two different DFB gratings of MEHPPV (**3b**). Reprinted with permission from ref 293. Copyright 2003 Wiley-VCH.

scattering.^{349,581} Highly crystalline nanowires of PyQs (**43a,c**) having distinct end-facets and low overlap of absorption and emission spectra were shown to exhibit active waveguiding of emitted fluorescence with an optical loss coefficient (α) of $0.014\text{--}0.043 \text{ dB}/\mu\text{m}$, which is comparable to that of low-loss inorganic semiconductor nanowires ($0.026 \text{ dB}/\mu\text{m}$).³⁴⁹ The waveguiding property of the organic nanowire is affected by its width. The minimum width required for light propagation can be calculated from the dielectric tensor components of the

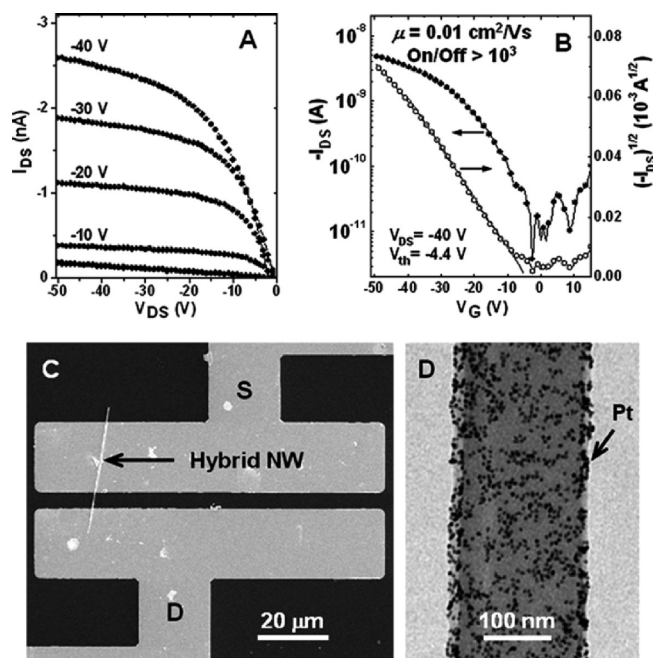


Figure 36. (A) Output and (B) transfer characteristics of an HTP (29)-Pt nanowire transistor. (C) SEM image of an HTP (29)-Pt hybrid nanowire transistor. (D) TEM image of a representative HTP (29)-Pt nanowire. Reprinted with permission from ref 315. Copyright 2008 Royal Society of Chemistry.

material and wavelength of the light, as shown from self-assembled nanowires of TC (42)^{348,519} and PTCDI (35h).³²⁹ Vertical arrays of nanowires of DAAQ (55) as waveguides have been shown to have a smaller optical loss than the horizontally placed arrays of the nanowires.⁴⁵⁹ An individual nanowire of light-emitting polymers has been further patterned in 1D nanograting to enhance the forward emission of nanowires.²³⁰

3.9. Other Applications. Many other applications of organic conductor and semiconductor nanowires have been demonstrated. HTP (29) nanowires decorated with gold, platinum, or palladium nanoparticles (Figure 36) were demonstrated to work not only as field-effect transistors but also as catalysts for hydrogenation reactions.³¹⁵ Because of the unique chemical interactions between noble metal nanoparticles and sulfur atoms of HTP (29) at the nanowire surface, the nanoparticles were uniformly distributed over the nanowire surfaces (Figure 36D), enabling highly reactive active catalytic sites on the nanowires.³¹⁵ Cu-TCNQ (52a) nanowires,⁴⁶⁰ made by vapor-phase deposition, and directly polymerized PANI (1) nanofibers decorated with gold nanoparticles⁵⁸² have been explored in bistable organic memory devices. PEDOT (5)^{114,583} and PNP3T-PN (19a)²⁵⁵ nanostructures have been shown to have fast electrochromic switching. The PEDOT (5) nanotubes prepared using a porous template were reported to exhibit fast electrochromic switching (less than 10 ms).¹¹⁴ Thin walls (10–20 nm) of the nanotubes are responsible for such a short switching time.¹¹⁴ Nanofibers of polynorbornylene with oligothiophene pendants (19a), prepared by electrospinning, exhibited electrochromism with color switching from blue to orange, depending on the oxidation state.²⁵⁵

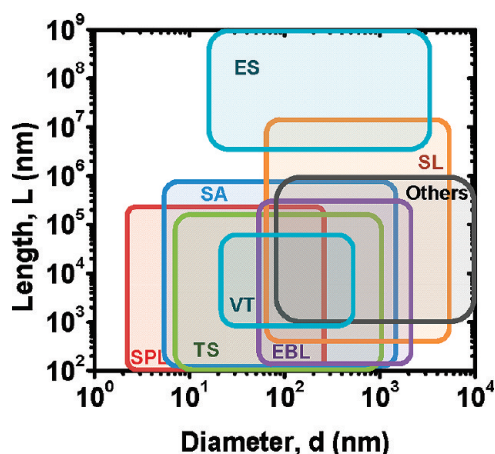


Figure 37. Dimensions (diameter or width d , length L) of nanowires synthesized by various techniques. (EBL, electron beam lithography; ES, electrospinning; SA, solution-phase self-assembly; SL, soft lithography; SPL, scanning probe lithography; TS, template-directed synthesis; VT, vapor transport and deposition).

The switching times of 2–3 s in the PNP3T-PN (19a) nanofiber was about 20 times faster than electrochemically prepared PEDOT (5) films with a similar thickness ($\sim 1 \mu\text{m}$).²⁵⁵ The large surface-to-volume ratio and high conductivity of PEDOT (5) nanowires make them promising for supercapacitor-based energy storage devices.^{185,584} PEDOT (5) nanotubes produced by electrochemical polymerization of the monomer onto poly(lactide-co-glycolide) nanofiber templates have shown controlled release of bioactive molecules by electrical stimulation.¹⁸² Organic spintronics,^{585–588} which deals with the injection, transport, manipulation, and detection of spins in organic semiconductor devices, is another application that has been explored with organic semiconductor nanowires. An array of 50 nm wide, 1 μm long nanowires that consist of 25–33 nm long Alq_3 (24) segments sandwiched between ferromagnetic electrodes, Co and Ni, has been produced by means of anodized alumina templates and demonstrated as nanowire-based spin valves.^{589,590} At low temperature ($T < 100 \text{ K}$), the spin relaxation length was calculated to be 3–6 nm.⁵⁹⁰ With this relaxation length and reported carrier mobility of Alq_3 (24), very long spin relaxation time of 2 ms to 1 s was estimated.⁵⁹⁰

4. Concluding Remarks and Future Outlook

The richness in the chemistry, physics, materials science, and engineering of π -conjugated organic semiconductors continues to unfold despite the considerable interdisciplinary advances in scientific understanding and technological applications of the materials in the past two decades. As is evident from this review, the increasing ability to assemble π -conjugated molecular building blocks (small molecules, oligomers, and polymers) into well-defined crystalline 1D nanostructures is opening new opportunities for discoveries and interdisciplinary research in many areas as well as for applications. The various approaches that have been developed for producing organic semiconductor nanowires, nanoribbons/nanobelts, and nanotubes and the range of

accessible dimensions (diameter or width d , length L) for each approach are summarized in Figure 37. Collectively, these strategies can offer a wide range of 1D nanomaterials and nanostructures with readily tunable electronic, optoelectronic, and photonic properties, suggesting ways toward high-volume, low-cost, affordable nanotechnologies.

The high degree of precision achieved in the control of dimensions (d , t , L), composition, shape, and crystal structure of inorganic semiconductor and metallic nanostructures^{1–10} is yet to be achieved in organic semiconductor nanostructures. Although such a precision is necessary to reveal the quantum size-dependent phenomena and properties of inorganic nanostructures, it may not be necessary for unmasking the supramolecular and mesoscopic phenomena and properties of organic nanostructures. Nevertheless, a better control of the diameter/width, aspect ratio, and single-crystallinity of organic semiconductor nanostructures is needed to facilitate systematic basic studies that can be expected to uncover the fundamental limits on properties ranging from charge, exciton, and photon transport to photovoltaic properties and mechanical strength. Methods for the facile alignment of organic nanowires in a preferred direction, beyond templated strategies,³²⁶ are also needed since such an alignment is beneficial for enhanced charge transport,^{63,447} production of polarized light emission,^{245,263} and improved absorption and photovoltaic properties,^{46,533} especially when dealing with an ensemble of nanowires.

π -Conjugated polymer semiconductors as molecular building blocks for the assembly of functional 1D nanostructures are of special interest because of their combination of various tunable electronic, optoelectronic, and photonic properties with excellent mechanical properties. As shown in this review, only a small number of conjugated polymers have been investigated as nanowires, most notably poly(3-alkylthiophene)s. Given the potential for enhanced performance of polymer semiconductor nanowire-based organic electronics (e.g., field-effect transistors, solar cells), there is a need for assembly and investigation of nanowires of other existing p-type and n-type conjugated polymers, especially those with donor–acceptor architectures⁵⁹¹ or the so-called third generation conjugated polymer semiconductors.²⁰ Although knowledge of the mechanical properties of organic semiconductor nanowires is essential for most applications, very little is currently known about the mechanical properties of π -conjugated organic/polymer nanowires.

One of the unique features of 1D organic semiconductor nanostructures is their great potential for hybridization with other classes of nanostructures (e.g., inorganic semiconductors, metals, biomaterials) to create novel hybrid nanocomposite systems, enabling integration of functions and properties and emergence of novel and multifunctional properties. Although only a very limited number of examples of effort along this line have been reported so far, they support our view of the numerous opportunities in this area.^{315,582,590,592} For example, 1D hybrid nanowires created by assembling gold, platinum,

and palladium nanoparticles onto the surfaces of single-crystalline hexathiapentacene (HTP) nanowires demonstrated good function in field-effect transistors while enabling catalysis.³¹⁵ Hybrid nanowires consisting of ferromagnetic metal/organic semiconductor/ferromagnetic metal have been demonstrated as promising spin-valves for applications in spintronics.^{590,592} Organic semiconductor nanowire-based hybrid nanocomposites have the potential to exhibit stimuli-responsive (adaptive) properties, unusual composition-dependent electrical, optical, thermal, magnetic, and mechanical properties, enabling new applications in sensors/biosensors, thermoelectrics, energy harvesting and storage, catalysis, nanoelectronics, nanophotonics, and spintronics.

Acknowledgment. Our research in the various areas covered by this review was supported by the NSF (DMR-0805259, DMR-1035196, and DMR-0120967), the U.S. DOE, Basic Energy Sciences, Division of Materials Science, under Award DE-FG02-07ER46467, the Office of Naval Research (N00014-08-1-1148), and the Boeing-Martin Endowed Professorship in Engineering. We are delighted to acknowledge discussions with colleagues in our research group.

References

- (1) Alivisatos, A. P. *Science* **1996**, *271*, 933–937.
- (2) Hu, J.; Odom, T. W.; Lieber, C. M. *Acc. Chem. Res.* **1999**, *32*, 435–445.
- (3) Xia, Y.; Yang, P.; Sun, Y.; Wu, Y.; Mayers, B.; Gates, B.; Yin, Y.; Kim, F.; Yan, H. *Adv. Mater.* **2003**, *15*, 353–389.
- (4) Cui, Y.; Lieber, C. M. *Science* **2001**, *291*, 851–853.
- (5) Pan, Z. W.; Dai, Z. R.; Wang, Z. L. *Science* **2001**, *291*, 1947–1949.
- (6) Murray, C. B.; Kagan, C. R.; Bawendi, M. G. *Annu. Rev. Mater. Sci.* **2000**, *30*, 545–610.
- (7) Yin, Y.; Alivisatos, A. P. *Nature* **2005**, *437*, 664–670.
- (8) Ozin, G. A. *Adv. Mater.* **1992**, *4*, 612–649.
- (9) Law, M.; Goldberger, J.; Yang, P. *Annu. Rev. Mater. Res.* **2004**, *34*, 83–122.
- (10) Lieber, C. M.; Wang, Z. L. *MRS Bull.* **2007**, *32*, 99–104.
- (11) Brus, L. E. *J. Chem. Phys.* **1984**, *80*, 4403–4409.
- (12) Whitesides, G. M. *Small* **2005**, *1*, 172–179.
- (13) Whitesides, G. M.; Lipomi, D. J. *Faraday Discuss.* **2009**, *143*, 373–384.
- (14) Ozin, G. A.; Cademartiri, L. *Small* **2009**, *5*, 1240–1244.
- (15) Baughman, R. H.; Zakhidov, A. A.; de Heer, W. A. *Science* **2002**, *297*, 787–792.
- (16) Tasis, D.; Tagmatarchis, N.; Bianco, A.; Prato, M. *Chem. Rev.* **2006**, *106*, 1105–1136.
- (17) Ajayan, P. M. *Chem. Rev.* **1999**, *99*, 1787–1800.
- (18) Dai, H. J. *Surf. Sci.* **2002**, *500*, 218–241.
- (19) Ouyang, M.; Huang, J. L.; Lieber, C. M. *Acc. Chem. Res.* **2002**, *35*, 1018–1025.
- (20) Heeger, A. J. *Chem. Soc. Rev.* **2010**, *39*, 2354–2371.
- (21) Heeger, A. J. *Angew. Chem., Int. Ed.* **2001**, *40*, 2591–2611.
- (22) Shirakawa, H. *Angew. Chem., Int. Ed.* **2001**, *40*, 2574–2580.
- (23) MacDiarmid, A. G. *Angew. Chem., Int. Ed.* **2001**, *40*, 2581–2590.
- (24) Tang, C. W.; VanSlyke, S. A. *Appl. Phys. Lett.* **1987**, *51*, 913–915.
- (25) Friend, R. H.; Gymer, R. W.; Holmes, A. B.; Burroughes, J. H.; Marks, R. N.; Taliani, C.; Bradley, D. D. C.; Santos, D. A. D.; Bredas, J. L.; Logdlund, M.; Salaneck, W. R. *Nature* **1999**, *397*, 121–128.
- (26) D'Andrade, B.; Forrest, S. R. *Adv. Mater.* **2004**, *16*, 1585–1595.
- (27) Grimsdale, A. C.; Chan, K. L.; Martin, R. E.; Jokisz, P. G.; Holmes, A. B. *Chem. Rev.* **2009**, *109*, 897–1091.
- (28) Kulkarni, A. P.; Tonzola, C. J.; Babel, A.; Jenekhe, S. A. *Chem. Mater.* **2004**, *16*, 4556–4573.
- (29) Reineke, S.; Lindner, F.; Schwartz, G.; Seidler, N.; Walzer, K.; Lussem, B.; Leo, K. *Nature* **2009**, *459*, 234–238.
- (30) Kido, J.; Kimura, M.; Nagai, K. *Science* **1995**, *267*, 1332–1334.
- (31) Allard, S.; Forster, M.; Souharce, B.; Thiem, H.; Scherf, U. *Angew. Chem., Int. Ed.* **2008**, *47*, 4070–4098.
- (32) Zausmeil, J.; Sirringhaus, H. *Chem. Rev.* **2007**, *107*, 1296–1323.
- (33) Gershenson, M. E.; Podzorov, V.; Morpurgo, A. F. *Rev. Mod. Phys.* **2006**, *78*, 973.
- (34) Coropceanu, V.; Cornil, J.; da Silva Filho, D. A.; Olivier, Y.; Silbey, R.; Bredas, J.-L. *Chem. Rev.* **2007**, *107*, 926–952.
- (35) Bao, Z. N.; Rogers, J. A.; Katz, H. E. *J. Mater. Chem.* **1999**, *9*, 1895–1904.

- (36) Kim, F. S.; Guo, X.; Watson, M. D.; Jenekhe, S. A. *Adv. Mater.* **2010**, *22*, 478–482.
- (37) LeMieux, M. C.; Bao, Z. *Nat. Nanotechnol.* **2008**, *3*, 585–586.
- (38) Forrest, S. R. *Nature* **2004**, *428*, 911–918.
- (39) Coakley, K. M.; McGehee, M. D. *Chem. Mater.* **2004**, *16*, 4533–4542.
- (40) Gunes, S.; Neugebauer, H.; Sariciftci, N. S. *Chem. Rev.* **2007**, *107*, 1324–1338.
- (41) Thompson, B. C.; Frechet, J. M. J. *Angew. Chem., Int. Ed.* **2008**, *47*, 58–77.
- (42) Peumans, P.; Yakimov, A.; Forrest, S. R. *J. Appl. Phys.* **2003**, *93*, 3693–3723.
- (43) Blom, P. W. M.; Mihailetchi, V. D.; Koster, L. J. A.; Markov, D. E. *Adv. Mater.* **2007**, *19*, 1551–1566.
- (44) Spanggaard, H.; Krebs, F. C. *Solar Energy Mater. Solar Cells* **2004**, *83*, 125–146.
- (45) Brunetti, F. G.; Kumar, R.; Wudl, F. J. *Mater. Chem.* **2010**, *20*, 2934–2948.
- (46) Xin, H.; Kim, F. S.; Jenekhe, S. A. *J. Am. Chem. Soc.* **2008**, *130*, 5424–5425.
- (47) Martin, R. E.; Diederich, F. *Angew. Chem., Int. Ed.* **1999**, *38*, 1350–1377.
- (48) Anthony, J. E. *Chem. Rev.* **2006**, *106*, 5028–5048.
- (49) Bunz, U. H. F. *Chem. Rev.* **2000**, *100*, 1605–1644.
- (50) Bendikov, M.; Wudl, F.; Perepichka, D. F. *Chem. Rev.* **2004**, *104*, 4891–4946.
- (51) Osaka, I.; McCullough, R. D. *Acc. Chem. Res.* **2008**, *41*, 1202–1214.
- (52) Anthony, J. E. *Angew. Chem., Int. Ed.* **2008**, *47*, 452–483.
- (53) Cheng, Y.-J.; Yang, S.-H.; Hsu, C.-S. *Chem. Rev.* **2009**, *109*, 5868–5923.
- (54) Wu, P.-T.; Bull, T.; Kim, F. S.; Luscombe, C. K.; Jenekhe, S. A. *Macromolecules* **2009**, *42*, 671–681.
- (55) Pron, A.; Gawrys, P.; Zagorska, M.; Djurado, D.; Demadrille, R. *Chem. Soc. Rev.* **2010**, *39*, 2577–2632.
- (56) Roncali, J. *Chem. Rev.* **1997**, *97*, 173–206.
- (57) van Mellekom, H. A. M.; Vekemans, J. A. J. M.; Havinga, E. E.; Meijer, E. W. *Mater. Sci. Eng. R Rep.* **2001**, *32*, 1–40.
- (58) Lehn, J. M. *Angew. Chem., Int. Ed.* **1988**, *27*, 89–112.
- (59) Lehn, J. M. *Angew. Chem., Int. Ed.* **1990**, *29*, 1304–1319.
- (60) Whitesides, G. M.; Mathias, J. P.; Seto, C. T. *Science* **1991**, *254*, 1312–1319.
- (61) Whitesides, G. M.; Grzybowski, B. *Science* **2002**, *295*, 2418–2421.
- (62) Lehn, J.-M. *Science* **2002**, *295*, 2400–2403.
- (63) Tsao, H. N.; Müllen, K. *Chem. Soc. Rev.* **2010**, *39*, 2372–2386.
- (64) Iijima, S. *Nature* **1991**, *354*, 56–58.
- (65) Berresheim, A. J.; Müller, M.; Mullen, K. *Chem. Rev.* **1999**, *99*, 1747–1786.
- (66) Jenekhe, S. A.; Alam, M.; Zhu, Y.; Jiang, S.; Shevade, A. *Adv. Mater.* **2007**, *19*, 536–542.
- (67) James, D. K.; Tour, J. M. *Top. Curr. Chem.* **2005**, *257*, 33–62.
- (68) Frampton, M.; Anderson, H. *Angew. Chem., Int. Ed.* **2007**, *46*, 1028–1064.
- (69) Zhao, Y. S.; Fu, H.; Peng, A.; Ma, Y.; Xiao, D.; Yao, J. *Adv. Mater.* **2008**, *20*, 2859–2876.
- (70) Pecher, J.; Mecking, S. *Chem. Rev.* **2010**, *110*, 6260–6279.
- (71) Martin, C. R. *Science* **1994**, *266*, 1961–1966.
- (72) Martin, C. R. *Acc. Chem. Res.* **1995**, *28*, 61–68.
- (73) Hurst, S. J.; Payne, E. K.; Qin, L.; Mirkin, C. A. *Angew. Chem., Int. Ed.* **2006**, *45*, 2672–2692.
- (74) Jang, J. *Adv. Polym. Sci.* **2006**, *199*, 189–259.
- (75) Kelly, T. L.; Wolf, M. O. *Chem. Soc. Rev.* **2010**, *39*, 1526–1535.
- (76) Zhang, D.; Wang, Y. *Mater. Sci. Eng., B* **2006**, *134*, 9–19.
- (77) Hulteen, J. C.; Martin, C. R. *J. Mater. Chem.* **1997**, *7*, 1075–1087.
- (78) Steinhart, M. *Adv. Polym. Sci.* **2008**, *220*, 123–187.
- (79) Yoon, H.-S.; Choi, M.-J.; Lee, K.-J.; Jang, J.-S. *Macromol. Res.* **2008**, *16*, 85–102.
- (80) Martin, C. R. *Chem. Mater.* **1996**, *8*, 1739–1746.
- (81) Wu, C.-G.; Bein, T. *Science* **1994**, *264*, 1757–1759.
- (82) Nguyen, T.-Q.; Wu, J.; Doan, V.; Schwartz, B. J.; Tolbert, S. H. *Science* **2000**, *288*, 652–656.
- (83) Penner, R. M.; Martin, C. R. *J. Electrochem. Soc.* **1986**, *133*, 2206–2207.
- (84) Van Dyke, L. S.; Martin, C. R. *Langmuir* **1990**, *6*, 1118–1123.
- (85) Cai, Z.; Martin, C. R. *J. Am. Chem. Soc.* **1989**, *111*, 4138–4139.
- (86) Cai, Z.; Lei, J.; Liang, W.; Menon, V.; Martin, C. R. *Chem. Mater.* **1991**, *3*, 960–967.
- (87) Martin, C. R.; Van Dyke, L. S.; Cai, Z.; Liang, W. *J. Am. Chem. Soc.* **1990**, *112*, 8976–8977.
- (88) Liang, W.; Martin, C. R. *J. Am. Chem. Soc.* **1990**, *112*, 9666–9668.
- (89) Martin, C. R. *Adv. Mater.* **1991**, *3*, 457–459.
- (90) Martin, C. R.; Parthasarathy, R.; Menon, V. *Synth. Met.* **1993**, *55*, 1165–1170.
- (91) Parthasarathy, R. V.; Martin, C. R. *Chem. Mater.* **1994**, *6*, 1627–1632.
- (92) Zuppiroli, L.; Beuneu, F.; Mory, J.; Enzel, P.; Bein, T. *Synth. Met.* **1993**, *57*, 5063–5068.
- (93) Enzel, P.; Bein, T. *Synth. Met.* **1993**, *55*, 1238–1245.
- (94) Wu, C.-G.; Bein, T. *Chem. Mater.* **1994**, *6*, 1109–1112.
- (95) Delvaux, M.; Duchet, J.; Stavaux, P.-Y.; Legras, R.; Demoustier-Champagne, S. *Synth. Met.* **2000**, *113*, 275–280.
- (96) Massuyeau, F.; Duval, J. L.; Athalin, H.; Lorcy, J. M.; Lefrant, S.; Wery, J.; Faulques, E. *Nanotechnology* **2009**, *20*, 155701.
- (97) Rahman, A.; Sanyal, M. K. *Adv. Mater.* **2007**, *19*, 3956–3960.
- (98) Demoustier-Champagne, S.; Stavaux, P.-Y. *Chem. Mater.* **1999**, *11*, 829–834.
- (99) Long, Y. Z.; Duval, J. L.; Chen, Z. J.; Jin, A. Z.; Gu, C. Z. *Polym. Adv. Technol.* **2009**, *20*, 541–544.
- (100) Duval, J. L.; Retho, P.; Fernandez, V.; Louarn, G.; Molinie, P.; Chauvet, O. *J. Phys. Chem. B* **2004**, *108*, 18552–18556.
- (101) Duval, J. L.; Retho, P.; Garreau, S.; Louarn, G.; Godon, C.; Demoustier-Champagne, S. *Synth. Met.* **2002**, *131*, 123–128.
- (102) Pra, L. D. D.; Ferain, E.; Legras, R.; Demoustier-Champagne, S. *Nucl. Instrum. Methods Phys. Res., Sect. B* **2002**, *196*, 81–88.
- (103) Duchet, J.; Legras, R.; Demoustier-Champagne, S. *Synth. Met.* **1998**, *98*, 113–122.
- (104) Demoustier-Champagne, S.; Ferain, E.; Jerome, C.; Jerome, R.; Legras, R. *Eur. Polym. J.* **1998**, *34*, 1767–1774.
- (105) Kim, K.; Jin, J.-I. *Nano Lett.* **2001**, *1*, 631–636.
- (106) Masuda, H.; Fukuda, K. *Science* **1995**, *268*, 1466–1468.
- (107) Al-Kaysi, R. O.; Ghaddar, T. H.; Guirado, G. J. *Nanomater.* **2009**, *14*, 108.
- (108) Berdichevsky, Y.; Lo, Y.-H. *Adv. Mater.* **2006**, *18*, 122–125.
- (109) Zhang, L.; Meng, F.; Chen, Y.; Liu, J.; Sun, Y.; Luo, T.; Li, M.; Liu, J. *Sens. Actuators B* **2009**, *142*, 204–209.
- (110) Joo, J.; Kim, B. H.; Park, D. H.; Kim, H. S.; Seo, D. S.; Shim, J. H.; Lee, S. J.; Ryu, K. S.; Kim, K.; Jin, J. I.; Lee, T. J.; Lee, C. J. *Synth. Met.* **2005**, *153*, 313–316.
- (111) Kim, B. H.; Park, D. H.; Joo, J.; Yu, S. G.; Lee, S. H. *Synth. Met.* **2005**, *150*, 279–284.
- (112) Xiao, R.; Cho, S. I.; Liu, R.; Lee, S. B. *J. Am. Chem. Soc.* **2007**, *129*, 4483–4489.
- (113) Han, M. G.; Foulger, S. H. *Chem. Commun.* **2005**, 3092–3094.
- (114) Cho, S. I.; Kwon, W. J.; Choi, S.-J.; Kim, P.; Park, S.-A.; Kim, J.; Son, S. J.; Xiao, R.; Kim, S.-H.; Lee, S. B. *Adv. Mater.* **2005**, *17*, 171–175.
- (115) Haberkorn, N.; Gutmann, J. S.; Theato, P. *ACS Nano* **2009**, *3*, 1415–1422.
- (116) Haberkorn, N.; Weber, S. A. L.; Berger, R.; Theato, P. *ACS Appl. Mater. Interfaces* **2010**, *2*, 1573–1580.
- (117) Park, D. H.; Kim, B. H.; Jang, M. G.; Bae, K. Y.; Joo, J. *Appl. Phys. Lett.* **2005**, *86*, 113116.
- (118) Lee, S. H.; Park, D. H.; Kim, K.; Joo, J.; Kim, D.-C.; Kim, H.-J.; Kim, J. *Appl. Phys. Lett.* **2007**, *91*, 263102.
- (119) Kim, J. S.; Park, Y.; Lee, D. Y.; Lee, J. H.; Park, J. H.; Kim, J. K.; Cho, K. *Adv. Funct. Mater.* **2010**, *20*, 540–545.
- (120) Santos, A.; Formentin, P.; Pallares, J.; Ferre-Borrull, J.; Marsal, L. F. *Solar Energy Mater. Solar Cells* **2010**, *94*, 1247–1253.
- (121) Coakley, K. M.; Srinivasan, B. S.; Ziebarth, J. M.; Goh, C.; Liu, Y.; McGehee, M. D. *Adv. Funct. Mater.* **2005**, *15*, 1927–1932.
- (122) Baek, S.; Park, J. B.; Lee, W.; Han, S. H.; Lee, J.; Lee, S. H. *New J. Chem.* **2009**, *33*, 986–990.
- (123) Moynihan, S.; Iacopino, D.; O'Carroll, D.; Lovera, P.; Redmond, G. *Chem. Mater.* **2007**, *20*, 996–1003.
- (124) O'Carroll, D.; Irwin, J.; Tanner, D. A.; Redmond, G. *Mater. Sci. Eng., B* **2008**, *147*, 298–302.
- (125) O'Carroll, D.; Iacopino, D.; O'Riordan, A.; Lovera, P.; O'Connor, E.; O'Brien, G. A.; Redmond, G. *Adv. Mater.* **2008**, *20*, 42–48.
- (126) O'Carroll, D.; Lieberwirth, I.; Redmond, G. *Nat. Nanotechnol.* **2007**, *2*, 180–184.
- (127) O'Brien, G. A.; Quinn, A. J.; Tanner, D. A.; Redmond, G. *Adv. Mater.* **2006**, *18*, 2379–2383.
- (128) Lee, J. W.; Kim, K.; Park, D. H.; Cho, M. Y.; Lee, Y. B.; Jung, J. S.; Kim, D.-C.; Kim, J.; Joo, J. *Adv. Funct. Mater.* **2009**, *19*, 704–710.
- (129) Park, D. H.; Hong, Y. K.; Cho, E. H.; Kim, M. S.; Kim, D.-C.; Bang, J.; Kim, J.; Joo, J. *ACS Nano* **2010**, *4*, 5155–5162.
- (130) Guo, Y.; Tang, Q.; Liu, H.; Zhang, Y.; Li, Y.; Hu, W.; Wang, S.; Zhu, D. *J. Am. Chem. Soc.* **2008**, *130*, 9198–9199.
- (131) Guo, Y.; Zhang, Y.; Liu, H.; Lai, S.-W.; Li, Y.; Li, Y.; Hu, W.; Wang, S.; Che, C.-M.; Zhu, D. *J. Phys. Chem. Lett.* **2009**, *1*, 327–330.
- (132) Guo, Y.; Liu, H.; Li, Y.; Li, G.; Zhao, Y.; Song, Y.; Li, Y. *J. Phys. Chem. C* **2009**, *113*, 12669–12673.
- (133) O'Brien, G. A.; Quinn, A. J.; Iacopino, D.; Pauget, N.; Redmond, G. *J. Mater. Chem.* **2006**, *16*, 3237–3241.
- (134) Wilson, J. N.; Bangcuyo, C. G.; Erdogan, B.; Myrick, M. L.; Bunz, U. H. F. *Macromolecules* **2003**, *36*, 1426–1428.
- (135) Jang, J.; Lim, B.; Lee, J.; Hyeon, T. *Chem. Commun.* **2001**, 83–84.
- (136) Bates, F. S.; Fredrickson, G. H. *Phys. Today* **1999**, *52*, 32–38.
- (137) Bates, F. S.; Fredrickson, G. H. *Annu. Rev. Phys. Chem.* **1990**, *41*, 525–557.
- (138) Hamley, I. W. *Prog. Polym. Sci.* **2009**, *34*, 1161–1210.
- (139) Kim, Y. H.; Yoon, D. K.; Jung, H.-T. *J. Mater. Chem.* **2009**, *19*, 9091–9102.
- (140) Spontak, R. J.; Alexandridis, P. *Curr. Opin. Colloid Interface Sci.* **1999**, *4*, 140–146.
- (141) Cohen, R. E. *Curr. Opin. Solid State Mater. Sci.* **1999**, *4*, 587–590.

- (142) Chai, J.; Buriak, J. M. *ACS Nano* **2008**, *2*, 489–501.
- (143) Lee, J. I.; Cho, S. H.; Park, S.-M.; Kim, J. K.; Kim, J. K.; Yu, J.-W.; Kim, Y. C.; Russell, T. P. *Nano Lett.* **2008**, *8*, 2315–2320.
- (144) Crossland, E. J. W.; Kamperman, M.; Nedelcu, M.; Ducati, C.; Wiesner, U.; Smilgies, D. M.; Toombes, G. E. S.; Hillmyer, M. A.; Ludwigs, S.; Steiner, U.; Snaith, H. J. *Nano Lett.* **2009**, *9*, 2807–2812.
- (145) Crossland, E. J. W.; Nedelcu, M.; Ducati, C.; Ludwigs, S.; Hillmyer, M. A.; Steiner, U.; Snaith, H. J. *Nano Lett.* **2009**, *9*, 2813–2819.
- (146) Li, X.; Tian, S.; Ping, Y.; Kim, D. H.; Knoll, W. *Langmuir* **2005**, *21*, 9393–9397.
- (147) Jang, J.; Yoon, H. *Chem. Commun.* **2003**, 720–721.
- (148) Yoon, H.; Chang, M.; Jang, J. *Adv. Funct. Mater.* **2007**, *17*, 431–436.
- (149) Zhang, X.; Zhang, J.; Liu, Z.; Robinson, C. *Chem. Commun.* **2004**, 1852–1853.
- (150) Zhang, X. T.; Zhang, J.; Song, W. H.; Liu, Z. F. *J. Phys. Chem. B* **2006**, *110*, 1158–1165.
- (151) Zhong, W.; Deng, J.; Yang, Y.; Yang, W. *Macromol. Rapid Commun.* **2005**, *26*, 395–400.
- (152) Hatano, T.; Takeuchi, M.; Ikeda, A.; Shinkai, S. *Org. Lett.* **2003**, *5*, 1395–1398.
- (153) Araya, K.; Mukoh, A.; Narahara, T.; Shirakawa, H. *Synth. Met.* **1986**, *14*, 199–206.
- (154) Akagi, K.; Katayama, S.; Ito, M.; Shirakawa, H.; Araya, K. *Synth. Met.* **1989**, *28*, D51–D56.
- (155) Akagi, K.; Piao, G.; Kaneko, S.; Sakamaki, K.; Shirakawa, H.; Kyotani, M. *Science* **1998**, *282*, 1683–1686.
- (156) Goto, H. *J. Polym. Sci., Part A: Polym. Chem.* **2007**, *45*, 1377–1387.
- (157) Goto, H.; Kawabata, K. *Macromolecules* **2008**, *41*, 4551–4554.
- (158) Kitamura, T.; Nakaso, S.; Mizoshita, N.; Tochigi, Y.; Shimomura, T.; Moriyama, M.; Ito, K.; Kato, T. *J. Am. Chem. Soc.* **2005**, *127*, 14769–14775.
- (159) Goto, H.; Akagi, K. *Macromolecules* **2005**, *38*, 1091–1098.
- (160) Samitsu, S.; Takanishi, Y.; Yamamoto, J. *Macromolecules* **2009**, *42*, 4366–4368.
- (161) Kato, T. *Science* **2002**, *295*, 2414–2418.
- (162) Mizoshita, N.; Hanabusa, K.; Kato, T. *Adv. Mater.* **1999**, *11*, 392–394.
- (163) Mizoshita, N.; Hanabusa, K.; Kato, T. *Adv. Funct. Mater.* **2003**, *13*, 313–317.
- (164) Braun, E.; Eichen, Y.; Sivan, U.; Ben-Yoseph, G. *Nature* **1998**, *391*, 775–778.
- (165) Houlton, A.; Pike, A. R.; Galindo, M. A.; Horrocks, B. R. *Chem. Commun.* **2009**, 1797–1806.
- (166) Ma, Y.; Zhang, J.; Zhang, G.; He, H. *J. Am. Chem. Soc.* **2004**, *126*, 7097–7101.
- (167) Nickels, P.; Dittmer, W. U.; Beyer, S.; Kotthaus, J. P.; Simmel, F. C. *Nanotechnology* **2004**, *15*, 1524–1529.
- (168) Bardavid, Y.; Ghabboun, J.; Porath, D.; Kotlyar, A. B.; Yitzchaik, S. *Polymer* **2008**, *49*, 2217–2222.
- (169) Dawn, A.; Nandi, A. K. *Macromolecules* **2005**, *38*, 10067–10073.
- (170) Dong, L.; Hollis, T.; Fishwick, S.; Connolly, B. A.; Wright, N. G.; Horrocks, B. R.; Houlton, A. *Chem.—Eur. J.* **2007**, *13*, 822–828.
- (171) Pruneanu, S.; Al-Said, S. A. F.; Dong, L.; Hollis, T. A.; Galindo, M. A.; Wright, N. G.; Houlton, A.; Horrocks, B. R. *Adv. Funct. Mater.* **2008**, *18*, 2444–2454.
- (172) Bjork, P.; Herland, A.; Scheblykin, I. G.; Inganas, O. *Nano Lett.* **2005**, *5*, 1948–1953.
- (173) Herland, A.; Bjork, P.; Nilsson, K. P. R.; Olsson, J. D. M.; Asberg, P.; Konradsson, P.; Hammarstrom, P.; Inganas, O. *Adv. Mater.* **2005**, *17*, 1466–1471.
- (174) Herland, A.; Bjork, P.; Hania, P.; Scheblykin, I.; Inganäs, O. *Small* **2007**, *3*, 318–325.
- (175) Herland, A.; Thomsson, D.; Mirzov, O.; Scheblykin, I. G.; Inganas, O. *J. Mater. Chem.* **2008**, *18*, 126–132.
- (176) Li, F.; Martens, A. A.; Aslund, A.; Konradsson, P.; de Wolf, F. A.; Cohen Stuart, M. A.; Sudholter, E. J. R.; Marcelis, A. T. M.; Leermakers, F. A. M. *Soft Matter* **2009**, *5*, 1668–1673.
- (177) Goren, M.; Qi, Z.; Lennox, R. B. *Chem. Mater.* **2000**, *12*, 1222–1228.
- (178) Kros, A.; Linhardt, J.; Bowman, H.; Tirrell, D. *Adv. Mater.* **2004**, *16*, 723–727.
- (179) Liu, L.; Duan, X.; Liu, H.; Wang, S.; Li, Y. *Chem. Commun.* **2008**, 5999–6001.
- (180) Bognitzki, M.; Hou, H.; Ishaque, M.; Frese, T.; Hellwig, M.; Schwarte, C.; Schaper, A.; Wendorff, J. H.; Greiner, A. *Adv. Mater.* **2000**, *12*, 637–640.
- (181) Caruso, R. A.; Schattka, J. H.; Greiner, A. *Adv. Mater.* **2001**, *13*, 1577–1579.
- (182) Abidian, M. R.; Kim, D.-H.; Martin, D. C. *Adv. Mater.* **2006**, *18*, 405–409.
- (183) Hou, H.; Jun, Z.; Reuning, A.; Schaper, A.; Wendorff, J. H.; Greiner, A. *Macromolecules* **2002**, *35*, 2429–2431.
- (184) Dong, H.; Prasad, S.; Nyame, V.; Jones, W. E. *Chem. Mater.* **2004**, *16*, 371–373.
- (185) Laforgue, A.; Robitaille, L. *Macromolecules* **2010**, *43*, 4194–4200.
- (186) Wang, X.; Kim, Y.-G.; Drew, C.; Ku, B.-C.; Kumar, J.; Samuelson, L. A. *Nano Lett.* **2004**, *4*, 331–334.
- (187) Döbbelin, M.; Tena-Zaera, R.; Carrasco, P. M.; Sarasua, J. R.; Cabañero, G.; Mecerreyes, D. *J. Polym. Sci., Part A: Polym. Chem.* **2010**, *48*, 4648–4653.
- (188) Lei, J.; Cai, Z.; Martin, C. R. *Synth. Met.* **1992**, *46*, 53–69.
- (189) Menon, V. P.; Lei, J.; Martin, C. R. *Chem. Mater.* **1996**, *8*, 2382–2390.
- (190) Park, S.; Lim, J.-H.; Chung, S.-W.; Mirkin, C. A. *Science* **2004**, *303*, 348–351.
- (191) Park, S.; Chung, S.-W.; Mirkin, C. A. *J. Am. Chem. Soc.* **2004**, *126*, 11772–11773.
- (192) Park, M.; Harrison, C.; Chaikin, P. M.; Register, R. A.; Adamson, D. H. *Science* **1997**, *276*, 1401–1404.
- (193) Thurn-Albrecht, T.; Schotter, J.; Kastle, G. A.; Emley, N.; Shibauchi, T.; Krusin-Elbaum, L.; Guarini, K.; Black, C. T.; Tuominen, M. T.; Russell, T. P. *Science* **2000**, *290*, 2126–2129.
- (194) Brinker, C. J.; Lu, Y.; Sellinger, A.; Fan, H. *Adv. Mater.* **1999**, *11*, 579–585.
- (195) Shirakawa, H.; Ikeda, S. *Synth. Met.* **1980**, *1*, 175–184.
- (196) McMillan, R. A.; Paavola, C. D.; Howard, J.; Chan, S. L.; Zaluzec, N. J.; Trent, J. D. *Nat. Mater.* **2002**, *1*, 247–252.
- (197) Li, Z.; Chung, S. W.; Nam, J. M.; Ginger, D. S.; Mirkin, C. A. *Angew. Chem., Int. Ed.* **2003**, *42*, 2306–2309.
- (198) Nam, K. T.; Kim, D.-W.; Yoo, P. J.; Chiang, C.-Y.; Meethong, N.; Hammond, P. T.; Chiang, Y.-M.; Belcher, A. M. *Science* **2006**, *312*, 885–888.
- (199) Mao, C.; Solis, D. J.; Reiss, B. D.; Kottmann, S. T.; Sweeney, R. Y.; Hayhurst, A.; Georgiou, G.; Iverson, B.; Belcher, A. M. *Science* **2004**, *303*, 213–217.
- (200) Lee, S.-W.; Mao, C.; Flynn, C. E.; Belcher, A. M. *Science* **2002**, *296*, 892–895.
- (201) Lee, S. W.; Lee, S.; Belcher, A. *Adv. Mater.* **2003**, *15*, 689–692.
- (202) Reneker, D. H.; Chun, I. *Nanotechnology* **1996**, *7*, 216–223.
- (203) Frenot, A.; Chronakis, I. S. *Curr. Opin. Colloid Interface Sci.* **2003**, *8*, 64–75.
- (204) Li, D.; Xia, Y. *Adv. Mater.* **2004**, *16*, 1151–1170.
- (205) Greiner, A.; Wendorff, J. *Angew. Chem., Int. Ed.* **2007**, *46*, 5670–5703.
- (206) Reneker, D. H.; Yarin, A. L.; Fong, H.; Koombhongse, S. *J. Appl. Phys.* **2000**, *87*, 4531–4547.
- (207) Deitzel, J. M.; Kleinmeyer, J.; Harris, D.; Beck Tan, N. C. *Polymer* **2001**, *42*, 261–272.
- (208) Wutticharoenmongkol, P.; Supaphol, P.; Sriksirin, T.; Kerdcharoen, T.; Osotchan, T. *J. Polym. Sci., Part B: Polym. Phys.* **2005**, *43*, 1881–1891.
- (209) Zhou, Y.; Freitag, M.; Hone, J.; Staii, C.; Johnson, J. A. T.; Pinto, N. J.; MacDiarmid, A. G. *Appl. Phys. Lett.* **2003**, *83*, 3800–3802.
- (210) MacDiarmid, A. G.; Jones, W. E.; Norris, I. D.; Gao, J.; Johnson, A. T.; Pinto, N. J.; Hone, J.; Han, B.; Ko, F. K.; Okuzaki, H.; Llaguno, M. *Synth. Met.* **2001**, *119*, 27–30.
- (211) Pinto, N. J.; Johnson, J. A. T.; MacDiarmid, A. G.; Mueller, C. H.; Theofylaktos, N.; Robinson, D. C.; Miranda, F. A. *Appl. Phys. Lett.* **2003**, *83*, 4244–4246.
- (212) Norris, I. D.; Shaker, M. M.; Ko, F. K.; MacDiarmid, A. G. *Synth. Met.* **2000**, *114*, 109–114.
- (213) Li, D.; Wang, Y.; Xia, Y. *Nano Lett.* **2003**, *3*, 1167–1171.
- (214) Kameoka, J.; Craighead, H. G. *Appl. Phys. Lett.* **2003**, *83*, 371–373.
- (215) Wang, C.-T.; Kuo, C.-C.; Chen, H.-C.; Chen, W.-C. *Nanotechnology* **2009**, *20*, 375604.
- (216) Kuo, C. C.; Wang, C. T.; Chen, W. C. *Macromol. Mater. Eng.* **2008**, *293*, 999–1008.
- (217) Campoy-Quiles, M.; Ishii, Y.; Sakai, H.; Murata, H. *Appl. Phys. Lett.* **2008**, *92*, 213305.
- (218) Li, D.; Babel, A.; Jenekhe, S. A.; Xia, Y. *Adv. Mater.* **2004**, *16*, 2062–2066.
- (219) Babel, A.; Li, D.; Xia, Y.; Jenekhe, S. A. *Macromolecules* **2005**, *38*, 4705–4711.
- (220) Zhu, Z. T.; Zhang, L. F.; Smith, S.; Fong, H.; Sun, Y. G.; Gosztola, D. *Synth. Met.* **2009**, *159*, 1454–1459.
- (221) Bergshoeff, M. M.; Vancso, G. J. *Adv. Mater.* **1999**, *11*, 1362–1365.
- (222) Gibson, P.; Schreuder-Gibson, H.; Rivin, D. *Colloids Surf. A* **2001**, *187*–188, 469–481.
- (223) Patel, A. C.; Li, S.; Wang, C.; Zhang, W.; Wei, Y. *Chem. Mater.* **2007**, *19*, 1231–1238.
- (224) Pham, Q. P.; Sharma, U.; Mikos, A. G. *Tissue Eng.* **2006**, *12*, 1197–1211.
- (225) Liu, H.; Kameoka, J.; Czaplewski, D. A.; Craighead, H. G. *Nano Lett.* **2004**, *4*, 671–675.
- (226) Wang, X.; Drew, C.; Lee, S.-H.; Senecal, K. J.; Kumar, J.; Samuelson, L. A. *Nano Lett.* **2002**, *2*, 1273–1275.
- (227) Moran-Mirabal, J. M.; Slinker, J. D.; DeFranco, J. A.; Verbridge, S. S.; Ilic, R.; Flores-Torres, S.; Abruna, H.; Malliaras, G. G.; Craighead, H. G. *Nano Lett.* **2007**, *7*, 458–463.
- (228) Pinto, N. J.; Carrasquillo, K. V.; Rodd, C. M.; Agarwal, R. *Appl. Phys. Lett.* **2009**, *94*, 083504.
- (229) Liu, H.; Reccius, C. H.; Craighead, H. G. *Appl. Phys. Lett.* **2005**, *87*, 253106.
- (230) Di Benedetto, F.; Camposeo, A.; Pagliara, S.; Mele, E.; Persano, L.; Stabile, R.; Cingolani, R.; Pisignano, D. *Nat. Nanotechnol.* **2008**, *3*, 614–619.

- (231) Chen, Z.; Foster, M. D.; Zhou, W.; Fong, H.; Reneker, D. H.; Resendes, R.; Manners, I. *Macromolecules* **2001**, *34*, 6156–6158.
- (232) Bianco, A.; Bertarelli, C.; Frisk, S.; Rabolt, J. F.; Gallazzi, M. C.; Zerbi, G. *Synth. Met.* **2007**, *157*, 276–281.
- (233) Kwak, G.; Fukao, S.; Fujiki, M.; Sakaguchi, T.; Masuda, T. *Chem. Mater.* **2006**, *18*, 5537–5542.
- (234) Liu, H. A.; Zepeda, D.; Ferraris, J. P.; Balkus, K. J. *ACS Appl. Mater. Interfaces* **2009**, *1*, 1958–1965.
- (235) Kuo, C.-C.; Lin, C.-H.; Chen, W.-C. *Macromolecules* **2007**, *40*, 6959–6966.
- (236) Yu, J. H.; Fridrikh, S. V.; Rutledge, G. C. *Adv. Mater.* **2004**, *16*, 1562–1566.
- (237) Xin, Y.; Huang, Z. H.; Li, W. W.; Jiang, Z. J.; Tong, Y. B.; Wang, C. *Eur. Polym. J.* **2008**, *44*, 1040–1045.
- (238) Chen, H.-C.; Wang, C.-T.; Liu, C.-L.; Liu, Y.-C.; Chen, W.-C. *J. Polym. Sci., Part B: Polym. Phys.* **2009**, *47*, 463–470.
- (239) Okuzaki, H.; Takahashi, T.; Miyajima, N.; Suzuki, Y.; Kuwabara, T. *Macromolecules* **2006**, *39*, 4276–4278.
- (240) Xin, Y.; Huang, Z. H.; Yang, P. P.; Jiang, Z. J.; Wang, C.; Shao, C. *J. Appl. Polym. Sci.* **2009**, *114*, 1864–1869.
- (241) Wang, C.; Yan, E.; Huang, Z.; Zhao, Q.; Xin, Y. *Macromol. Rapid Commun.* **2007**, *28*, 205–209.
- (242) Jiang, Z.; Huang, Z.; Yang, P.; Chen, J.; Xin, Y.; Xu, J. *Compos. Sci. Technol.* **2008**, *68*, 3240–3244.
- (243) Madhugiri, S.; Dalton, A.; Gutierrez, J.; Ferraris, J. P.; Balkus, K. J. *J. Am. Chem. Soc.* **2003**, *125*, 14531–14538.
- (244) Camposeo, A.; Di Benedetto, F.; Cingolani, R.; Pisignano, D. *Appl. Phys. Lett.* **2009**, *94*, 043109.
- (245) Pagliara, S.; Camposeo, A.; Mele, E.; Persano, L.; Cingolani, R.; Pisignano, D. *Nanotechnology* **2010**, *21*, 215304.
- (246) Vohra, V.; Calzaferri, G.; Destri, S.; Pasini, M.; Porzio, W.; Botta, C. *ACS Nano* **2010**, *4*, 1409–1416.
- (247) Sun, Z.; Zussman, E.; Yarin, A. L.; Wendorff, J. H.; Greiner, A. *Adv. Mater.* **2003**, *15*, 1929–1932.
- (248) Lee, S.; Moon, G. D.; Jeong, U. *J. Mater. Chem.* **2009**, *19*, 743–748.
- (249) Wang, Y.; Park, J. S.; Lee, J. P.; Miao, S.; Bunz, U. H. F. *Macromolecules* **2007**, *40*, 1843–1850.
- (250) Yoon, J.; Kim, J. M. *Macromol. Chem. Phys.* **2008**, *209*, 2195–2203.
- (251) Chae, S.; Park, H.; Yoon, J.; Lee, C.; Ahn, D.; Kim, J. M. *Adv. Mater.* **2007**, *19*, 521–524.
- (252) Yoon, J.; Chae, S. K.; Kim, J.-M. *J. Am. Chem. Soc.* **2007**, *129*, 3038–3039.
- (253) Chronakis, I. S.; Grapenson, S.; Jakob, A. *Polymer* **2006**, *47*, 1597–1603.
- (254) Kim, J.-S.; Reneker, D. H. *Polym. Eng. Sci.* **1999**, *39*, 849–854.
- (255) Jang, S.-Y.; Seshadri, V.; Khil, M.-S.; Kumar, A.; Marquez, M.; Mather, P. T.; Sotzing, G. A. *Adv. Mater.* **2005**, *17*, 2177–2180.
- (256) Gates, B. D.; Xu, Q.; Love, J. C.; Wolfe, D. B.; Whitesides, G. M. *Annu. Rev. Mater. Sci.* **2004**, *34*, 339–372.
- (257) Sotomayor Torres, C. M.; Zankovych, S.; Seekamp, J.; Kam, A. P.; Clavijo Cedeno, C.; Hoffmann, T.; Ahopelto, J.; Reuther, F.; Pfeiffer, K.; Bleidissel, G.; Gruetzner, G.; Maximov, M. V.; Heidari, B. *Mater. Sci. Eng., C* **2003**, *23*, 23–31.
- (258) Tseng, A. A.; Notargiacomo, A.; Chen, T. P. *J. Vac. Sci. Technol., B* **2005**, *23*, 877–894.
- (259) Xia, Y.; Whitesides, G. M. *Angew. Chem., Int. Ed.* **1998**, *37*, 550–575.
- (260) Holdcroft, S. *Adv. Mater.* **2001**, *13*, 1753–1765.
- (261) Cavallini, M.; Stoliar, P.; Moulin, J.-F.; Surin, M.; Leclerc, P.; Lazzaroni, R.; Breiby, D. W.; Andreasen, J. W.; Nielsen, M. M.; Sonar, P.; Grimsdale, A. C.; Mullen, K.; Biscarini, F. *Nano Lett.* **2005**, *5*, 2422–2425.
- (262) Aryal, M.; Trivedi, K.; Hu, W. C. *ACS Nano* **2009**, *3*, 3085–3090.
- (263) Zheng, Z. J.; Yim, K. H.; Saifullah, M. S. M.; Welland, M. E.; Friend, R. H.; Kim, J. S.; Huck, W. T. S. *Nano Lett.* **2007**, *7*, 987–992.
- (264) Hu, Z.; Muls, B.; Gence, L.; Serban, D. A.; Hofkens, J.; Melinte, S.; Nysten, B.; Demoustier-Champagne, S.; Jonas, A. M. *Nano Lett.* **2007**, *7*, 3639–3644.
- (265) Dong, B.; Zhong, D. Y.; Chi, L. F.; Fuchs, H. *Adv. Mater.* **2005**, *17*, 2736–2741.
- (266) Wanekaya, A. K.; Bangar, M. A.; Yun, M.; Chen, W.; Myung, N. V.; Mulchandani, A. J. *Phys. Chem. C* **2007**, *111*, 5218–5221.
- (267) Yun, M.; Myung, N. V.; Vasquez, R. P.; Lee, C.; Menke, E.; Penner, R. M. *Nano Lett.* **2004**, *4*, 419–422.
- (268) Ramanathan, K.; Bangar, M. A.; Yun, M.; Chen, W.; Mulchandani, A.; Myung, N. V. *Nano Lett.* **2004**, *4*, 1237–1239.
- (269) Chen, Y. X.; Luo, Y. *Adv. Mater.* **2009**, *21*, 2040–2044.
- (270) Doi, Y.; Saeki, A.; Koizumi, Y.; Seki, S.; Okamoto, K.; Kozawa, T.; Tagawa, S. *J. Vac. Sci. Technol. B* **2005**, *23*, 2051–2055.
- (271) Persson, S. H. M.; Dyreklev, P.; Inganas, O. *Adv. Mater.* **1996**, *8*, 405–408.
- (272) Park, J. G.; Kim, G. T.; Park, J. H.; Yu, H. Y.; McIntosh, G.; Krstic, V.; Jhang, S. H.; Kim, B.; Lee, S. H.; Lee, S. W.; Burghard, M.; Roth, S.; Park, Y. W. *Thin Solid Films* **2001**, *393*, 161–167.
- (273) Stabile, R.; Camposeo, A.; Persano, L.; Tavazzi, S.; Cingolani, R.; Pisignano, D. *Appl. Phys. Lett.* **2007**, *91*, 101110.
- (274) Okawa, Y.; Aono, M. *Nature* **2001**, *409*, 683–684.
- (275) Granstrom, M. *Acta Polym.* **1998**, *49*, 514–517.
- (276) Maynor, B. W.; Filocamo, S. F.; Grinstaff, M. W.; Liu, J. J. *Am. Chem. Soc.* **2001**, *124*, 522–523.
- (277) Jang, S.-Y.; Marquez, M.; Sotzing, G. A. *J. Am. Chem. Soc.* **2004**, *126*, 9476–9477.
- (278) Fenwick, O.; Bozec, L.; Credgington, D.; Hammiche, A.; Lazzarini, G. M.; Silberberg, Y. R.; Cacialli, F. *Nat. Nanotechnol.* **2009**, *4*, 664–668.
- (279) Lim, J.-H.; Mirkin, C. A. *Adv. Mater.* **2002**, *14*, 1474–1477.
- (280) Riehn, R.; Charas, A.; Morgado, J.; Cacialli, F. *Appl. Phys. Lett.* **2003**, *82*, 526–528.
- (281) Wang, D. B.; Kim, S.; Underwood, W. D.; Giordano, A. J.; Henderson, C. L.; Dai, Z. T.; King, W. P.; Marder, S. R.; Riedo, E. *Appl. Phys. Lett.* **2009**, *95*, 233108.
- (282) Noy, A.; Miller, A. E.; Klare, J. E.; Weeks, B. L.; Woods, B. W.; DeYoreo, J. J. *Nano Lett.* **2001**, *2*, 109–112.
- (283) Lu, H.-H.; Lin, C.-Y.; Hsiao, T.-C.; Fang, Y.-Y.; Ho, K.-C.; Yang, D.; Lee, C.-K.; Hsu, S.-M.; Lin, C.-W. *Anal. Chim. Acta* **2009**, *640*, 68–74.
- (284) Wang, J.; Sun, X.; Chen, L.; Chou, S. Y. *Appl. Phys. Lett.* **1999**, *75*, 2767–2769.
- (285) Lawrence, J. R.; Andrew, P.; Barnes, W. L.; Buck, M.; Turnbull, G. A.; Samuel, I. D. W. *Appl. Phys. Lett.* **2002**, *81*, 1955–1957.
- (286) Cheyns, D.; Vasseur, K.; Rolin, C.; Genoe, J.; Poortmans, J.; Heremans, P. *Nanotechnology* **2008**, *19*, 424016.
- (287) Aryal, M.; Buyukserin, F.; Mielczarek, K.; Zhao, X.-M.; Gao, J.; Zakhidov, A.; Hu, W. *J. Vac. Sci. Technol. B* **2008**, *26*, 2562–2566.
- (288) Kim, M. S.; Kim, J. S.; Cho, J. C.; Shtein, M.; Guo, L. J.; Kim, J. *Appl. Phys. Lett.* **2007**, *90*, 123113.
- (289) Dong, B.; Lu, N.; Zelsmann, M.; Kehagias, N.; Fuchs, H.; Torres, C. M. S.; Chi, L. F. *Adv. Funct. Mater.* **2006**, *16*, 1937–1942.
- (290) Mele, E.; Di Benedetto, F.; Persano, L.; Cingolani, R.; Pisignano, D. *Nano Lett.* **2005**, *5*, 1915–1919.
- (291) Mele, E.; Camposeo, A.; Stabile, R.; Del Carro, P.; Di Benedetto, F.; Persano, L.; Cingolani, R.; Pisignano, D. *Appl. Phys. Lett.* **2006**, *89*, 131109.
- (292) Mele, E.; Camposeo, A.; Del Carro, P.; Di Benedetto, F.; Stabile, R.; Persano, L.; Cingolani, R.; Pisignano, D. *Mater. Sci. Eng., C* **2007**, *27*, 1428–1433.
- (293) Gaal, M.; Gadermaier, C.; Plank, H.; Moderegger, E.; Pogantsch, A.; Leising, G.; List, E. J. W. *Adv. Mater.* **2003**, *15*, 1165–1167.
- (294) Zhang, F. L.; Nyberg, T.; Inganas, O. *Nano Lett.* **2002**, *2*, 1373–1377.
- (295) Park, H.; Cheng, X. *Nanotechnology* **2009**, *20*, 245308.
- (296) Cavallini, M.; Murgia, M.; Biscarini, F. *Nano Lett.* **2001**, *1*, 193–195.
- (297) Beh, W. S.; Kim, I. T.; Qin, D.; Xia, Y.; Whitesides, G. M. *Adv. Mater.* **1999**, *11*, 1038–1041.
- (298) Massi, M.; Albonetti, C.; Facchini, M.; Cavallini, M.; Biscarini, F. *Adv. Mater.* **2006**, *18*, 2739–2742.
- (299) Cavallini, M.; Biscarini, F. *Nano Lett.* **2003**, *3*, 1269–1271.
- (300) Lipomi, D. J.; Chiechi, R. C.; Dickey, M. D.; Whitesides, G. M. *Nano Lett.* **2008**, *8*, 2100–2105.
- (301) Lipomi, D. J.; Chiechi, R. C.; Reus, W. F.; Whitesides, G. M. *Adv. Funct. Mater.* **2008**, *18*, 3469–3477.
- (302) Gigli, G.; Rinaldi, R.; Turco, C.; Visconti, P.; Cingolani, R.; Cacialli, F. *Appl. Phys. Lett.* **1998**, *73*, 3926–3928.
- (303) Zhang, X.; Shetty, A. S.; Jenekhe, S. A. *Macromolecules* **1999**, *32*, 7422–7429.
- (304) Zhang, X.; Jenekhe, S. A. *Macromolecules* **2000**, *33*, 2069–2082.
- (305) Earmme, T.; Ahmed, E.; Jenekhe, S. A. *Adv. Mater.* **2010**, *22*, 4744–4748.
- (306) Lehn, J.-M. *Supramolecular Chemistry: Concepts and Perspectives*; John Wiley & Sons: Hoboken, NJ, 1995.
- (307) Hoebe, F. J. M.; Jonkheijm, P.; Meijer, E. W.; Schenning, A. P. H. J. *Chem. Rev.* **2005**, *105*, 1491–1546.
- (308) Schenning, A. P. H. J.; Meijer, E. W. *Chem. Commun.* **2005**, 3245–3258.
- (309) Leclerc, P.; Surin, M.; Brocorens, P.; Cavallini, M.; Biscarini, F.; Lazzaroni, R. *Mater. Sci. Eng., R* **2006**, *55*, 1–56.
- (310) Nguyen, T.-Q.; Martel, R.; Bushey, M.; Avouris, P.; Carlsen, A.; Nuckolls, C.; Brus, L. *Phys. Chem. Chem. Phys.* **2007**, *9*, 1515–1532.
- (311) Muthukumar, M.; Ober, C. K.; Thomas, E. L. *Science* **1997**, *277*, 1225–1232.
- (312) Halperin, A.; Tirrell, M.; Lodge, T. *Adv. Polym. Sci.* **1992**, *100*, 31–71.
- (313) Kim, D. H.; Lee, D. Y.; Lee, H. S.; Lee, W. H.; Kim, Y. H.; Han, J. I.; Cho, K. *Adv. Mater.* **2007**, *19*, 678–682.
- (314) Briseno, A. L.; Mannsfeld, S. C. B.; Lu, X.; Xiong, Y.; Jenekhe, S. A.; Bao, Z.; Xia, Y. *Nano Lett.* **2007**, *7*, 668–675.
- (315) Briseno, A. L.; Mannsfeld, S. C. B.; Formo, E.; Yujie Xiong, Lu, X.; Bao, Z.; Jenekhe, S. A.; Xia, Y. *J. Mater. Chem.* **2008**, *18*, 5395–5398.
- (316) Zhou, Y.; Liu, W. J.; Ma, Y. G.; Wang, H. L.; Qi, L. M.; Cao, Y.; Wang, J.; Pei, J. *J. Am. Chem. Soc.* **2007**, *129*, 12386–12387.
- (317) Zhou, Y.; Lei, T.; Wang, L.; Pei, J.; Cao, Y.; Wang, J. *Adv. Mater.* **2010**, *22*, 1484–1487.
- (318) Zhang, S.; Guo, Y.; Zhang, Y.; Liu, R.; Li, Q.; Zhan, X.; Liu, Y.; Hu, W. *Chem. Commun.* **2010**, 2841–2843.
- (319) Guo, Y.; Du, C.; Yu, G.; Di, C. a.; Jiang, S.; Xi, H.; Zheng, J.; Yan, S.; Yu, C.; Hu, W.; Liu, Y. *Adv. Funct. Mater.* **2010**, *20*, 1019–1024.
- (320) Lee, D.-C.; McGrath, K. K.; Jang, K. *Chem. Commun.* **2008**, 3636–3638.

- (321) McGrath, K.; Jang, K.; Robins, K.; Lee, D. C. *Chem.—Eur. J.* **2009**, *15*, 4070–4077.
- (322) Ahmed, E.; Earmme, T.; Ren, G.; Jenekhe, S. A. *Chem. Mater.* **2010**, *22*, 5786–5796.
- (323) Datar, A.; Balakrishnan, K.; Yang, X.; Zuo, X.; Huang, J.; Oitker, R.; Yen, M.; Zhao, J.; Tiede, D. M.; Zang, L. *J. Phys. Chem. B* **2006**, *110*, 12327–12332.
- (324) Balakrishnan, K.; Datar, A.; Oitker, R.; Chen, H.; Zuo, J.; Zang, L. *J. Am. Chem. Soc.* **2005**, *127*, 10496–10497.
- (325) Briseno, A. L.; Mannsfeld, S. C. B.; Reese, C.; Hancock, J. M.; Xiong, Y.; Jenekhe, S. A.; Bao, Z.; Xia, Y. *Nano Lett.* **2007**, *7*, 2847–2853.
- (326) Oh, J. H.; Lee, H. W.; Mannsfeld, S.; Stoltenberg, R. M.; Jung, E.; Jin, Y. W.; Kim, J. M.; Yoo, J.-B.; Bao, Z. *Proc. Natl. Acad. Sci. U.S.A.* **2009**, *106*, 6065–6070.
- (327) Zang, L.; Che, Y.; Moore, J. S. *Acc. Chem. Res.* **2008**, *41*, 1596–1608.
- (328) Balakrishnan, K.; Datar, A.; Naddo, T.; Huang, J.; Oitker, R.; Yen, M.; Zhao, J.; Zang, L. *J. Am. Chem. Soc.* **2006**, *128*, 7390–7398.
- (329) Che, Y.; Yang, X.; Balakrishnan, K.; Zuo, J.; Zang, L. *Chem. Mater.* **2009**, *21*, 2930–2934.
- (330) Che, Y.; Datar, A.; Balakrishnan, K.; Zang, L. *J. Am. Chem. Soc.* **2007**, *129*, 7234–7235.
- (331) Che, Y.; Yang, X.; Liu, G.; Yu, C.; Ji, H.; Zuo, J.; Zhao, J.; Zang, L. *J. Am. Chem. Soc.* **2010**, *132*, 5743–5750.
- (332) Würthner, F. *Chem. Commun.* **2004**, 1564–1579.
- (333) Briseno, A. L.; Mannsfeld, S. C. B.; Jenekhe, S. A.; Bao, Z.; Xia, Y. *Mater. Today* **2008**, *11*, 38–47.
- (334) Che, Y.; Yang, X.; Loser, S.; Zang, L. *Nano Lett.* **2008**, *8*, 2219–2223.
- (335) Zhang, X. J.; Yuan, G. D.; Li, Q. S.; Wang, B.; Zhang, X. H.; Zhang, R. Q.; Chang, J. C.; Lee, C. S.; Lee, S. T. *Chem. Mater.* **2008**, *20*, 6945–6950.
- (336) Ajayaghosh, A.; Praveen, V. K. *Acc. Chem. Res.* **2007**, *40*, 644–656.
- (337) George, S. J.; Ajayaghosh, A. *Chem.—Eur. J.* **2005**, *11*, 3217–3227.
- (338) Ajayaghosh, A.; George, S. J. *J. Am. Chem. Soc.* **2001**, *123*, 5148–5149.
- (339) Prasanthkumar, S.; Saeki, A.; Seki, S.; Ajayaghosh, A. *J. Am. Chem. Soc.* **2010**, *132*, 8866–8867.
- (340) Bae, J.; Choi, J.-H.; Yoo, Y.-S.; Oh, N.-K.; Kim, B.-S.; Lee, M. *J. Am. Chem. Soc.* **2005**, *127*, 9668–9669.
- (341) Jeukens, C. R. L. P. N.; Jonkheijm, P.; Wijnen, F. J. P.; Gielen, J. C.; Christianen, P. C. M.; Schenning, A. P. H. J.; Meijer, E. W.; Maan, J. C. *J. Am. Chem. Soc.* **2005**, *127*, 8280–8281.
- (342) Schenning, A. P. H. J.; Jonkheijm, P.; Peeters, E.; Meijer, E. W. *J. Am. Chem. Soc.* **2000**, *123*, 409–416.
- (343) Schenning, A. P. H. J.; v. Herrikhuysen, J.; Jonkheijm, P.; Chen, Z.; Würthner, F.; Meijer, E. W. *J. Am. Chem. Soc.* **2002**, *124*, 10252–10253.
- (344) Jonkheijm, P.; Miura, A.; Zdanowska, M.; Hoebe, F. J. M.; De Feyter, S.; Schenning, A. P. H. J.; De Schryver, F. C.; Meijer, E. W. *Angew. Chem., Int. Ed.* **2004**, *43*, 74–78.
- (345) Beljonne, D.; Hennebicq, E.; Daniel, C.; Herz, L. M.; Silva, C.; Scholes, G. D.; Hoebe, F. J. M.; Jonkheijm, P.; Schenning, A. P. H. J.; Meskers, S. C. J.; Phillips, R. T.; Friend, R. H.; Meijer, E. W. *J. Phys. Chem. B* **2005**, *109*, 10594–10604.
- (346) Balakrishnan, K.; Datar, A.; Zhang, W.; Yang, X.; Naddo, T.; Huang, J.; Zuo, J.; Yen, M.; Moore, J. S.; Zang, L. *J. Am. Chem. Soc.* **2006**, *128*, 6576–6577.
- (347) Naddo, T.; Che, Y.; Zhang, W.; Balakrishnan, K.; Yang, X.; Yen, M.; Zhao, J.; Moore, J. S.; Zang, L. *J. Am. Chem. Soc.* **2007**, *129*, 6978–6979.
- (348) Takazawa, K.; Kitahama, Y.; Kimura, Y.; Kido, G. *Nano Lett.* **2005**, *5*, 1293–1296.
- (349) Wang, X.; Zhou, Y.; Lei, T.; Hu, N.; Chen, E.-Q.; Pei, J. *Chem. Mater.* **2010**, *22*, 3735–3745.
- (350) Hong, D.-J.; Lee, E.; Lee, M. *Chem. Commun.* **2007**, 1801–1803.
- (351) Moon, K. S.; Kim, H. J.; Lee, E.; Lee, M. *Angew. Chem., Int. Ed.* **2007**, *46*, 6807–6810.
- (352) Huang, Z.; Lee, E.; Kim, H.-J.; Lee, M. *Chem. Commun.* **2009**, 6819–6821.
- (353) Lee, E.; Huang, Z.; Ryu, J. H.; Lee, M. *Chem.—Eur. J.* **2008**, *14*, 6957–6966.
- (354) Cho, B. K.; Kim, H. J.; Chung, Y. W.; Lee, B. I.; Lee, M. *Adv. Polym. Sci.* **2008**, *219*, 69–106.
- (355) Wang, Z.; Medforth, C. J.; Shelnutt, J. A. *J. Am. Chem. Soc.* **2004**, *126*, 15954–15955.
- (356) Schwab, A. D.; Smith, D. E.; Rich, C. S.; Young, E. R.; Smith, W. F.; de Paula, J. C. *J. Phys. Chem. B* **2003**, *107*, 11339–11345.
- (357) Schwab, A. D.; Smith, D. E.; Bond-Watts, B.; Johnston, D. E.; Hone, J.; Johnson, A. T.; de Paula, J. C.; Smith, W. F. *Nano Lett.* **2004**, *4*, 1261–1265.
- (358) Rotomskis, R.; Augulis, R.; Snitka, V.; Valiokas, R.; Liedberg, B. *J. Phys. Chem. B* **2004**, *108*, 2833–2838.
- (359) Wang, Z.; Medforth, C. J.; Shelnutt, J. A. *J. Am. Chem. Soc.* **2004**, *126*, 16720–16721.
- (360) Radivojevic, I.; Likhtina, I.; Shi, X.; Singh, S.; Drain, C. M. *Chem. Commun.* **2010**, 1643–1645.
- (361) Dimitrakopoulos, C. D.; Malenfant, P. R. L. *Adv. Mater.* **2002**, *14*, 99–117.
- (362) Newman, C. R.; Frisbie, C. D.; da Silva Filho, D. A.; Bredas, J.-L.; Ewbank, P. C.; Mann, K. R. *Chem. Mater.* **2004**, *16*, 4436–4451.
- (363) Bao, Z.; Dodabalapur, A.; Lovinger, A. J. *Appl. Phys. Lett.* **1996**, *69*, 4108–4110.
- (364) Sirringhaus, H.; Tessler, N.; Friend, R. H. *Science* **1998**, *280*, 1741–1744.
- (365) Sirringhaus, H.; Brown, P. J.; Friend, R. H.; Nielsen, M. M.; Bechgaard, K.; Langeveld-Voss, B. M. W.; Spiering, A. J. H.; Janssen, R. A. J.; Meijer, E. W.; Herwig, P.; de Leeuw, D. M. *Nature* **1999**, *401*, 685–688.
- (366) Yang, H. C.; Shin, T. J.; Yang, L.; Cho, K.; Ryu, C. Y.; Bao, Z. N. *Adv. Funct. Mater.* **2005**, *15*, 671–676.
- (367) Li, G.; Shrotriya, V.; Huang, J.; Yao, Y.; Moriarty, T.; Emery, K.; Yang, Y. *Nat. Mater.* **2005**, *4*, 864–868.
- (368) Ma, W.; Yang, C.; Gang, X.; Lee, K.; Heeger, A. J. *Adv. Funct. Mater.* **2005**, *15*, 1617–1622.
- (369) Ihn, K. J.; Moulton, J.; Smith, P. J. *Polym. Sci., Part B: Polym. Phys.* **1993**, *31*, 735–742.
- (370) Oosterbaan, W. D.; Vrindts, V.; Berson, S.; Guillerez, S.; Douhéret, O.; Ruttens, B.; D'Haen, J.; Adriaenssens, P.; Manca, J.; Lutsen, L.; Vanderzande, D. *J. Mater. Chem.* **2009**, *19*, 5424–5435.
- (371) Lu, G.; Li, L.; Yang, X. *Macromolecules* **2008**, *41*, 2062–2070.
- (372) Yang, H. C.; Shin, T. J.; Bao, Z. N.; Ryu, C. Y. *J. Polym. Sci., Part B: Polym. Phys.* **2007**, *45*, 1303–1312.
- (373) Mardalen, J.; Samuelsen, E. J.; Pedersen, A. *Synth. Met.* **1993**, *55*, 378–383.
- (374) Samitsu, S.; Shimomura, T.; Heike, S.; Hashizume, T.; Ito, K. *Macromolecules* **2008**, *41*, 8000–8010.
- (375) Prosa, T. J.; Winokur, M. J.; Moulton, J.; Smith, P.; Heeger, A. J. *Macromolecules* **1992**, *25*, 4364–4372.
- (376) Prosa, T. J.; Winokur, M. J.; McCullough, R. D. *Macromolecules* **1996**, *29*, 3654–3656.
- (377) Kim, D. H.; Park, Y. D.; Jang, Y.; Kim, S.; Cho, K. *Macromol. Rapid Commun.* **2005**, *26*, 834–839.
- (378) Merlo, J. A.; Frisbie, C. D. *J. Polym. Sci., Part B: Polym. Phys.* **2003**, *41*, 2674–2680.
- (379) Merlo, J. A.; Frisbie, C. D. *J. Phys. Chem. B* **2004**, *108*, 19169–19179.
- (380) Liu, J.; Arif, M.; Zou, J.; Khondaker, S. I.; Zhai, L. *Macromolecules* **2009**, *42*, 9390–9393.
- (381) Meille, S. V.; Romita, V.; Caronna, T.; Lovinger, A. J.; Catellani, M.; Belobrzekaja, L. *Macromolecules* **1997**, *30*, 7898–7905.
- (382) Samitsu, S.; Shimomura, T.; Ito, K. *Thin Solid Films* **2008**, *516*, 2478–2486.
- (383) Wu, P.-T.; Xin, H.; Kim, F. S.; Ren, G.; Jenekhe, S. A. *Macromolecules* **2009**, *42*, 8817–8826.
- (384) Malik, S.; Nandi, A. K. *J. Polym. Sci., Part B: Polym. Phys.* **2002**, *40*, 2073–2085.
- (385) Ungar, G.; Stejny, J.; Keller, A.; Bidd, I.; Whiting, M. C. *Science* **1985**, *229*, 386–389.
- (386) Magonov, S. N.; Yerina, N. A. *Langmuir* **2003**, *19*, 500–504.
- (387) Mena-Osteritz, E.; Meyer, A.; Langeveld-Voss, B. M. W.; Janssen, R. A. J.; Meijer, E. W.; Bauerle, P. *Angew. Chem., Int. Ed.* **2000**, *39*, 2679–2684.
- (388) Grevin, B.; Rannou, P.; Payerne, R.; Pron, A.; Travers, J.-P. *Adv. Mater.* **2003**, *15*, 881–884.
- (389) Berson, S.; Bettignies, R. D.; Bailly, S.; Guillerez, S. *Adv. Funct. Mater.* **2007**, *17*, 1377–1384.
- (390) Zen, A.; Saphiannikova, M.; Neher, D.; Asawapirom, U.; Scherf, U. *Chem. Mater.* **2005**, *17*, 781–786.
- (391) Barton, A. F. M., *CRC Handbook of Solubility Parameters and Other Cohesion Parameters*; CRC Press: Boca Raton, FL, 1991.
- (392) Sperling, L. H. *Introduction to Physical Polymer Science*; John Wiley & Sons: New York, 2001.
- (393) Wu, C.-G.; Chien, L.-N. *Synth. Met.* **2000**, *110*, 251–255.
- (394) Kiriy, N.; Jahne, E.; Adler, H.-J.; Schneider, M.; Kiriy, A.; Gorodyska, G.; Minko, S.; Jehnichen, D.; Simon, P.; Fokin, A. A.; Stamm, M. *Nano Lett.* **2003**, *3*, 707–712.
- (395) Kim, B. G.; Kim, M. S.; Kim, J. *ACS Nano* **2010**, *4*, 2160–2166.
- (396) Liu, J.; Sheina, E.; Kowalewski, T.; McCullough, R. D. *Angew. Chem., Int. Ed.* **2002**, *41*, 329–332.
- (397) Leclerc, P.; Calderone, A.; Marsitzky, D.; Francke, V.; Geerts, Y.; Mullen, K.; Bredas, J. L.; Lazzaroni, R. *Adv. Mater.* **2000**, *12*, 1042–1046.
- (398) Leclerc, P.; Calderone, A.; Mullen, K.; Bredas, J. L.; Lazzaroni, R. *Mater. Sci. Technol.* **2002**, *18*, 749–754.
- (399) Leclerc, P.; Hennebicq, E.; Calderone, A.; Brocorens, P.; Grimsdale, A. C.; Mullen, K.; Bredas, J. L.; Lazzaroni, R. *Prog. Polym. Sci.* **2003**, *28*, 55–81.
- (400) Wu, P.-T.; Ren, G.; Li, C.; Mezzenga, R.; Jenekhe, S. A. *Macromolecules* **2009**, *42*, 2317–2320.
- (401) He, M.; Zhao, L.; Wang, J.; Han, W.; Yang, Y.; Qiu, F.; Lin, Z. *ACS Nano* **2010**, *4*, 3241–3247.
- (402) Wu, P.-T.; Ren, G.; Kim, F. S.; Li, C.; Mezzenga, R.; Jenekhe, S. A. *J. Polym. Sci., Part A: Polym. Chem.* **2010**, *48*, 614–626.
- (403) Jenekhe, S. A.; Chen, X. L. *Science* **1998**, *279*, 1903–1907.
- (404) Jenekhe, S. A.; Chen, X. L. *J. Phys. Chem. B* **2000**, *104*, 6332–6335.

- (405) Liu, H.; Wang, S.; Luo, Y.; Tang, W.; Yu, G.; Li, L.; Chen, C.; Liu, Y.; Xi, F. *J. Mater. Chem.* **2001**, *11*, 3063–3067.
- (406) Luo, Y.-H.; Liu, H.-W.; Xi, F.; Li, L.; Jin, X.-G.; Han, C. C.; Chan, C.-M. *J. Am. Chem. Soc.* **2003**, *125*, 6447–6451.
- (407) Kim, J.; McQuade, D. T.; McHugh, S. K.; Swager, T. M. *Angew. Chem., Int. Ed.* **2000**, *39*, 3868–3872.
- (408) Briseno, A. L.; Mannsfeld, S. C. B.; Shamberger, P. J.; Ohuchi, F. S.; Bao, Z.; Jenekhe, S. A.; Xia, Y. *Chem. Mater.* **2008**, *20*, 4712–4719.
- (409) Onodera, T.; Oshikiri, T.; Katagi, H.; Kasai, H.; Okada, S.; Oikawa, H.; Terauchi, M.; Tanaka, M.; Nakanishi, H. *J. Cryst. Growth* **2001**, *229*, 586–590.
- (410) De Witte, P. A. J.; Hernando, J.; Neuteboom, E. E.; van Dijk, E. M. H. P.; Meskers, S. C. J.; Janssen, R. A. J.; van Hulst, N. F.; Nolte, R. J. M.; Garcia-Parajo, M. F.; Rowan, A. E. *J. Phys. Chem. B* **2006**, *110*, 7803–7812.
- (411) Finlayson, C. E.; Friend, R. H.; Otten, M. B. J.; Schwartz, E.; Cornelissen, J. J. L. M.; Nolte, R. J. M.; Rowan, A. E.; Samori, P.; Palermo, V.; Liscio, A.; Peneva, K.; Müllen, K.; Trapani, S.; Beljonne, D. *Adv. Funct. Mater.* **2008**, *18*, 3947–3955.
- (412) Dabirian, R.; Palermo, V.; Liscio, A.; Schwartz, E.; Otten, M. B. J.; Finlayson, C. E.; Treossi, E.; Friend, R. H.; Calestani, G.; Müllen, K.; Nolte, R. J. M.; Rowan, A. E.; Samori, P. *J. Am. Chem. Soc.* **2009**, *131*, 7055–7063.
- (413) Zhang, C.; Zhang, X.; Ou, X.; Zhang, W.; Jie, J.; Chang, J. C.; Lee, C. S.; Lee, S. T. *Adv. Mater.* **2009**, *21*, 4172–4175.
- (414) Yan, P.; Chowdhury, A.; Holman, M. W.; Adams, D. M. *J. Phys. Chem. B* **2004**, *109*, 724–730.
- (415) Jiang, L.; Yao, X.; Li, H.; Fu, Y.; Chen, L.; Meng, Q.; Hu, W.; Jiang, L. *Adv. Mater.* **2010**, *22*, 376–379.
- (416) Gao, B. X.; Li, J. J.; Li, M. Y.; Cheng, Y. X.; Wang, L. X. *Chem-PhysChem* **2009**, *10*, 3197–3200.
- (417) Chung, J. W.; Yang, H.; Singh, B.; Moon, H.; An, B.-k.; Lee, S. Y.; Park, S. Y. *J. Mater. Chem.* **2009**, *19*, 5920–5925.
- (418) An, B.-K.; Gihm, S. H.; Chung, J. W.; Park, C. R.; Kwon, S.-K.; Park, S. Y. *J. Am. Chem. Soc.* **2009**, *131*, 3950–3957.
- (419) Hill, J. P.; Jin, W.; Kosaka, A.; Fukushima, T.; Ichihara, H.; Shimomura, T.; Ito, K.; Hashizume, T.; Ishii, N.; Aida, T. *Science* **2004**, *304*, 1481–1483.
- (420) Xiao, S.; Tang, J.; Beetz, T.; Guo, X.; Tremblay, N.; Siegrist, T.; Zhu, Y.; Steigerwald, M.; Nuckolls, C. *J. Am. Chem. Soc.* **2006**, *128*, 10700–10701.
- (421) Kastler, M.; Pisula, W.; Wasserfallen, D.; Pakula, T.; Müllen, K. *J. Am. Chem. Soc.* **2005**, *127*, 4286–4296.
- (422) Wang, L.; Zhou, Y.; Yan, J.; Wang, J.; Pei, J.; Cao, Y. *Langmuir* **2009**, *25*, 1306–1310.
- (423) Wang, L.; Liu, B.; Liu, D.; Yao, M.; Hou, Y.; Yu, S.; Cui, T.; Li, D.; Zou, G.; Iwasiewicz, A.; Sundqvist, B. *Adv. Mater.* **2006**, *18*, 1883–1888.
- (424) Geng, J.; Zhou, W.; Skelton, P.; Yue, W.; Kinloch, I. A.; Windle, A. H.; Johnson, B. F. G. *J. Am. Chem. Soc.* **2008**, *130*, 2527–2534.
- (425) Hoagland, J. J.; Wang, X. D.; Hipps, K. W. *Chem. Mater.* **1993**, *5*, 54–60.
- (426) Kline, R. J.; McGehee, M. D.; Kadnikova, E. N.; Liu, J. S.; Frechet, J. M. J.; Toney, M. F. *Macromolecules* **2005**, *38*, 3312–3319.
- (427) Zen, A.; Saphiannikova, M.; Neher, D.; Grenzer, J.; Grigorian, S.; Pietsch, U.; Asawapirom, U.; Janietz, S.; Scherf, U.; Lieberwirth, I.; Wegner, G. *Macromolecules* **2006**, *39*, 2162–2171.
- (428) Guo, X.; Kim, F. S.; Jenekhe, S. A.; Watson, M. D. *J. Am. Chem. Soc.* **2009**, *131*, 7206–7207.
- (429) Savenije, T. J.; Kroeze, J. E.; Yang, X.; Loos, J. *Thin Solid Films* **2006**, *511–512*, 2–6.
- (430) Ren, G.; Wu, P.-T.; Jenekhe, S. A. *Chem. Mater.* **2010**, *22*, 2020–2026.
- (431) Samori, P.; Francke, V.; Müllen, K.; Rabe, J. P. *Thin Solid Films* **1998**, *336*, 13–15.
- (432) Samori, P.; Francke, V.; Müllen, K.; Rabe, J. P. *Chem.—Eur. J.* **1999**, *5*, 2312–2317.
- (433) Perahia, D.; Traiphol, R.; Bunz, U. H. F. *Macromolecules* **2000**, *34*, 151–155.
- (434) Hu, W.; Nakashima, H.; Furukawa, K.; Kashimura, Y.; Ajito, K.; Torimitsu, K. *Appl. Phys. Lett.* **2004**, *85*, 115–117.
- (435) Dong, H.; Jiang, S.; Jiang, L.; Liu, Y.; Li, H.; Hu, W.; Wang, E.; Yan, S.; Wei, Z.; Xu, W.; Gong, X. *J. Am. Chem. Soc.* **2009**, *131*, 17315–17320.
- (436) Ofer, D.; Swager, T. M.; Wrighton, M. S. *Chem. Mater.* **1995**, *7*, 418–425.
- (437) De Luca, G.; Liscio, A.; Maccagnani, P.; Nolde, F.; Palermo, V.; Müllen, K.; Samori, P. *Adv. Funct. Mater.* **2007**, *17*, 3791–3798.
- (438) Mativetsky, J. M.; Kastler, M.; Savage, R. C.; Gentilini, D.; Palma, M.; Pisula, W.; Müllen, K.; Samori, P. *Adv. Funct. Mater.* **2009**, *19*, 2486–2494.
- (439) Chung, J. W.; An, B.-K.; Hirato, F.; Kim, J. H.; Jinnai, H.; Park, S. Y. *J. Mater. Chem.* **2010**, *20*, 7715–7720.
- (440) Reese, C.; Bao, Z. *Mater. Today* **2007**, *10*, 20–27.
- (441) Horowitz, G.; Bachet, B.; Yassar, A.; Lang, P.; Demanze, F.; Fave, J.-L.; Garnier, F. *Chem. Mater.* **1995**, *7*, 1337–1341.
- (442) Laudise, R. A.; Kloc, C.; Simpkins, P. G.; Siegrist, T. *J. Cryst. Growth* **1998**, *187*, 449–454.
- (443) Fichou, D.; Bachet, B.; Demanze, F.; Billy, I.; Horowitz, G.; Garnier, F. *Adv. Mater.* **1996**, *8*, 500–504.
- (444) Kloc, C.; Simpkins, P. G.; Siegrist, T.; Laudise, R. A. *J. Cryst. Growth* **1997**, *182*, 416–427.
- (445) Sundar, V. C.; Zaumseil, J.; Podzorov, V.; Menard, E.; Willett, R. L.; Someya, T.; Gershenson, M. E.; Rogers, J. A. *Science* **2004**, *303*, 1644–1646.
- (446) Briseno, A. L.; Mannsfeld, S. C. B.; Ling, M. M.; Liu, S.; Tseng, R. J.; Reese, C.; Roberts, M. E.; Yang, Y.; Wudl, F.; Bao, Z. *Nature* **2006**, *444*, 913–917.
- (447) Ahmed, E.; Briseno, A. L.; Xia, Y.; Jenekhe, S. A. *J. Am. Chem. Soc.* **2008**, *130*, 1118–1119.
- (448) Podzorov, V.; Sysoev, S. E.; Loginova, E.; Pudalov, V. M.; Gershenson, M. E. *Appl. Phys. Lett.* **2003**, *83*, 3504–3506.
- (449) Briseno, A.; Tseng, R.; Ling, M. M.; Falcao, E.; Yang, Y.; Wudl, F.; Bao, Z. *Adv. Mater.* **2006**, *18*, 2320–2324.
- (450) Tang, Q.; Li, H.; He, M.; Hu, W.; Liu, C.; Chen, K.; Wang, C.; Liu, Y.; Zhu, D. *Adv. Mater.* **2006**, *18*, 65–68.
- (451) Zeis, R.; Siegrist, T.; Kloc, C. *Appl. Phys. Lett.* **2005**, *86*, 022103.
- (452) Tang, Q.; Li, H.; Liu, Y.; Hu, W. *J. Am. Chem. Soc.* **2006**, *128*, 14634–14639.
- (453) Tang, Q.; Li, H.; Song, Y.; Xu, W.; Hu, W.; Jiang, L.; Liu, Y.; Wang, X.; Zhu, D. *Adv. Mater.* **2006**, *18*, 3010–3014.
- (454) Tang, Q.; Tong, Y.; Hu, W.; Wan, Q.; Bjørnholm, T. *Adv. Mater.* **2009**, *21*, 4234–4237.
- (455) Zhao, Y. S.; Wu, J. S.; Huang, J. X. *J. Am. Chem. Soc.* **2009**, *131*, 3158–3159.
- (456) Zhang, Y.; Dong, H.; Tang, Q.; Ferdous, S.; Liu, F.; Mannsfeld, S. C. B.; Hu, W.; Briseno, A. L. *J. Am. Chem. Soc.* **2010**, *132*, 11580–11584.
- (457) Chiu, J.-J.; Kei, C.-C.; Perng, T.-P.; Wang, W.-S. *Adv. Mater.* **2003**, *15*, 1361–1364.
- (458) Sun, Y.; Tan, L.; Jiang, S.; Qian, H.; Wang, Z.; Yan, D.; Di, C.; Wang, Y.; Wu, W.; Yu, G.; Yan, S.; Wang, C.; Hu, W.; Liu, Y.; Zhu, D. *J. Am. Chem. Soc.* **2007**, *129*, 1882–1883.
- (459) Zhao, Y. S.; Zhan, P.; Kim, J.; Sun, C.; Huang, J. X. *ACS Nano* **2010**, *4*, 1630–1636.
- (460) Xiao, K.; Tao, J.; Pan, Z.; Puzosky, A. A.; Ivanov, I. N.; Pennycook, S. J.; Geoghegan, D. B. *Angew. Chem., Int. Ed.* **2007**, *46*, 2650–2654.
- (461) Xiao, K.; Tao, J.; Puzosky, A. A.; Ivanov, I. N.; Retterer, S. T.; Pennycook, S. J.; Geoghegan, D. B. *Adv. Funct. Mater.* **2008**, *18*, 3043–3048.
- (462) Xiao, K.; Rondinone, A. J.; Puzosky, A. A.; Ivanov, I. N.; Retterer, S. T.; Geoghegan, D. B. *Chem. Mater.* **2009**, *21*, 4275–4281.
- (463) Leznoff, C. C.; Lever, A. B. P. *Phthalocyanines, Properties and Applications*; Wiley: New York, 1996; Vols. 1–4.
- (464) Kobayashi, N. *Curr. Opin. Solid State Mater. Sci.* **1999**, *4*, 345–353.
- (465) Schoch, J. K. F.; Gregg, J. J.; Temofonte, T. A. *J. Vac. Sci. Technol. A* **1988**, *6*, 155–158.
- (466) Tong, W. Y.; Djuricic, A. B.; Xie, M. H.; Ng, A. C. M.; Cheung, K. Y.; Chan, W. K.; Leung, Y. H.; Lin, H. W.; Gwo, S. *J. Phys. Chem. B* **2006**, *110*, 17406–17413.
- (467) Peumans, P.; Forrest, S. R. *Appl. Phys. Lett.* **2001**, *79*, 126–128.
- (468) Lee, Y.-L.; Tsai, W.-C.; Maa, J.-R. *Appl. Surf. Sci.* **2001**, *173*, 352–361.
- (469) Tong, W. Y.; Djuricic, A. B.; Ng, A. M. C.; Chan, W. K. *Thin Solid Films* **2007**, *515*, 5270–5274.
- (470) Bao, Z.; Lovinger, A. J.; Brown, J. *J. Am. Chem. Soc.* **1998**, *120*, 207–208.
- (471) Barrena, E.; Zhang, X. N.; Mbenkum, B. N.; Lohmueller, T.; Krauss, T. N.; Kelsch, M.; Aken, P. A. v.; Spatz, J. P.; Dosch, H. *Chem-PhysChem* **2008**, *9*, 1114–1116.
- (472) Chiu, J.-J.; Wang, W.-S.; Kei, C.-C.; Cho, C.-P.; Perng, T. P.; Wei, P.-K.; Chiu, S.-Y. *Appl. Phys. Lett.* **2003**, *83*, 4607–4609.
- (473) Chiu, J. J.; Wang, W. S.; Kei, C. C.; Perng, T. P. *Appl. Phys. Lett.* **2003**, *83*, 347–349.
- (474) Cheung, C. H.; Djuricic, A. B.; Leung, Y. H.; Wei, Z. F.; Xu, S. J.; Chan, W. K. *Chem. Phys. Lett.* **2004**, *394*, 203–206.
- (475) Zhao, Y.; Di, C.; Yang, W.; Yu, G.; Liu, Y.; Yao, J. *Adv. Funct. Mater.* **2006**, *16*, 1985–1991.
- (476) Hrudehy, P. C. P.; Szeto, B.; Brett, M. J. *Appl. Phys. Lett.* **2006**, *88*, 251106.
- (477) Hrudehy, P.; Westra, K.; Brett, M. *Adv. Mater.* **2006**, *18*, 224–228.
- (478) Bjørnholm, T.; Greve, D. R.; Reitzel, N.; Hassenkam, T.; Kjaer, K.; Howes, P. B.; Larsen, N. B.; Bogelund, J.; Jayaraman, M.; Ewbank, P. C.; McCullough, R. D. *J. Am. Chem. Soc.* **1998**, *120*, 7643–7644.
- (479) Bjørnholm, T.; Hassenkam, T.; Greve, D. R.; McCullough, R. D.; Jayaraman, M.; Savoy, S. M.; Jones, C. E.; McDevitt, J. T. *Adv. Mater.* **1999**, *11*, 1218–1221.
- (480) Brinkmann, M.; Chandezon, F.; Pansu, R. B.; Julien-Rabant, C. *Adv. Funct. Mater.* **2009**, *19*, 2759–2766.
- (481) Li, D.; Huang, J.; Kaner, R. B. *Acc. Chem. Res.* **2008**, *42*, 135–145.
- (482) Ding, H.; Wan, M.; Wei, Y. *Adv. Mater.* **2007**, *19*, 465–469.
- (483) Zhang, X.; Kolla, H. S.; Wang, X.; Raja, K.; Manohar, S. K. *Adv. Funct. Mater.* **2006**, *16*, 1145–1152.
- (484) Michaelson, J. C.; McEvoy, A. J. *Chem. Commun.* **1994**, 79–80.
- (485) Virji, S.; Huang, J.; Kaner, R. B.; Weiller, B. H. *Nano Lett.* **2004**, *4*, 491–496.

- (486) Goel, S.; Gupta, A.; Singh, K. P.; Mehrotra, R.; Kandpal, H. C. *Mater. Sci. Eng., A* **2007**, *443*, 71–76.
- (487) Huang, J.; Virji, S.; Weiller, B. H.; Kaner, R. B. *J. Am. Chem. Soc.* **2002**, *125*, 314–315.
- (488) Nuraje, N.; Su, K.; Yang, N.-I.; Matsui, H. *ACS Nano* **2008**, *2*, 502–506.
- (489) Chiou, N.-R.; Epstein, A. J. *Adv. Mater.* **2005**, *17*, 1679–1683.
- (490) Chiou, N.-R.; Lu, C.; Guan, J.; Lee, L. J.; Epstein, A. J. *Nat. Nanotechnol.* **2007**, *2*, 354–357.
- (491) Chiou, N.-R.; Epstein, A. J. *Synth. Met.* **2005**, *153*, 69–72.
- (492) Wang, J.; Chan, S.; Carlson, R. R.; Luo, Y.; Ge, G.; Ries, R. S.; Heath, J. R.; Tseng, H.-R. *Nano Lett.* **2004**, *4*, 1693–1697.
- (493) Liu, H.; Li, Y.; Xiao, S.; Gan, H.; Jiu, T.; Li, H.; Jiang, L.; Zhu, D.; Yu, D.; Xiang, B.; Chen, Y. *J. Am. Chem. Soc.* **2003**, *125*, 10794–10795.
- (494) Kobayashi, T. *J-aggregates*; World Scientific: Singapore, 1996.
- (495) Agranovich, V. M.; La Rocca, G. C. *Organic Nanostructures: Science and Applications*; IOS Press: Amsterdam, 2002.
- (496) Spano, F. C.; Kuklinski, J. R.; Mukamel, S. *Phys. Rev. Lett.* **1990**, *65*, 211.
- (497) Abramavicius, D.; Palmieri, B.; Voronine, D. V.; Sanda, F.; Mukamel, S. *Chem. Rev.* **2009**, *109*, 2350–2408.
- (498) Scholes, G. D.; Rumbles, G. *Nat. Mater.* **2006**, *5*, 683–696.
- (499) Spano, F. C. *Annu. Rev. Phys. Chem.* **2006**, *57*, 217–243.
- (500) Spano, F. C. *Acc. Chem. Res.* **2009**, *43*, 429–439.
- (501) Scholes, G. D. *Annu. Rev. Phys. Chem.* **2003**, *54*, 57–87.
- (502) Eisele, D. M.; Knoester, J.; Kirstein, S.; Rabe, J. P.; Vanden Bout, D. A. *Nat. Nanotechnol.* **2009**, *4*, 658–663.
- (503) Lin, H.; Camacho, R.; Tian, Y.; Kaiser, T. E.; Wurthner, F.; Scheblykin, I. G. *Nano Lett.* **2009**, *10*, 620–626.
- (504) Law, K. Y. *Chem. Rev.* **1993**, *93*, 449–486.
- (505) Kazmaier, P. M.; Hoffmann, R. J. *Am. Chem. Soc.* **1994**, *116*, 9684–9691.
- (506) An, B.-K.; Lee, D.-S.; Lee, J.-S.; Park, Y.-S.; Song, H.-S.; Park, S. Y. *J. Am. Chem. Soc.* **2004**, *126*, 10232–10233.
- (507) Luo, J.; Xie, Z.; Lam, J. W. Y.; Cheng, L.; Tang, B. Z.; Chen, H.; Qiu, C.; Kwok, H. S.; Zhan, X.; Liu, Y.; Zhu, D. *Chem. Commun.* **2001**, 1740–1741.
- (508) Weiss, D. S.; Abkowitz, M. *Chem. Rev.* **2009**, *110*, 479–526.
- (509) Jenekhe, S. A.; Osaheni, J. A. *Science* **1994**, *265*, 765–768.
- (510) Jenekhe, S. A.; Yi, S. *Adv. Mater.* **2000**, *12*, 1274–1278.
- (511) Takazawa, K.; Inoue, J.-i.; Mitsuishi, K.; Takamasu, T. *Phys. Rev. Lett.* **2010**, *105*, 067401.
- (512) Zhao, Y. S.; Peng, A.; Fu, H.; Ma, Y.; Yao, J. *Adv. Mater.* **2008**, *20*, 1661–1665.
- (513) Zhao, Y.; Xu, J.; Peng, A.; Fu, H.; Ma, Y.; Jiang, L.; Yao, J. *Angew. Chem., Int. Ed.* **2008**, *47*, 7301–7305.
- (514) Wang, H.; Liao, Q.; Fu, H.; Zeng, Y.; Jiang, Z.; Ma, J.; Yao, J. *J. Mater. Chem.* **2009**, *19*, 89–96.
- (515) Balzer, F.; Bordo, V. G.; Simonsen, A. C.; Rubahn, H. G. *Appl. Phys. Lett.* **2003**, *82*, 10–12.
- (516) Balzer, F.; Bordo, V. G.; Simonsen, A. C.; Rubahn, H. G. *Phys. Rev. B* **2003**, *67*, 115408.
- (517) Wasielewski, M. R. *Chem. Rev.* **1992**, *92*, 435–461.
- (518) Takazawa, K. *Chem. Phys. Lett.* **2008**, *452*, 168–172.
- (519) Takazawa, K. *J. Phys. Chem. C* **2007**, *111*, 8671–8676.
- (520) Zhao, Y.; Fu, H.; Hu, F.; Peng, A.; Yang, W.; Yao, J. *Adv. Mater.* **2008**, *20*, 79–83.
- (521) Liao, Q.; Fu, H.; Yao, J. *Adv. Mater.* **2009**, *21*, 4153–4157.
- (522) Li, R.; Hu, W.; Liu, Y.; Zhu, D. *Acc. Chem. Res.* **2010**, *43*, 529–540.
- (523) Baughman, R. H.; Bredas, J. L.; Chance, R. R.; Elsenbaumer, R. L.; Shacklette, L. W. *Chem. Rev.* **1982**, *82*, 209–222.
- (524) Shirakawa, H.; Louis, E. J.; Macdiarmid, A. G.; Chiang, C. K.; Heeger, A. J. *J. Chem. Soc., Chem. Commun.* **1977**, 578–580.
- (525) Jang, J.; Bae, J.; Lee, K. *Polymer* **2005**, *46*, 3677–3684.
- (526) Granstrom, M.; Inganas, O. *Polymer* **1995**, *36*, 2867–2872.
- (527) Thapa, P. S.; Yu, D. J.; Wicksted, J. P.; Hadwiger, J. A.; Barisci, J. N.; Baughman, R. H.; Flanders, B. N. *Appl. Phys. Lett.* **2009**, *94*, 033104.
- (528) Kemp, N. T.; McGrouther, D.; Cochrane, J. W.; Newbury, R. *Adv. Mater.* **2007**, *19*, 2634–2638.
- (529) Yamamoto, Y.; Jin, W.; Fukushima, T.; Minari, T.; Tsukagoshi, K.; Saeki, A.; Seki, S.; Tagawa, S.; Aida, T. *Chem. Lett.* **2009**, *38*, 888–889.
- (530) Wang, C.; Liu, Y.; Ji, Z.; Wang, E.; Li, R.; Jiang, H.; Tang, Q.; Li, H.; Hu, W. *Chem. Mater.* **2009**, *21*, 2840–2845.
- (531) Yamamoto, Y.; Fukushima, T.; Suna, Y.; Ishii, N.; Saeki, A.; Seki, S.; Tagawa, S.; Taniguchi, M.; Kawai, T.; Aida, T. *Science* **2006**, *314*, 1761–1764.
- (532) Xin, H.; Ren, G.; Kim, F. S.; Jenekhe, S. A. *Chem. Mater.* **2008**, *20*, 6199–6207.
- (533) Xin, H.; Reid, O. G.; Ren, G. Q.; Kim, F. S.; Ginger, D. S.; Jenekhe, S. A. *ACS Nano* **2010**, *4*, 1861–1872.
- (534) Oosterbaan, W. D.; Bolsee, J.-C.; Gadisa, A.; Vrindts, V.; Bertho, S.; D'Haen, J.; Cleij, T. J.; Lutsen, L.; McNeill, C. R.; Thomsen, L.; Manca, J. V.; Vanderzande, D. *Adv. Funct. Mater.* **2010**, *20*, 792–802.
- (535) Qiu, L.; Lee, W. H.; Wang, X.; Kim, J. S.; Lim, J. A.; Kwak, D.; Lee, S.; Cho, K. *Adv. Mater.* **2009**, *21*, 1349–1353.
- (536) Kim, D. H.; Han, J. T.; Park, Y. D.; Jang, Y.; Cho, J. H.; Hwang, M.; Cho, K. *Adv. Mater.* **2006**, *18*, 719–723.
- (537) Babel, A.; Jenekhe, S. A. *J. Am. Chem. Soc.* **2003**, *125*, 13656–13657.
- (538) Lee, S. W.; Lee, H. J.; Choi, J. H.; Koh, W. G.; Myoung, J. M.; Hur, J. H.; Park, J. J.; Cho, J. H.; Jeong, U. *Nano Lett.* **2009**, *10*, 347–351.
- (539) Bube, R. H. *Photoelectronic Properties of Semiconductors*; Cambridge University Press: Cambridge, U.K., 1992.
- (540) Osaheni, J. A.; Jenekhe, S. A.; Perlstein, J. J. *Phys. Chem.* **1994**, *98*, 12727–12736.
- (541) Tang, Q.; Li, L.; Song, Y.; Liu, Y.; Li, H.; Xu, W.; Hu, W.; Zhu, D. *Adv. Mater.* **2007**, *19*, 2624–2628.
- (542) Ng, A. M.-C.; Djuriscaroni, A. B.; cacute; Tam, K.-H.; Kwok, W.-M.; Chan, W.-K.; Tam, W. Y.; Phillips, D. L.; Cheah, K.-W. *Adv. Funct. Mater.* **2008**, *18*, 566–574.
- (543) Granstrom, M.; Berggren, M.; Inganas, O. *Science* **1995**, *267*, 1479–1481.
- (544) Boroumand, F. A.; Fry, P. W.; Lidzey, D. G. *Nano Lett.* **2005**, *5*, 67–71.
- (545) Pope, M.; Swenberg, C. E., *Electronic Processes in Organic Crystals and Polymers*, 2nd ed.; Oxford: New York, 1999.
- (546) Simon, J.; Andre, J. J., *Molecular Semiconductors: Photoelectrical Properties and Solar Cells*. Springer: Berlin, 1985.
- (547) Brédas, J. L.; Cornil, J.; Heeger, A. J. *Adv. Mater.* **1996**, *8*, 447–452.
- (548) Bredas, J.-L.; Beljonne, D.; Coropceanu, V.; Cornil, J. *Chem. Rev.* **2004**, *104*, 4971–5004.
- (549) Green, M. A., *Silicon Solar Cells: Advanced Principles and Practice*; Bridge Printery: Sydney, Australia, 1995.
- (550) Gregg, B. A. *J. Phys. Chem. B* **2003**, *107*, 4688–4698.
- (551) Yu, G.; Gao, J.; Hummelen, J. C.; Wudl, F.; Heeger, A. J. *Science* **1995**, *270*, 1789–1791.
- (552) Halls, J. J. M.; Walsh, C. A.; Greenham, N. C.; Marseglia, E. A.; Friend, R. H.; Moratti, S. C.; Holmes, A. B. *Nature* **1995**, *376*, 498–500.
- (553) Piliago, C.; Holcombe, T. W.; Douglas, J. D.; Woo, C. H.; Beaujuge, P. M.; Frechet, J. M. J. *J. Am. Chem. Soc.* **2010**, *132*, 7595–7597.
- (554) Liang, Y.; Xu, Z.; Xia, J.; Tsai, S. T.; Wu, Y.; Li, G.; Ray, C.; Yu, L. *Adv. Mater.* **2010**, *22*, E135–E138.
- (555) Park, S. H.; Roy, A.; Beaupre, S.; Cho, S.; Coates, N.; Moon, J. S.; Moses, D.; Leclerc, M.; Lee, K.; Heeger, A. J. *Nat. Photon* **2009**, *3*, 297–302.
- (556) Liu, J.; Namboothiry, M. A. G.; Carroll, D. L. *Appl. Phys. Lett.* **2007**, *90*, 063501.
- (557) O'Connor, B.; Pipe, K. P.; Shtein, M. *Appl. Phys. Lett.* **2008**, *92*, 193306.
- (558) Li, Y.; Zhou, W.; Xue, D.; Liu, J.; Peterson, E. D.; Nie, W.; Carroll, D. L. *Appl. Phys. Lett.* **2009**, *95*, 203503.
- (559) Lee, M. R.; Eckert, R. D.; Forberich, K.; Dennler, G.; Brabec, C. J.; Gaudiana, R. A. *Science* **2009**, *324*, 232–235.
- (560) Bertho, S.; Oosterbaan, W. D.; Vrindts, V.; D'Haen, J.; Cleij, T. J.; Lutsen, L.; Manca, J.; Vanderzande, D. *Org. Electron.* **2009**, *10*, 1248–1251.
- (561) Salim, T.; Sun, S. Y.; Wong, L. H.; Xi, L. F.; Foo, Y. L.; Lam, Y. M. *J. Phys. Chem. C* **2010**, *114*, 9459–9468.
- (562) Reid, O. G.; Xin, H.; Jenekhe, S. A.; Ginger, D. S. *J. Appl. Phys.* **2010**, *108*, 084320.
- (563) Wang, H. S.; Lin, L. H.; Chen, S. Y.; Wang, Y. L.; Wei, K. H. *Nanotechnology* **2009**, *20*, 075201.
- (564) Schmidt-Mende, L.; Fechtenkötter, A.; Mullen, K.; Moons, E.; Friend, R. H.; MacKenzie, J. D. *Science* **2001**, *293*, 1119–1122.
- (565) Karak, S.; Ray, S. K.; Dhar, A. *Appl. Phys. Lett.* **2010**, *97*, 043306.
- (566) McQuade, D. T.; Pullen, A. E.; Swager, T. M. *Chem. Rev.* **2000**, *100*, 2537–2574.
- (567) Thomas, S. W.; Joly, G. D.; Swager, T. M. *Chem. Rev.* **2007**, *107*, 1339–1386.
- (568) Wanekaya, A.; Chen, W.; Myung, N.; Mulchandani, A. *Electroanalysis* **2006**, *18*, 533–550.
- (569) Cui, Y.; Wei, Q.; Park, H.; Lieber, C. M. *Science* **2001**, *293*, 1289–1292.
- (570) Law, M.; Kind, H.; Messer, B.; Kim, F.; Yang, P. *Angew. Chem., Int. Ed.* **2002**, *41*, 2405–2408.
- (571) Strelcov, E.; Kolmakov, A. *J. Nanosci. Nanotechnol.* **2008**, *8*, 212–221.
- (572) Che, Y.; Datar, A.; Yang, X.; Naddo, T.; Zhao, J.; Zang, L. *J. Am. Chem. Soc.* **2007**, *129*, 6354–6355.
- (573) Wang, Y. J.; Coti, K. K.; Jun, W.; Alam, M. M.; Shyue, J. J.; Lu, W. X.; Padture, N. P.; Tseng, H. R. *Nanotechnology* **2007**, *18*, 424021.
- (574) Huang, J.; Virji, S.; Weiller, B. H.; Kaner, R. B. *Chem.—Eur. J.* **2004**, *10*, 1314–1319.
- (575) Dan, Y. P.; Cao, Y. Y.; Mallouk, T. E.; Evoy, S.; Johnson, A. T. C. *Nanotechnology* **2009**, *20*, 434014.
- (576) Jung, Y. S.; Jung, W.; Tuller, H. L.; Ross, C. A. *Nano Lett.* **2008**, *8*, 3776–3780.
- (577) Samuel, I. D. W.; Turnbull, G. A. *Chem. Rev.* **2007**, *107*, 1272–1295.
- (578) Barrelet, C. J.; Greytak, A. B.; Lieber, C. M. *Nano Lett.* **2004**, *4*, 1981–1985.
- (579) Quochi, F.; Saba, M.; Cordella, F.; Gocalska, A.; Corpino, R.; Marceddu, M.; Anedda, A.; Andreev, A.; Sitter, H.; Sariciffci, N. S.; Mura, A.; Bongiovanni, G. *Adv. Mater.* **2008**, *20*, 3017–3021.
- (580) O'Carroll, D.; Redmond, G. *Physica E* **2008**, *40*, 2468–2473.

- (581) O'Carroll, D.; Lieberwirth, I.; Redmond, G. *Small* **2007**, *3*, 1178–1183.
- (582) Tseng, R. J.; Huang, J.; Ouyang, J.; Kaner, R. B.; Yang, Y. *Nano Lett.* **2005**, *5*, 1077–1080.
- (583) Duvail, J. L.; Long, Y.; Retho, P.; Louarn, G.; De Pra, L. D.; Demoustier-Champagne, S. *Mol. Cryst. Liq. Cryst.* **2008**, *485*, 835–842.
- (584) Liu, R.; Cho, S. I.; Lee, S. B. *Nanotechnology* **2008**, *19*, 215710.
- (585) Wolf, S. A.; Awschalom, D. D.; Buhrman, R. A.; Daughton, J. M.; von Molnar, S.; Roukes, M. L.; Chtchelkanova, A. Y.; Treger, D. M. *Science* **2001**, *294*, 1488–1495.
- (586) Xiong, Z. H.; Wu, D.; Vardeny, Z. V.; Shi, J. *Nature* **2004**, *427*, 821–824.
- (587) Rocha, A. R.; Garcia-suarez, V. M.; Bailey, S. W.; Lambert, C. J.; Ferrer, J.; Sanvito, S. *Nat. Mater.* **2005**, *4*, 335–339.
- (588) Zhan, Y. Q.; de Jong, M. P.; Li, F. H.; Dediu, V.; Fahlman, M.; Salaneck, W. R. *Phys. Rev. B* **2008**, *78*, 045208.
- (589) Pramanik, S.; Bandyopadhyay, S.; Garre, K.; Cahay, M. *Phys. Rev. B* **2006**, *74*, 235329.
- (590) Pramanik, S.; Stefanita, C. G.; Patibandla, S.; Bandyopadhyay, S.; Garre, K.; Harth, N.; Cahay, M. *Nat. Nanotechnol.* **2007**, *2*, 216–219.
- (591) Jenekhe, S. A.; Lu, L.; Alam, M. M. *Macromolecules* **2001**, *34*, 7315–7324.
- (592) Sanvito, S.; Rocha, A. R. *J. Comput. Theor. Nanosci.* **2006**, *3*, 624–642.